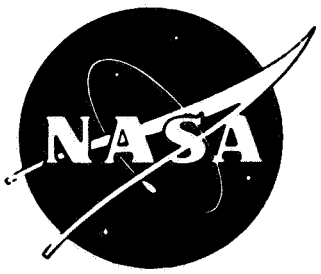

DAC-60804

Final Report

AN EXPERIMENTAL STUDY OF THE ENTROPY LAYER SURROUNDING A BLUNT BODY AT ANGLE OF ATTACK

OCTOBER 1967

Prepared by
J. XERIKOS AND W. A. ANDERSON

Prepared under Contract No. NAS-7-461
by Douglas Aircraft Company
Missile and Space Systems Division,
Santa Monica, California
for
NATIONAL AERONAUTICS AND SPACE ADMINISTRATION

CONTENTS

AN EXPERIMENTAL STUDY OF THE ENTROPY LAYER SURROUNDING A BLUNT BODY AT ANGLE OF ATTACK

By J. Xerikos and W. A. Anderson*
Douglas Aircraft Company

SUMMARY

An experimental investigation of three-dimensional blunt body shock layer phenomena was conducted at a Mach number of 4.468 and at angles of attack up to 20° using an ellipsoid of revolution and an Apollo-type model. The principal objective of the study was to investigate the behavior of the stagnation streamline in asymmetric flow by means of a definitive measurement of the isentropic total pressure on the surface of the body. A traversing probe was used to establish accurate total pressure profiles which could then be extrapolated to the body surface. The effect of asymmetry on the measured values was found to be of the order of 0.5% indicating that the maximum entropy streamline does not, in general, coincide exactly with the stagnation streamline. In addition to the shock layer total pressure profiles, detailed surface pressure, shock shape and sonic line data were obtained.

INTRODUCTION

During the past several years, both steady inverse and direct methods as well as time dependent numerical methods have been developed for determining the inviscid flow field about yawed, blunt axisymmetric bodies. In these analyses, consideration of physical boundary conditions has introduced a basic question regarding the behavior of the stagnation, or dividing, streamline. An early study (ref. 1) assumed, a priori, that the stagnation streamline, which subsequently wets the body surface, originally passed through the point at which the shock was normal to the free stream. Thus, the body entropy was specified at the outset of the flow field calculation. In applying the PLK method to inverse and direct solutions of asymmetric flow problems, the same assumption was introduced in ref. 2.

More recently, the results of an inverse or shock-specified analysis (ref. 3), for treating flow past two-dimensional and axisymmetric blunt bodies at small angles of attack, indicated that the stagnation streamline at the shock wave was slightly displaced from the normal point. Therefore, the body was not covered by the maximum-entropy streamline. A solution was obtained for a body supporting a parabolic or paraboloidal shock wave set at 10° angle of attack to a hypersonic free stream ($M_\infty \to \infty$, $\gamma = 1.4$). The maximum entropy streamline was found to be slightly displaced to the windward side of the stagnation

---

*Research and Development Directorate, Advance Systems and Technology, Missile and Space Systems Division. The authors wish to acknowledge the able assistance of Mr. Dale Klahn during preparation of this report.

streamline. A later study by the same author (ref. 4) dealt with the direct or body-specified version of this problem. An inverse approach to the perfect gas and equilibrium air solution of blunt-body flow fields at large angles of attack (ref. 5) has also yielded a displaced maximum entropy streamline. An Apollo configuration set at 22° angle of attack (U_∞ = 22, 754 ft/sec, altitude = 150, 480 ft) was considered. In this case, the displacement was to the leeward side of the stagnation streamline.

The behavior of the maximum entropy streamline for the numerical examples cited above coincides with the results of ref. 6 (as described in ref. 7) which are based on a hypersonic, constant density solution of the blunt body rotational stagnation point region considering weak two-dimensional asymmetry. The study concludes that the maximum entropy streamline is not coincident with the stagnation streamline and that it turns in the direction of decreasing body or shock curvature.

The application of the N-strip method of integral relations to symmetric flow cases requires the specification of 3N boundary conditions (for the 3N governing differential equations) in order to form a properly set two point boundary value problem. Symmetry requirements at the axis provide 2N conditions while analyticity requirements along the "sonic" singular line provide the remaining N conditions. For the asymmetric case, only the latter conditions remain valid. If the solution is sought in a plane of symmetry of the flow (assuming, for example, a sinusoidal meridianal variation of properties), 2N conditions are given by analyticity requirements at the N "sonic" singular points on both the windward and leeward sides of the body. Additional conditions must therefore be sought.

Applications of the integral method to asymmetric flows have been restricted to one strip (N = 1) versions treating two-dimensional or axisymmetric configurations at angle of attack. In this case the most rigorous approach includes, as unknowns, the initial conditions: (1) stagnation point location, (2) body entropy, (3) shock detachment distance, and (4) shock angle opposite the stagnation point. Three formulations of the integral method have been presented to date. The most simplified version (refs. 2 and 8) reverts to the maximum entropy stagnation streamline assumption, thus eliminating body entropy as an unknown parameter. Conditions for determining the remaining parameters are provided by the requirement that the solution be analytic in the neighborhood of the two body sonic points in the plane of symmetry and that a mass conservation relationship is satisfied in the stagnation region.

A second large angle of attack approach (refs. 9 and 10) provides for the possibility that the maximum entropy streamline does not wet the body, but does not furnish necessary supplemental conditions for the determination of the additional parameters. For example, in ref. 9 which treats a two dimensional flat plate, use of the assumption that the stagnation streamline passes through the normal point on the shock leads to inconsistencies in the solution for angles of attack in excess of 30°

Ref. 11 treats the full four-parameter problem by establishing two additional conditions based upon the requirement of analyticity at the stagnation point. Entropy data are not presented in the numerical results; therefore, no

quantitative information is provided regarding the direction or magnitude of the stagnation streamline displacement from the shock normal point.

A critical examination of the characteristics of the stagnation streamline yielded by the one strip integral method (ref. 12) results in the conclusion that the behavior of the stagnation streamline is primarily a consequence of the coordinate system and the functional approximations employed, e. g., it is required to coincide with a coordinate system direction.

Summarizing the present status of the integral method as applied to asymmetric flows, independent of the approach taken, the one strip ($N = 1$) version yields an oversimplified description of the stagnation region while for $N > 1$, additional conditions required for a properly set problem are not as yet resolved.

At this point it is instructive to briefly cite the results of a generalized rotational, constant density, stagnation-point analysis encompassing asymmetric perturbations on both two-dimensional and axisymmetric flows (refs. 7, 13). It should be noted that ref. 14 offers a correction to the exact solution of ref. 7 which does not appear to invalidate two basic conclusions of the earlier work: (1) for two-dimensional asymmetric blunt body flow, the stagnation streamline intersects the body at a finite angle and the rotational flow is analytic in the neighborhood of the stagnation point (2) for an asymmetric quasi-spherical stagnation region, the stagnation streamline is tangent to the body at the stagnation point and the solution is non-analytic. The latter conclusion obviously contradicts the analyticity assumptions of ref. 11.

In dealing with the more recently developed direct unsteady approach to calculating three-dimensional blunt body flow fields, the body entropy need not be specified in advance, in the sense of a known parameter or initial condition. However, available numerical data yielded by these methods (e. g., refs. 15 and 16) are not sufficiently detailed to conclusively establish the behavior of the stagnation streamline.

The purpose of the present experimental investigation of three-dimensional shock layer phenomena is to provide basic data not presently available for the critical evaluation of analytical and numerical studies of asymmetric supersonic flow. The principal objective of the study is to investigate the behavior of the stagnation streamline by means of a definitive measurement of the entropy on the surface of a blunt axisymmetric body at angle of attack. The determination of the body entropy involves the measurement of static and total pressures in the shock-layer region along several paths normal to the body surface using a traversing probe. An extrapolation procedure, excluding data points within the boundary layer, is then applied to establish the inviscid value of the surface entropy.

The secondary objectives of the experimental program are to provide high-quality surface pressure and shock-shape data. Since most three-dimensional methods are in the developmental stage, it is essential that accurate data be obtained for classical configurations which are more readily susceptible of analysis, as opposed to complex three-dimensional shapes which can only be treated by advanced versions of the current analyses.

EXPERIMENTAL TECHNIQUE

The present experimental study employs conventional instrumentation in a specialized mode of operation that is particularly suited to shock-layer measurements. A prototype Douglas study (ref. 17) has previously established the feasibility of accurately determining shock-layer properties in the transonic zone of a blunt body.

Determination of Surface Entropy

Primary emphasis has been placed in this study on the determination of the value of entropy on the surface of the body, since this information essentially identifies the point of origin of the stagnation streamline. The results of this measurement can provide a direct answer as to whether the maximum entropy streamline wets the body or almost equivalently, from a practical standpoint, lies within the confines of the boundary layer. For the test conditions chosen, the following two assumptions governing the flow-field behavior will be applicable:

1. The shock-layer flow excluding the boundary layer is particle-isentropic: the value of entropy along a given streamline is a constant which is determined at the point at which the streamline crosses the bow shock.

2. The isentropic flow relation between entropy and total pressure is valid, i.e.,

$$\frac{\Delta S}{\mathcal{R}} = -\ln_e \left[p_t\,(\theta;\, M_\infty,\, \gamma)/p_{t_\infty}(M_\infty,\, \gamma) \right], \quad \theta = \text{bow shock angle}$$

Subsequent discussion of the experimental approach related to the stagnation streamline will therefore be concerned with the measurement of the total pressure in the shock-layer region.

Pressure Measurement Sensitivity

The variation of post-shock total pressure (relative to the normal shock value) with shock angle is indicated in Fig. 1. For example, at $M_\infty = 5$ and $\gamma = 1.4$, a 0.5% change in total pressure takes place if the streamline under consideration passes through the bow shock at a point where the shock slope, θ, is 87.1°, measured relative to the free stream direction. A pressure measurement accuracy of 0.5% is readily attainable; therefore, it should be possible to identify a stagnation streamline which is displaced only a few degrees in terms of shock angle from the normal point. Increasing the Mach number to 10 increases the sensitivity by only 0.2° at $\Delta p_t = 0.5$ and introduces instrumentation difficulties associated with high Mach-number testing. Based on the preceding considerations, a nominal test Mach number, $M_\infty = 4.5$ was selected in order to provide adequate pressure measurement sensitivity while avoiding real gas effects which would complicate the thermodynamic relationships involved in the present investigation.

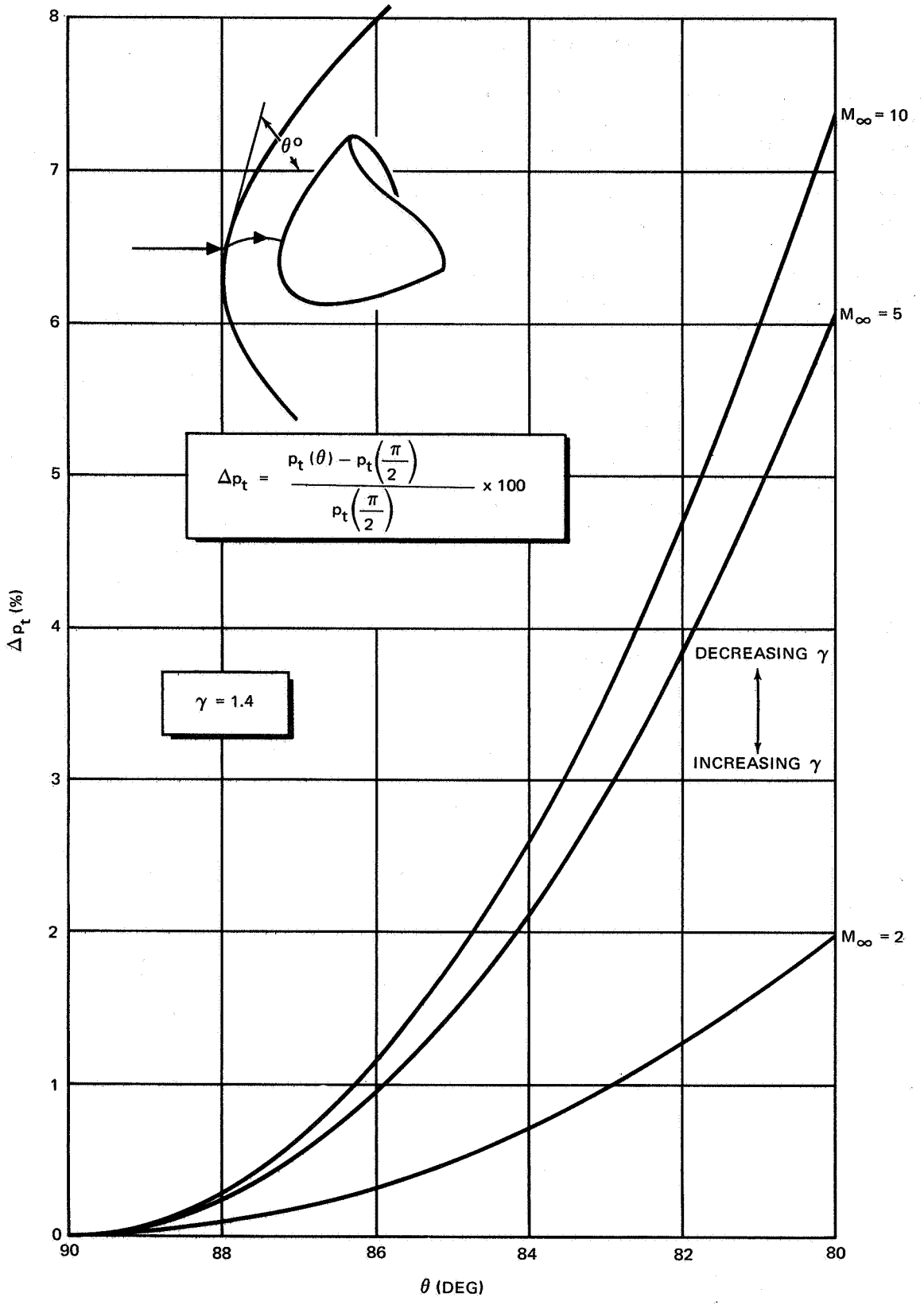

Figure 1. Variation in Post-Shock Total Pressure Relative to Normal Shock Value with Shock Angle

Theoretical Considerations

Because of viscous dissipation in the boundary layer, the inviscid value of surface total or stagnation pressure, considered in the aforementioned theoretical investigations is not directly measurable away from the stagnation point in a real fluid for the symmetric flow case. Further, as previously mentioned, the asymmetric quasi-spherical stagnation region analysis described in ref. 7 indicates that the stagnation streamline becomes tangent to the body at the stagnation point. It is therefore not clear that the maximum in the surface static pressure variation is necessarily equal to the body stagnation pressure when three-dimensional asymmetric flow configurations are considered.

A displacement, d, of the maximum entropy (or, equivalently, minimum total pressure) streamline in the plane containing the body axis and the free stream vector, where $d > \delta$ (δ = boundary layer thickness), can produce a discernible minimum in the total pressure profile on one side of the body, e.g., fig. 2. If a minimum cannot be detected outside of the boundary layer, then an upper bound on the magnitude of a possible displacement effect will immediately be established. It should be noted, however, that use of a total pressure profile extrapolation procedure for determining the surface entropy may not preclude detection of a displacement effect for the case $d < \delta$. As indicated in fig. 3, the behavior of an experimental p_t profile, relative to the minimum attainable inviscid value of p_t, could provide information regarding the probable location of the maximum entropy streamline.

If one accepts the possibility of the maximum entropy streamline not wetting the body, a further theoretical consideration arises. The stagnation streamline for the axisymmetric or full three-dimensional case is now contained in a complete constant entropy stream surface. The manner in which it intersects the body surface is not obvious, i.e., whether along a line contained in the plane of symmetry or along a general curve on the body surface (fig. 4).

The preceding considerations form the basis for the use of a traversing probe in the present study which is capable of making detailed total and static pressure surveys along paths approximately normal to the body surface. As opposed to a single pitot-static probe, separate total and static pressure probes were employed in order to minimize probe diameter and to record pressures at the same point in the flow field; the tip of the total pressure probe and the orifices in the static probe traced coincident paths across the shock layer. With the probe axis fixed parallel to the local body slope, measurements were limited in most cases to those relatively near the body surface in order to avoid significant angular deviations from the local flow direction. It is therefore possible to establish an isentropic total-pressure profile outside of the boundary layer that can be extrapolated to the body surface in order to determine the inviscid value of the body entropy.

The nature of the disturbance caused by a probe of finite diameter, D, in a shear flow has been investigated both theoretically and experimentally (ref. 18). In effect, the probe senses a value of total pressure corresponding to an incoming streamline shifted a distance Δ off the probe axis. It has been shown that for subsonic flow, an empirical expression for Δ, considering a

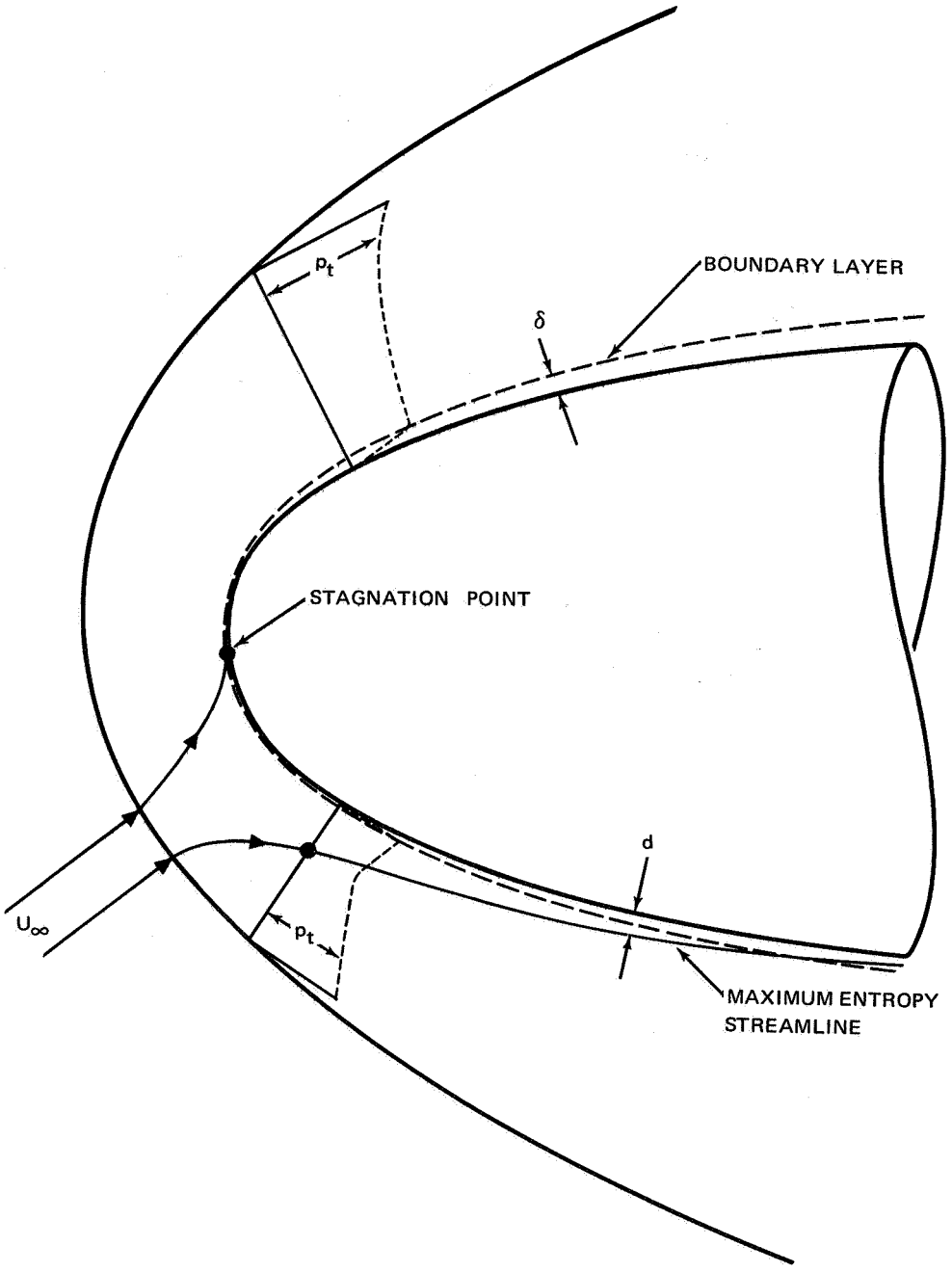

Figure 2. Shock-Layer Total Pressure Profiles Considering the Stagnation Streamline Displaced From the Normal Point on the Bow Shock Wave

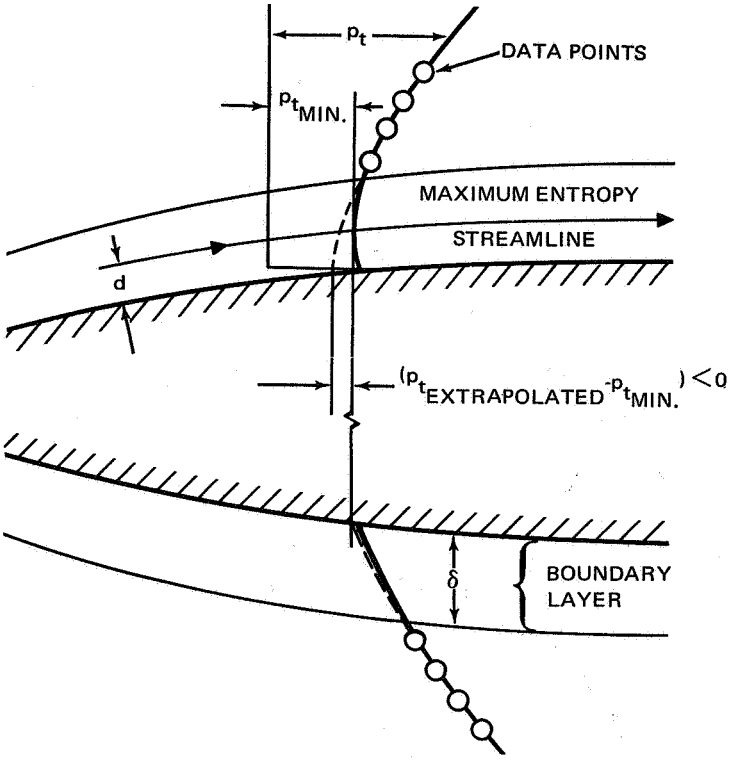

Figure 3. Experimental Extrapolation Procedure Considering Maximum Entropy Streamline Lying Within Boundary Layer

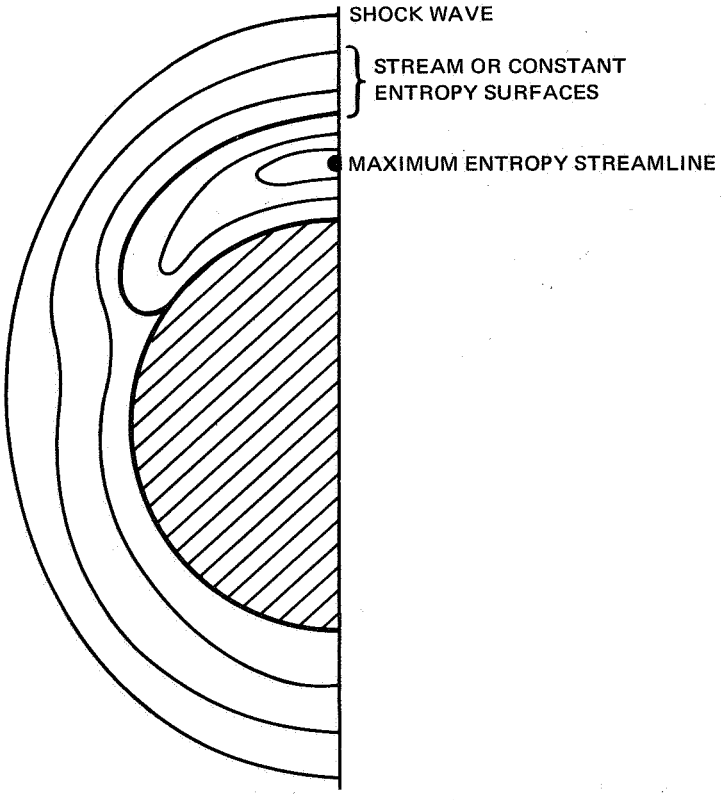

Figure 4. Cross-Section of Hypothetical Asymmetric Stream Surfaces

shear flow defined by $V = U_\infty + Ay$, is given by $\Delta/D = 0.18 \text{ sgn } K$, $K = (AD/2U_\infty) > 0$. Therefore, the shift is negligible, particularly near a maximum or minimum in the pressure profile (fig. 5).

EXPERIMENTAL EQUIPMENT AND TEST PROCEDURE

Test Facility

The tests were conducted in the McDonnell-Douglas Aerophysics Laboratory trisonic 4-ft tunnel. The tunnel is an intermittent blowdown to atmosphere facility capable of operating over a continuously variable Mach number range from 0.2 to 5.0 with running times on the order of 40 to 60 sec. The Mach number in the 4-ft sq test section (4 x 4 x 6 ft) in absence of the model is uniform within ±0.01 with a flow angularity not exceeding ±0.2°.

The entire test was run at a fixed Mach number, $M_\infty = 4.468$. The nominal values of free stream stagnation pressure and temperature were $p_{t_\infty} = 220$ psia and $T_{t_\infty} = 140°$ F., respectively. The average value of Reynolds number during the test was 1.1×10^6/in. or 16.5×10^6 based on maximum model diameter.

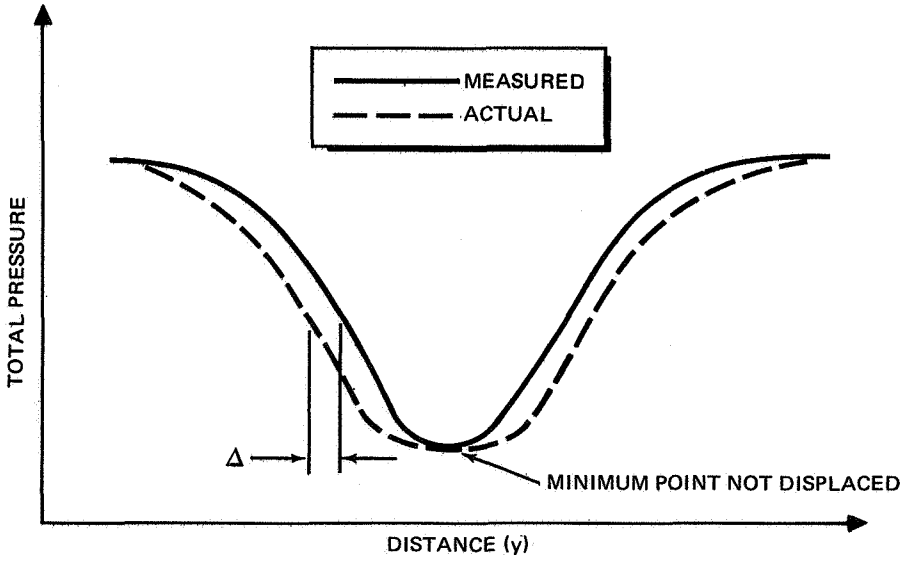

Figure 5. Shear-Flow Effect on Probe Reading

Model Selection and Description

In selecting a model which is compatible with the primary test objectives, the following points were considered: given a family of ellipsoids of revolution, a configuration may be selected which is either significantly more blunt or less blunt than a sphere. In the former case, the shock shape will be quite sensitive to angle of attack; however, the entire shock remains rather flat in the subsonic region and a considerable shift in the stagnation streamline must take place in order to detect a total pressure change on the body surface. In the latter case, the shock curves back more rapidly, but the corresponding change in shock shape and stagnation streamline shift with a given angle of attack is less. It was therefore decided to test two models, since an a priori quantitative evaluation of the tradeoff between these effects could not be made. Subsequently, the analysis of ref. 6 indicated a marked difference in the behavior of the maximum entropy streamline for the configurations selected based on a hypersonic, constant density stagnation flow model. Use of configurations involving sharp corners was ruled out in view of the possibility of the appearance of separation bubbles which may introduce a significant Reynolds number dependence in the experimental results.

The two models selected are shown in figs. 6 and 7. Model E is an ellipsoid of revolution while Model A is an Apollo-type configuration. The models consist of hollow, 17-4PH stainless-steel shells with provisions for internal mounting of all instrumentation. The traversing probe and sting adapter are common to both models. Three ports are available on each model for accommodating the traversing probe shaft. In order to minimize the disturbing effect of the probe on the shock-layer properties, the models both have a maximum diameter of 15 in., thereby establishing a favorable ratio between the scale of the flow field and the probe dimensions.

Central Data Gathering System

The data were recorded by a high-speed, computer-controlled data acquisition system known as the CDGS. The new CDGS is one of the most advanced systems available and is unique as the first application of a computer to control both a wind-tunnel run and all data recording. The data, up to 96 channels, are sampled automatically by an SDS 930 computer, under control of a stored program. Analog millivolt signals from pressure transducers and thermocouples are digitized in the data recording system by a series of multiplexers, amplifiers, and an analog-to-digital converter. These signals are stored in the SDS 930 computer memory. Simultaneously, digital signals from an angle of attack encoder are stored directly into the SDS 930 computer memory core. When all data necessary to form a single data point have been stored, the computer records this information on magnetic tape.

After all data points have been recorded for a run, the magnetic tape is read back into the computer which calculates the final data. The raw and final data are printed in tabulated form by an SDS 300 line-per-minute printer.

ORIFICE	s	x	r
1	0.0	0.0	0.0
2	0.5	0.025	0.499
3	1.0	0.099	0.993
A	1.334	0.168	1.319
4	1.5	0.221	1.478
5	2.0	0.387	1.950
6	2.5	0.594	2.405
7	3.0	0.838	2.841
8	3.5	1.116	3.256
9 & 31	4.0	1.423	3.651
10	4.5	1.756	4.024
B	4.690	1.889	4.160
11	5.0	2.112	4.375
12	5.5	2.488	4.704
13	6.0	2.882	5.012
14	6.5	3.290	5.300
15	7.0	3.713	5.568
16	7.5	4.147	5.816
17	8.0	4.591	6.045
18	8.5	5.044	6.256
19	9.0	5.506	6.449
20	9.5	5.974	6.624
21	10.0	6.448	6.783
22	10.5	6.928	6.924
C	10.632	7.055	6.959
23	11.0	7.412	7.050
24	11.5	7.899	7.160
25	12.0	8.390	7.254
26	12.5	8.884	7.332
27	13.0	9.380	7.396
28	13.5	9.878	7.444
29	14.0	10.377	7.477
30	14.5	10.876	7.496

(All dimensions in inches)

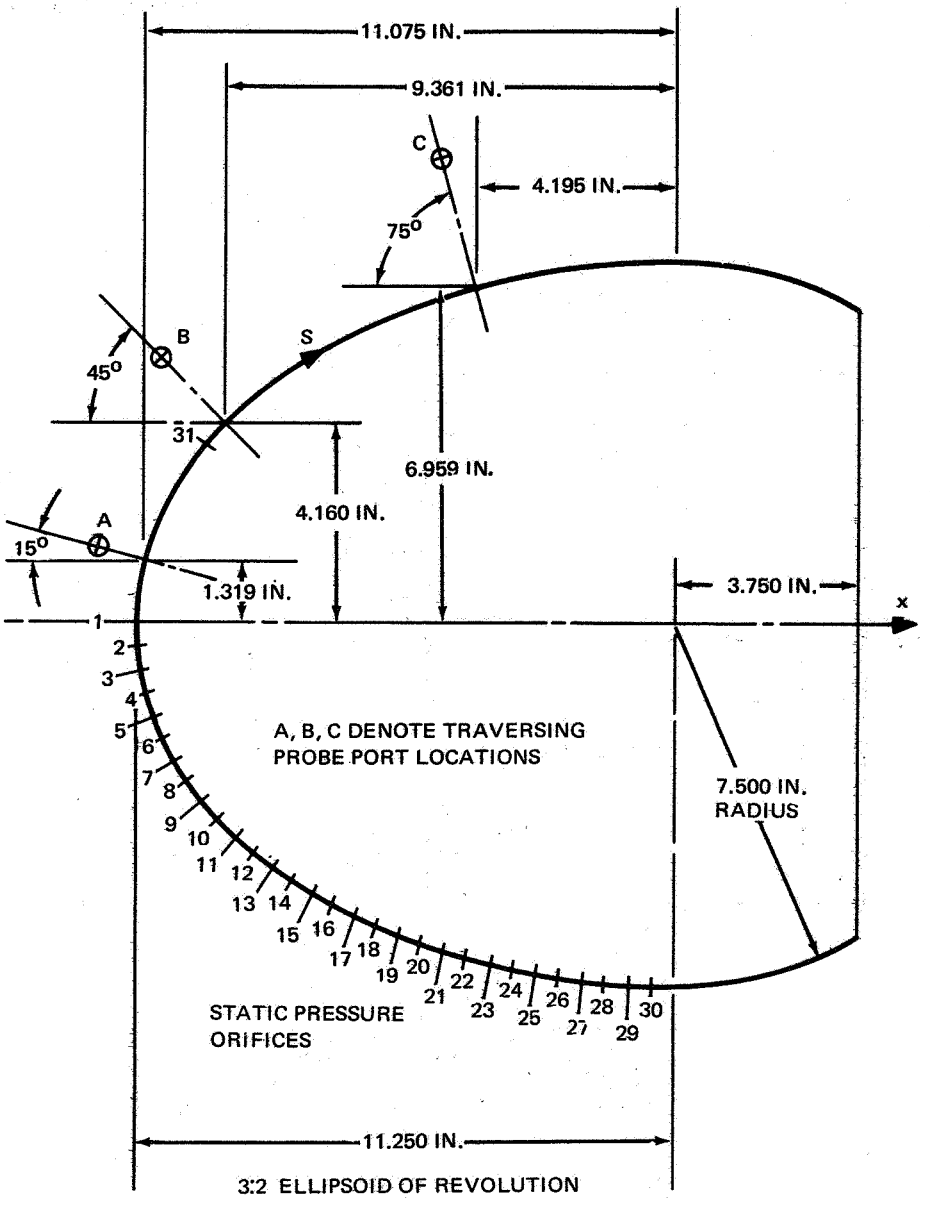

Figure 6. Model Geometry , Model E (1 of 2)

ORIFICE	s	x	r
1	0.0	0.0	0.0
2	0.471	0.006	0.471
3	0.942	0.025	0.992
4	1.414	0.055	1.412
5	1.885	0.099	1.882
6	2.356	0.154	2.350
7	2.827	0.222	2.816
8	3.299	0.302	3.280
9	3.770	0.393	3.742
10 & A	4.241	0.497	4.202
11	4.712	0.613	4.659
12	5.184	0.741	5.112
13	5.655	0.881	5.562
14	6.126	1.032	6.009
15	6.597	1.196	6.451
16	7.069	1.360	6.664
17 & TP	7.237	1.435	7.043
18	7.400	1.515	7.186
19 & 28	7.564	1.624	7.308
20	7.728	1.756	7.403
21 & B	7.891	1.907	7.467
22	8.055	2.067	7.498
23	8.228	2.230	7.493
24	8.372	2.388	7.452
25 & TP	8.545	2.534	7.379
26 & C	9.045	2.953	7.107
27	9.545	3.373	6.834

(All dimensions in inches)

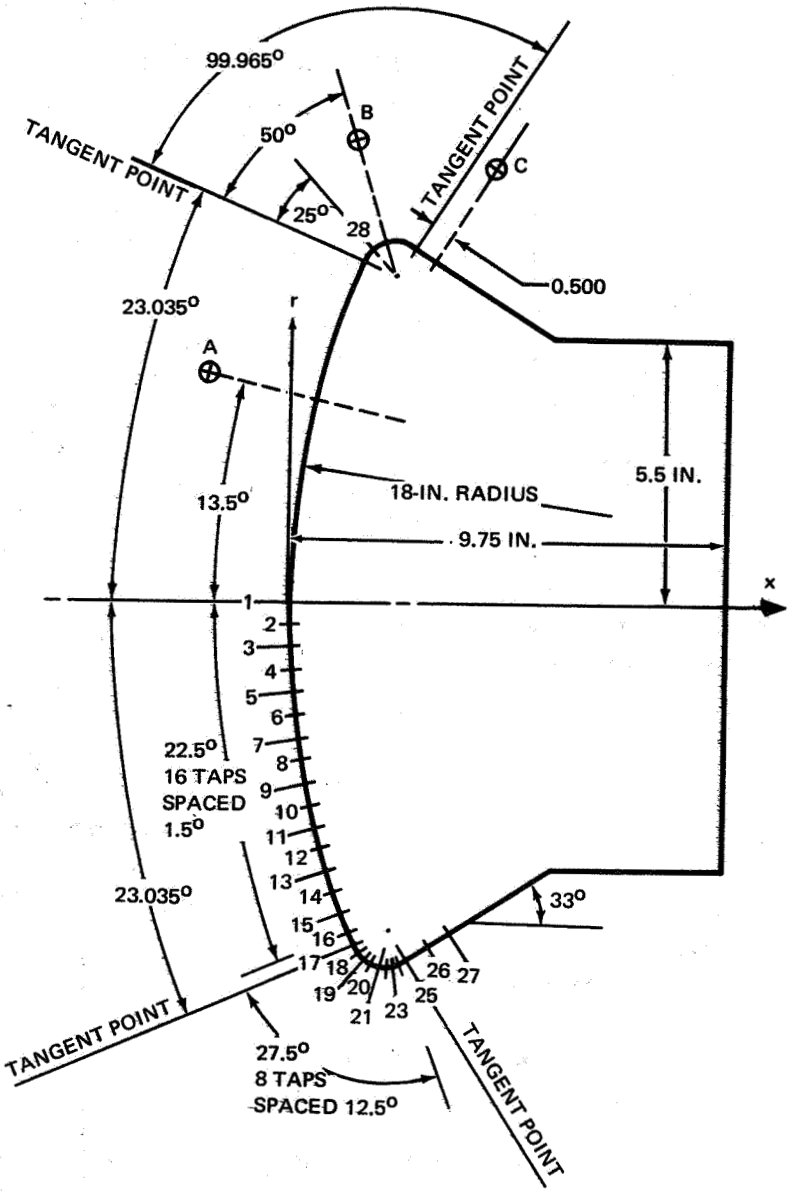

Figure 6. Model Geometry , Model A (2 of 2)

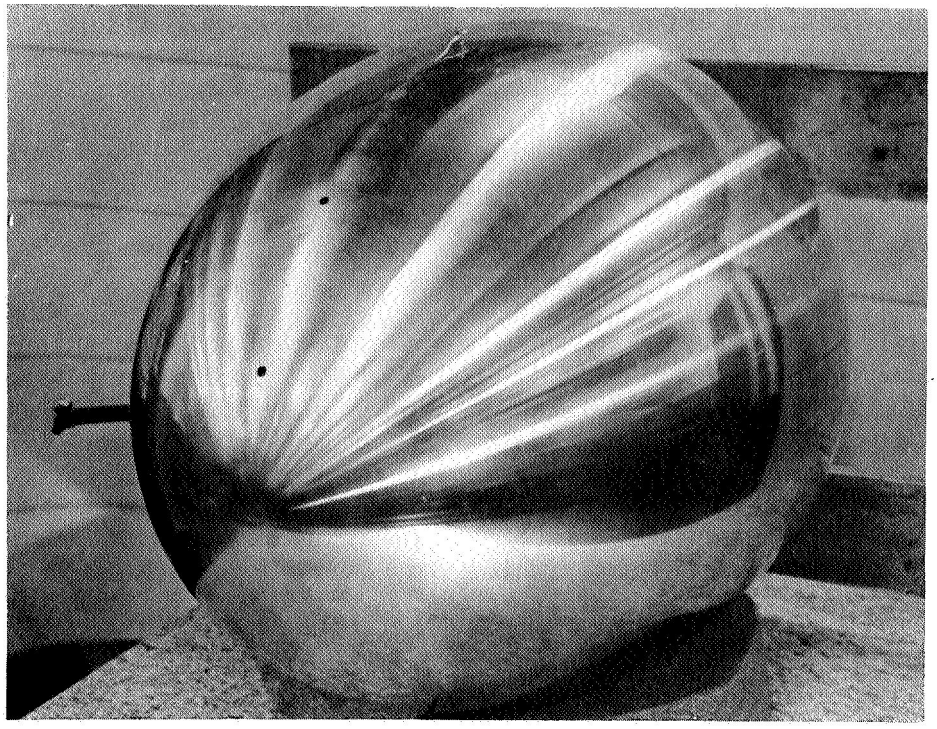

(a) MODEL E

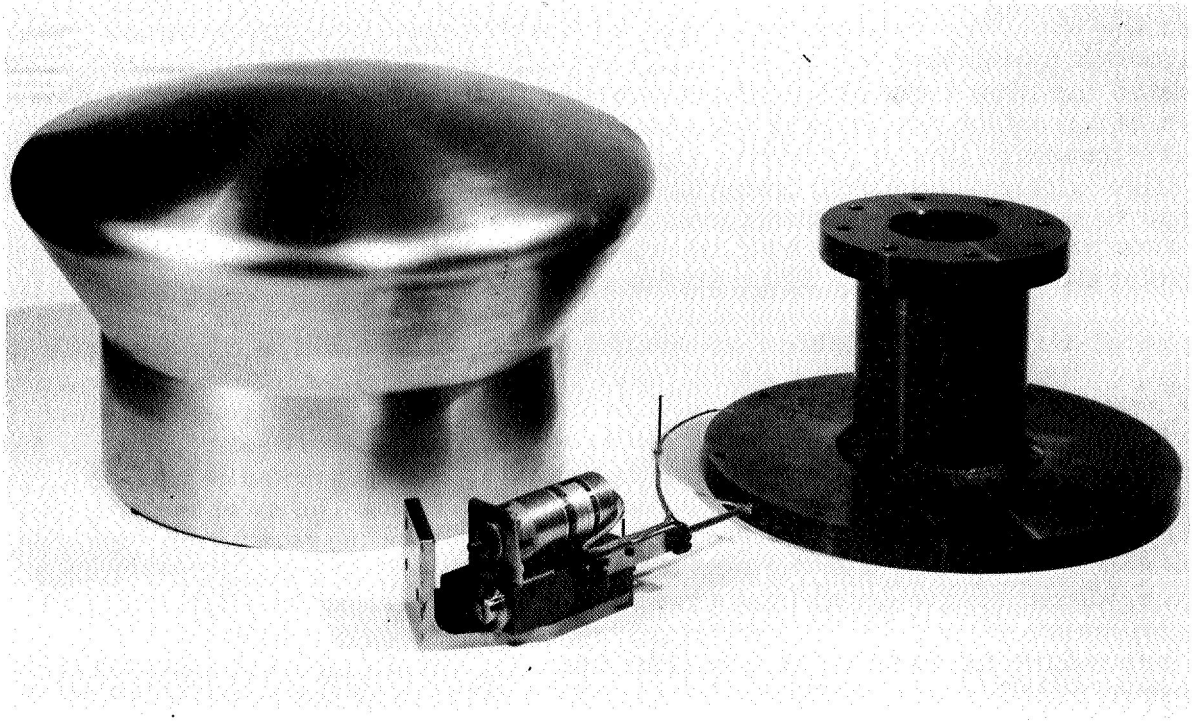

(b) MODEL A

Figure 7. Model Photos

The pressure measurement accuracy in the present test is a function of (1) transducer linearity, (2) transducer scatter or repeatability, (3) calibration system accuracy, and (4) data-acquisition system accuracy. The transducer non-linearity is normally of the order of 0.2 to 0.3% of full scale, transducer repeatability is of the order of 0.05% full scale, and data acquisition and calibration system accuracies are of the order of 0.1%.

Traversing Probe

The traversing probe mechanism consists of a drive unit and interchangeable total and static pressure probe heads (fig. 8). The probe shaft is driven by a Globe model 5A2316-1 electric motor through a gear train and its position is sensed by a Bourns model 108 precision linear motion potentiometer with a resolution of 0.001 in. The motor was electrically braked in order to minimize coasting following shut off. Three Statham diaphragm-type pressure transducers, with ranges of 5, 10 and 100 psia, were mounted on the back of the model. This location minimized lag time in recording data and allowed rapid switching of pressure ranges for best accuracy as the probe position and/or head was changed.

The output from the precision potentiometer readout device served as a control signal which was fed to the central data gathering system. When the wind tunnel start was confirmed, the probe moved through a sequence of preprogrammed steps based upon the calibration of the potentiometer output versus distance from the body surface. When the probe reached a predetermined stop position, the electric motor was switched off by the computer. When the pressure reading stabilized within the specified limits based upon continuous monitoring of the pressure transducer signal, the computer actuated the motor and the probe proceeded to the next stop position. This mode of operation maximized the data for a given tunnel run and minimized erratic readings due to pressure lag. If a given pressure reading did not stabilize within a specified interval of time (e.g., 0.5 sec), the probe then moved to the next programmed position and an identifying flag was noted on the data printout. A filter was incorporated in the data system to eliminate consideration of pressure fluctuations above 100 cps.

The most direct and reliable non-optical measurement which can be made in the supersonic region of the shock layer is that of pitot pressure since precise orientation of the total pressure probe with local flow direction is not required. In order to obtain local isentropic stagnation pressure, p_t, in the shock layer, an additional measurement such as static pressure must obviously be made. If the probe is moved forward into the subsonic region, a correction for the pitot-probe shock is no longer necessary; however, the influence of the probe will then be felt throughout the subsonic zone; therefore, the magnitude of this disturbance must be kept extremely small.

The procedure followed in the present study for obtaining isentropic total pressure profiles was as follows. A static pressure probe run was made for a given angle of attack and port location and the pressure versus probe location data were stored by the data systems computer. A corresponding pitot pressure run was then made with programmed stop positions not necessarily

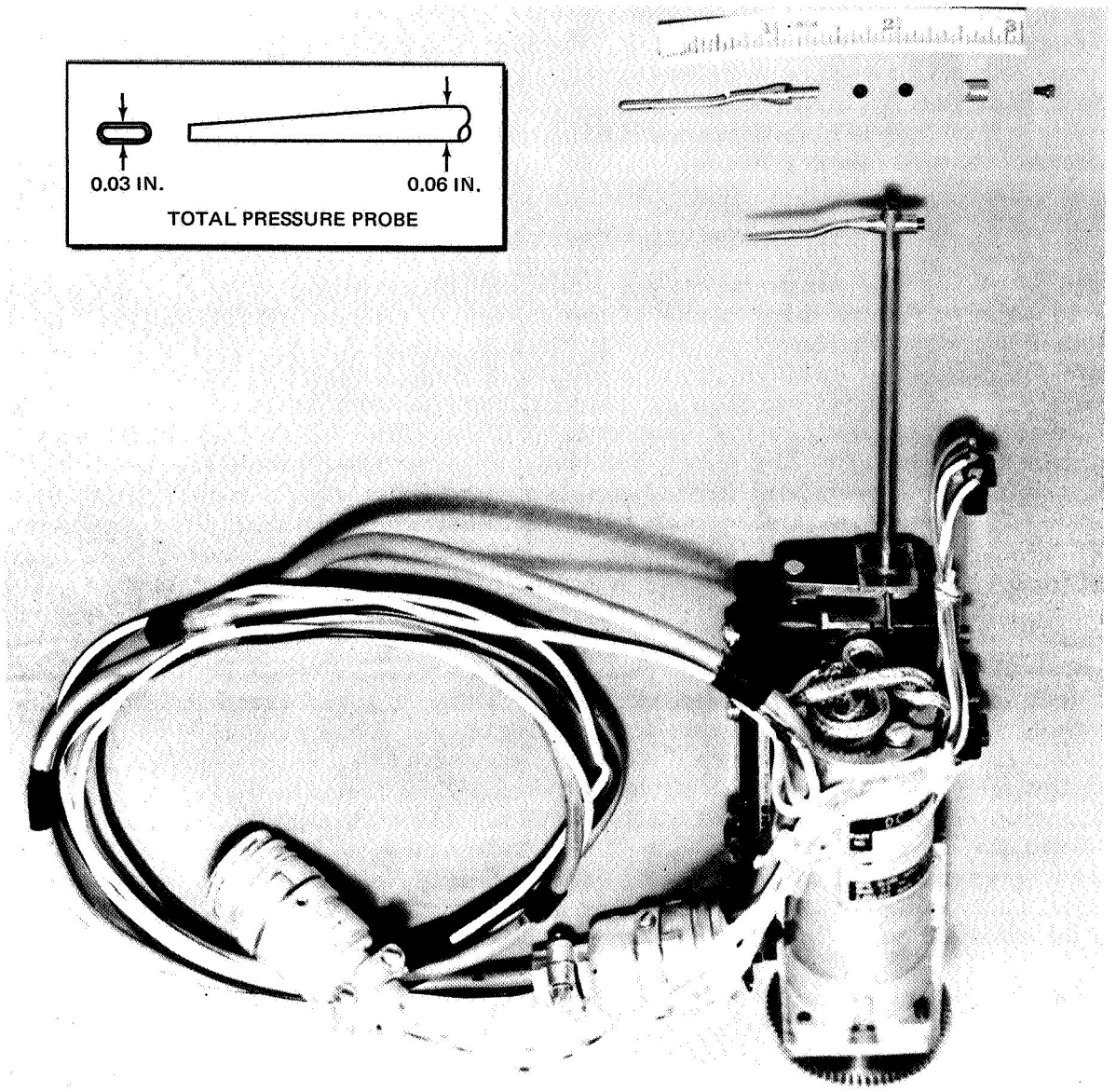

Figure 8. Traversing Probe Details

corresponding to those of the static run. A series of second order polynomial fits of the static data using two points above and one point below each pitot probe position provided the necessary interpolated static pressure value. This operation was automatically performed by the computer which then calculated local Mach number and isentropic total pressure. The free stream stagnation pressure, p_{t_∞}, was continuously monitored on a 500 psia transducer referenced to atmospheric pressure. Instantaneous values of p_{t_∞}, were used to normalize all pressure data recorded as opposed to an average value for an entire tunnel run. Tunnel stagnation temperature was sensed in the settling chamber with a copper-constantan thermocouple referenced to a Pace 150°F thermocouple reference junction.

Surface Pressures

A number of surface static pressure orifices, 31 on Model E and 28 on Model A, were located in the pitching plane of the model-sting configuration (see fig. 6). Circumferential rotation of the model, that is, rotation, ϕ, about the axis of symmetry, provided surface pressure data at each angle of attack at intervals, $\Delta\phi$, of 30°. The model surface pressures were sensed on three Scanivalves, pressure sampling devices for sequentially connecting up to 24 pressures to a common transducer. The three Scanivalves, mounted within the model shell, contained two 15 psid (differential) transducers and a 5 psia (absolute) transducer for Model A and two 15 psid transducers and a 10 psia transducer for Model E. The 15 psid transducers were zeroed at atmospheric pressure while the 5 and 10 psia transducers were zeroed at a vacuum (20 μHg).

The data recording program was written so that it would record data and step the Scanivalves to the next pressure port when either of the following events occurred: (1) All pressures had stabilized eithin a given transducer output tolerance, corresponding to a pressure tolerance. This pressure stabilization was based on 5 consecutive data samples for each pressure channel being within the specified transducer output tolerance; or (2) The maximum stabilization time allowable had elapsed. This allowable time was based on a calculated pressure lag and could be modified during the test if required. When all pressure measuring ports of the Scanivalve had been sampled, the model was advanced to the next pre-set angle of attack. This procedure was repeated until all programmed angles had been obtained.

To verify the correct operation of the Scanivalves, a common pressure was manifolded to a pressure port on each of the Scanivalves. The common pressure for the 5 and 10 psia transducers was the tunnel side wall static pressure. The 15 psid transducers used atmospheric pressure for their common pressure. The tunnel side wall static pressure was sensed by a 5 psia transducer zeroed at vacuum. Atmospheric pressure was measured on a mercury column barometer and entered into the data system through the computer header board. Each time the Scanivalve made one complete scan, it would measure and record this common pressure as sensed by each Scanivalve pressure transducer. Simultaneously, the common pressure was compared with these Scanivalve pressures.

Optical Flow Visualization

Associated with the 4-ft wind tunnel facility is a 30-in. schlieren system. This system permits visual observation of the flow field about the wind-tunnel models, which can be viewed directly and simultaneously photographed. During the test, single-frame schlieren photographs, recorded on a 70-mm negative, were taken at rates of one or two per second. The Z-type Toepler schlieren system is comprised of four independent units, connected optically through the tunnel test section and a control panel. Development of a double-knife-edge schlieren technique permits visualization of flow field density gradients down to the 500 μHg static pressure regime.

Shock-Wave Shapes and Sonic Line Determination

The schlieren system was used for recording shock shapes and sonic line data. Measurements were made directly from the 70-mm negatives using an optical comparator incorporating a micrometer readout device on a film mounting table with two perpendicular directions of travel. The sonic line determination involved the introduction of weak shock disturbances ahead of the model bow shock wave. The shock generator is shown in fig. 9. The interaction of the impinging and bow shock waves results in a transmitted wave (assuming that the post-shock flow is supersonic) which terminates at the sonic line since a stationary shock wave cannot continue into the subsonic zone. This technique has been used previously in the transonic zone of blunt axisymmetric and two-dimensional bodies (refs. 19 and 20, respectively).

Figure 9. Shock Generator

EXPERIMENTAL RESULTS

Shock Layer Probe Data

The computer-controlled traversing probe device satisfactorily performed all programmed operations. Twenty stabilized pressure readings were taken during each tunnel run with actual probe position histories closely following pre-set schedules. The shock layer pressure profiles obtained can be categorized into three groups: (1) isentropic total pressure profiles recorded directly in the subsonic region, (2) isentropic total pressure profiles calculated on the basis of pitot and static pressures recorded in the supersonic region, and (3) pitot pressure profiles recorded in viscous-dominated regions of the flow. A summary and identification of the pressure plots is given in table I. It was found necessary to correct static pressure profiles near the body surface since erratic reading were typically obtained during the first 0.1 to 0.2 in. of probe travel. This probe interference correction was accomplished by fitting a smooth curve through the remainder of the data and the independently measured surface static pressure at the point in question, e.g., fig. 10.

For a Mach number of 4.468, the total pressure ratio across a normal shock wave, $p_t/p_{t_\infty}=0.0941$. At the forward probe position on both models (figs. 11 and 15) extrapolation of the pressure profile to the model surface for the zero angle of attack case recovers this value almost exactly. (The apparent data scatter in fig. 15 results from a greatly expanded pressure scale.) These "subsonic" runs are inherently the most accurate since no additional data processing is required. Note that the points corresponding to the probe lying on the surface ($N \cong 0.015$ in.) tend to reflect some degree of viscous dissipation indicated by a decrease in p_t in excess of the trend established by the remainder of the points.

Before proceeding to a discussion of the data, a further consistency check can be made to support the validity of the measured total pressure profiles. Following the procedure outlined in ref. 21, an exact inviscid relation was derived for the normal gradient of isentropic total pressure at the body surface for an axisymmetric configuration at zero angle of attack:

$$G = \left[\frac{\partial\left(p_t/p_{t_\infty}\right)}{\partial N}\right]_{\alpha = 0} = \left(\frac{\rho_B}{\rho_{t_\infty}}\right)\left(\frac{u_B}{V_{MAX}}\right)\left(\frac{r_B}{R_{s_o}^2}\right) F(M_\infty, \gamma)$$

$$F(M_\infty, \gamma) = \left(\frac{p_{t_B}}{p_{t_\infty}}\right) \frac{4\gamma(M_\infty^2 - 1)^2 \left[\frac{2}{(\gamma-1)M_\infty^2}\left(1 + \frac{\gamma-1}{2} M_\infty^2\right)^{\frac{\gamma+1}{\gamma-1}}\right]^{\frac{1}{2}}}{\left[2\gamma M_\infty^2 - (\gamma-1)\right]\left[(\gamma-1)M_\infty^2 + 2\right]}$$

where the subscript B denotes surface values of the noted flow properties and R_{s_o} is the shock radius of curvature at the axis. Under the assumption

TABLE I

SUMMARY AND IDENTIFICATION OF SHOCK LAYER PRESSURE PLOTS

MODEL	ANGLE OF ATTACK (DEG)	POSITION	FIGURE
E	0°	1	11
		2	12
		3	13
	20°	1	11
		2	12
		3	14
		4	–
		5	12
		6	13
A	0°	1	15
		2	16
		3	17
	15°	1	15
		2	16
		3	18
		4	15
		5	16
		6	17

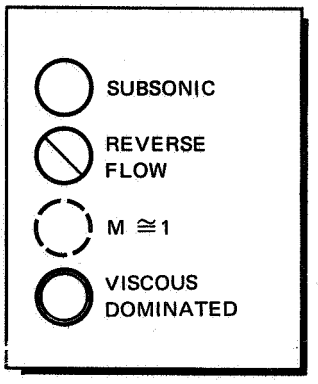

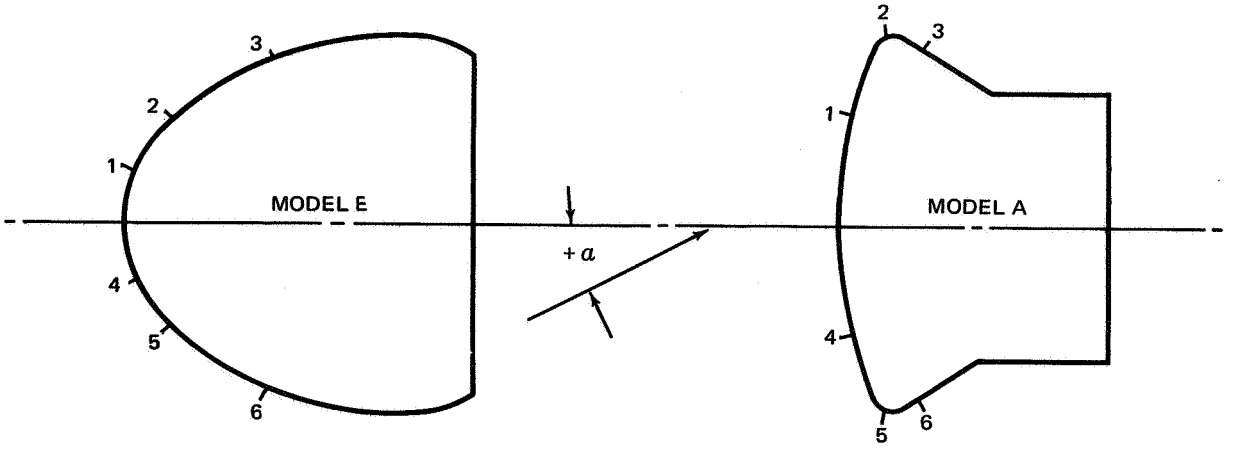

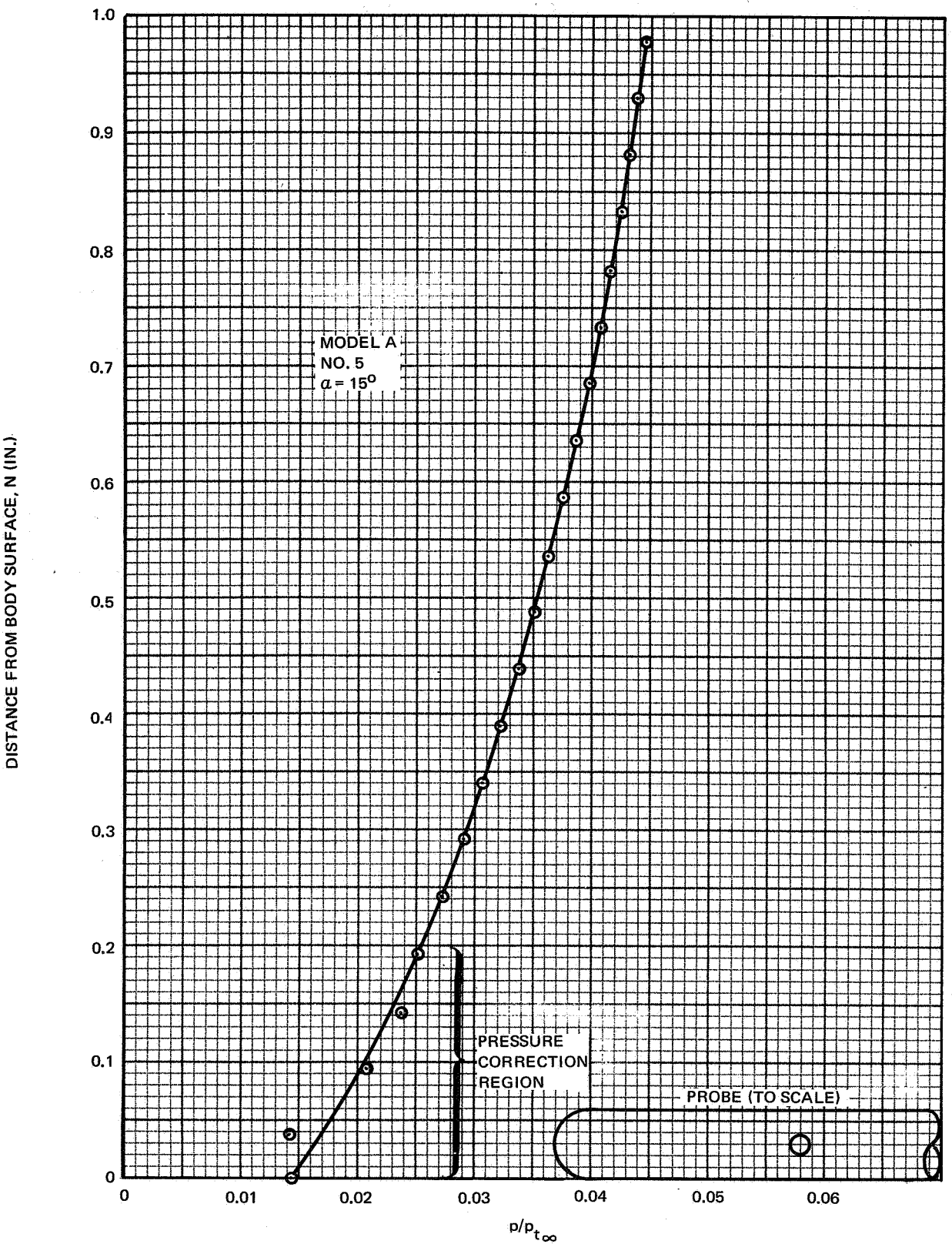

Figure 10. Representative Static Pressure Profile

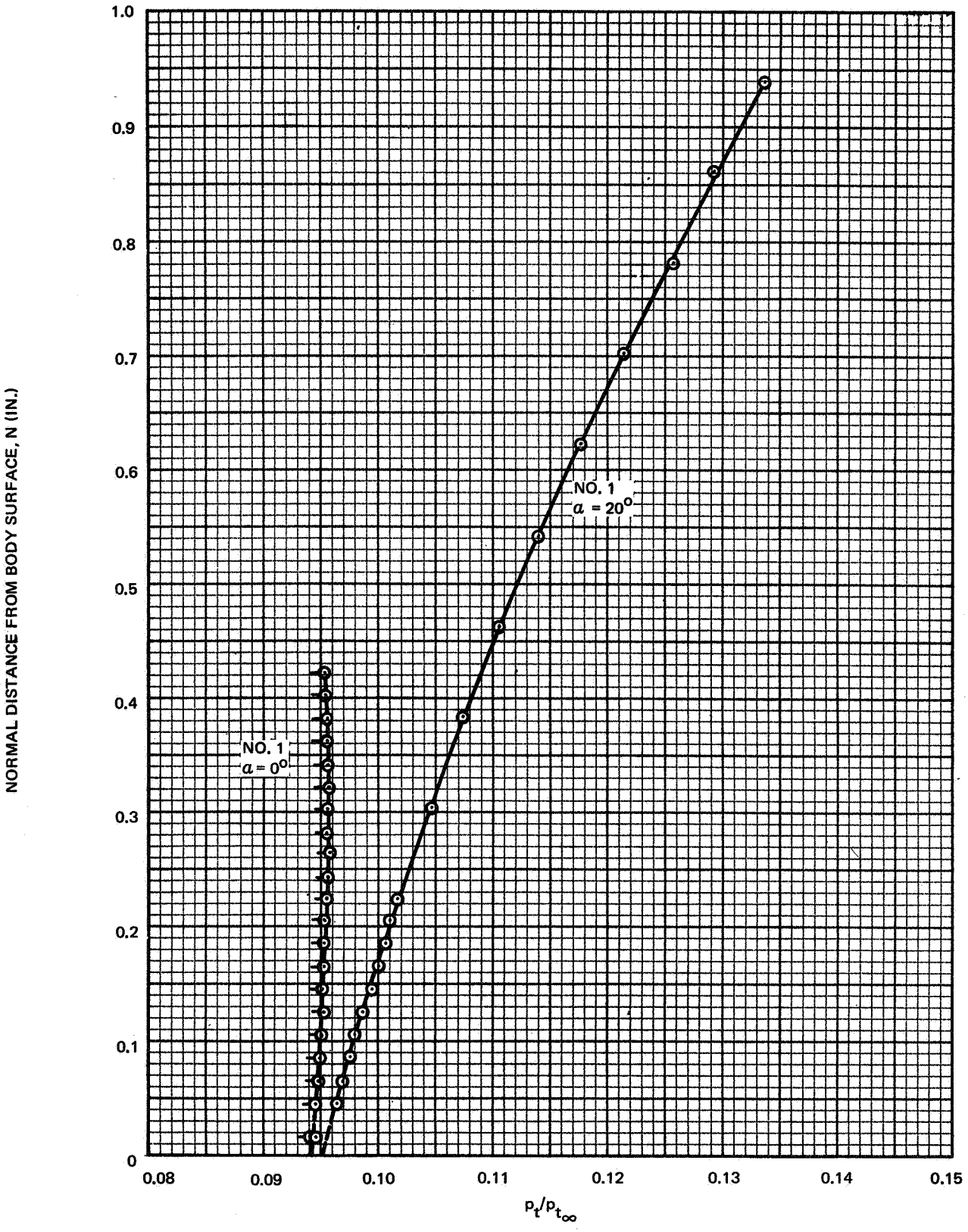

Figure 11. Shock Layer Total Pressure: Model E; Position 1; $\alpha = 0^{0}, 20^{0}$

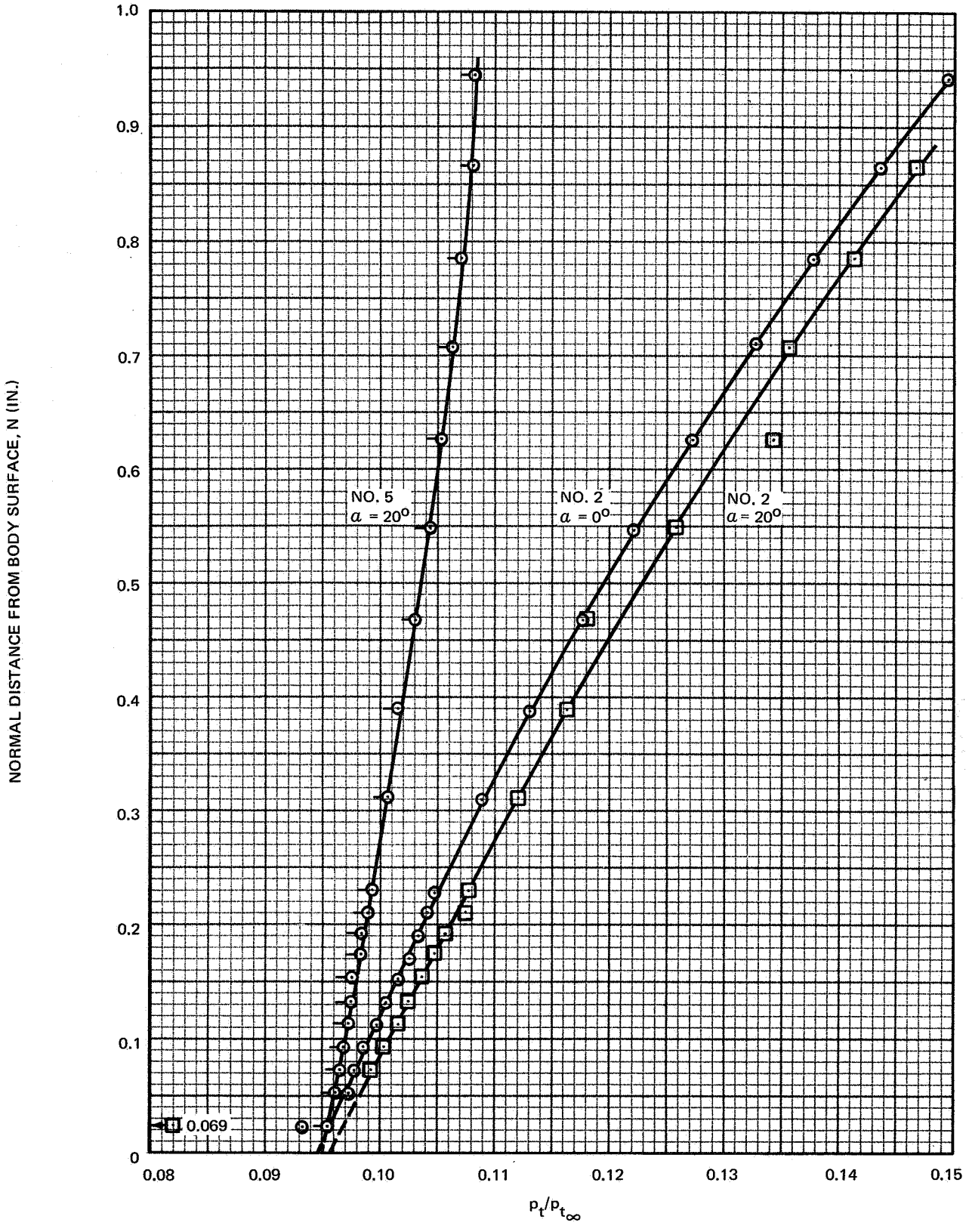

Figure 12. Shock Layer Total Pressure: Model E; Positions 2, 5; $\alpha = 0^o, 20^o$

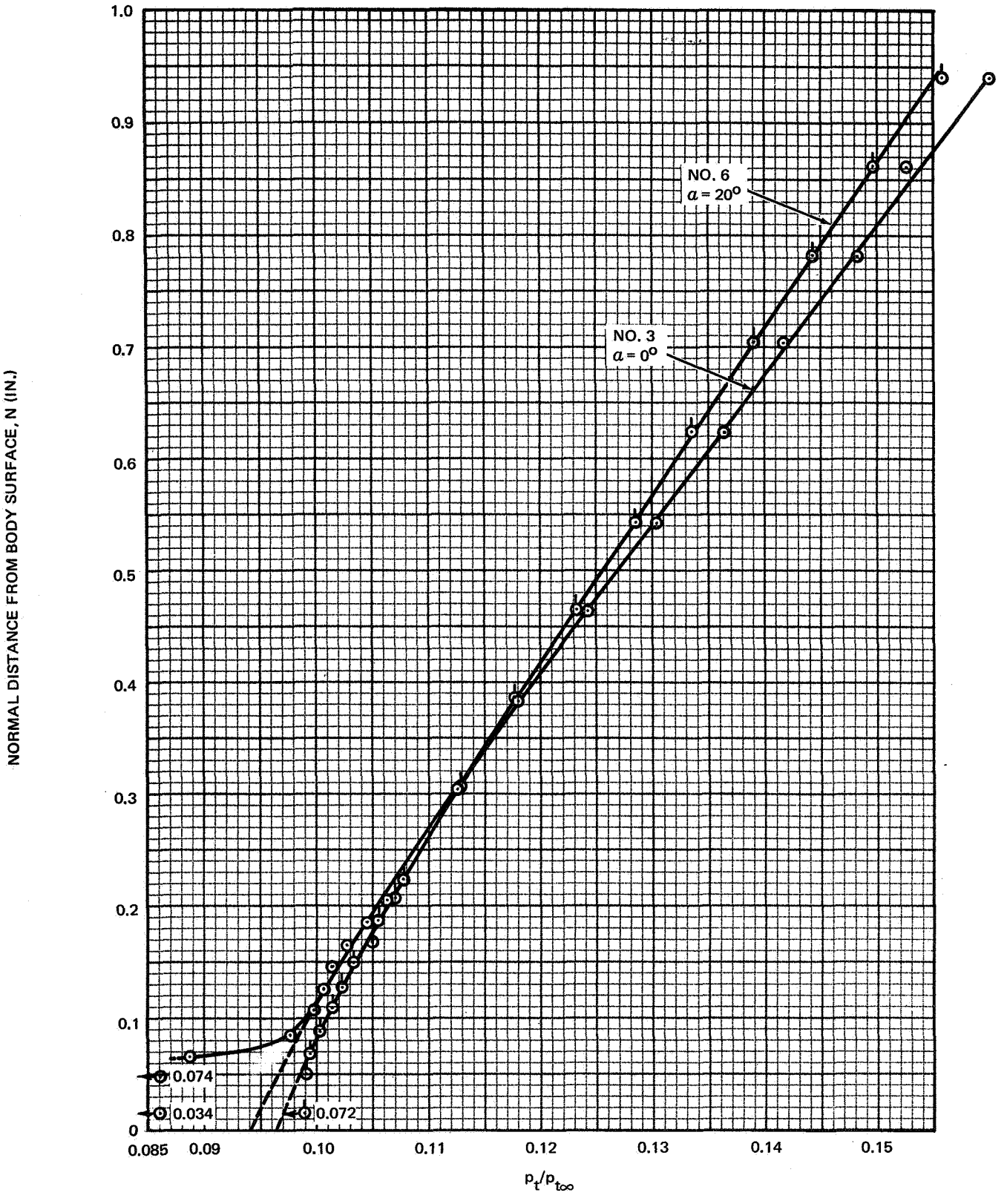

Figure 13. Shock Layer Total Pressure: Model E; Positions 3, 6; $a = 0^0, 20^0$

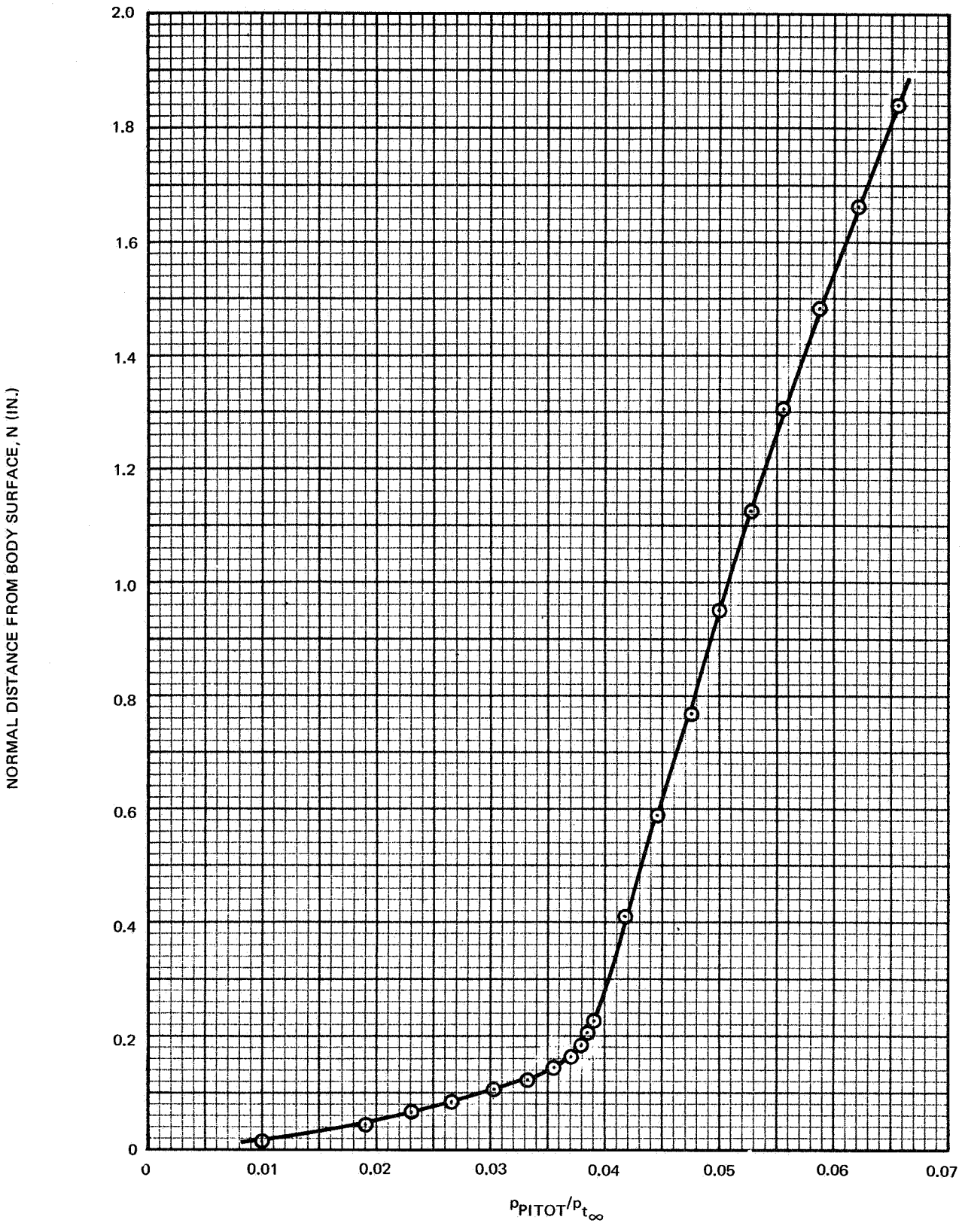

Figure 14. Shock Layer Pitot Pressure: Model E; Position 3; $\alpha = 20^0$

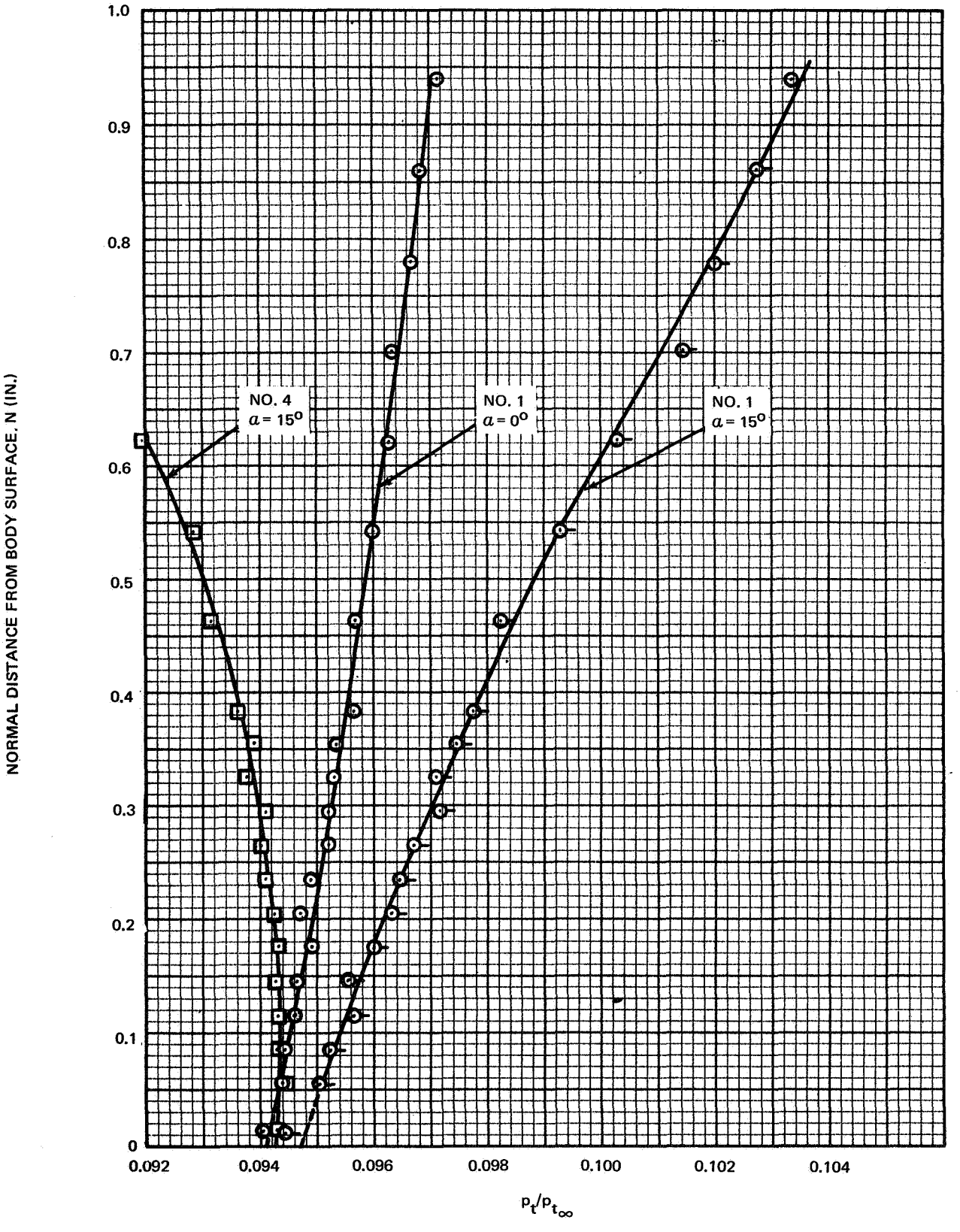

Figure 15. Shock Layer Total Pressure: Model A; Positions 1, 4; $\alpha = 0^0, 15^0$

of particle isentropic flow, experimentally determined values of surface static pressure and R_{s_o} (obtained from schlieren photographs) were used to evaluate the normal gradient at the three probe positions for both models. Measured and calculated slopes were in close agreement, except for the viscous dominated total pressure profiles. For example, a value of $G = 0.0413/\text{in.}$ was calculated for Model E, position 2 (using a measured shock radius of curvature, $R_{s_o} = 7.22$ in.), which coincided almost exactly with the initial slope of the total pressure curve established by the locus of experimental points near the body surface.

Restricting attention to Model E data, the surface total pressure at position 1, $\alpha = 20°$ (fig. 11) is approximately 1% higher than the symmetric flow value. Fig. 12 is particularly interesting since a slightly shifted 1% differential is maintained at the body surface between the $\alpha = 0°$ and 20° curves corresponding to position 2, while the windward, position 5 curve approaches the zero total pressure value and, in principle, could reverse direction near the body ($N < 0.04$ in.) and meet the leeward curve. Although this interpretation of the data is speculative, the implied direction of the maximum entropy streamline displacement, i.e., windward, would agree with the results of refs. 3 and 6.

The most rearward probe location on Model E showed pronounced viscous effects as evidenced by the off-scale points noted on fig. 13 and the pitot pressure plot (fig. 14). The latter curve was left in unreduced form owing to the difficulty in obtaining accurate static pressure data at this most leeward ($\alpha = 20°$) position. Comparing extrapolated surface total pressure values on fig. 13, the trend towards higher p_t values at angle of attack is again noted.

Considering Model A data, fig. 15 (subsonic location) shows a 0.6% increase in surface p_t at $\alpha = 15°$, position 1, over the $\alpha = 0°$ value. The windward position, 4, in this case is just downstream of the stagnation point implying significant probe misalignment with respect to the local flow direction as the distance from the surface is increased. Unfortunately the remaining probe plots, figs. 16, 17 and 18, are inconclusive owing to strong inviscid flow gradients in the neighborhood of the rounded corner of the body, the possible presence of a lip shock, and the separated viscous shear flow at positions 3 and 6. The inclusion of the pitot pressure plots may prove useful to investigators concerned with viscous flow behavior downstream of a rapid, continuous expansion region.

Surface Pressures

The surface pressure distributions shown in figs. 19 and 20 were obtained in a sequence of tunnel runs during which the roll or meridianal angle, ϕ, was varied from 0° to 180° in 30° increments ($\phi = 0°$ corresponds to the windward plane of symmetry at positive angle of attack). A misalignment in the model

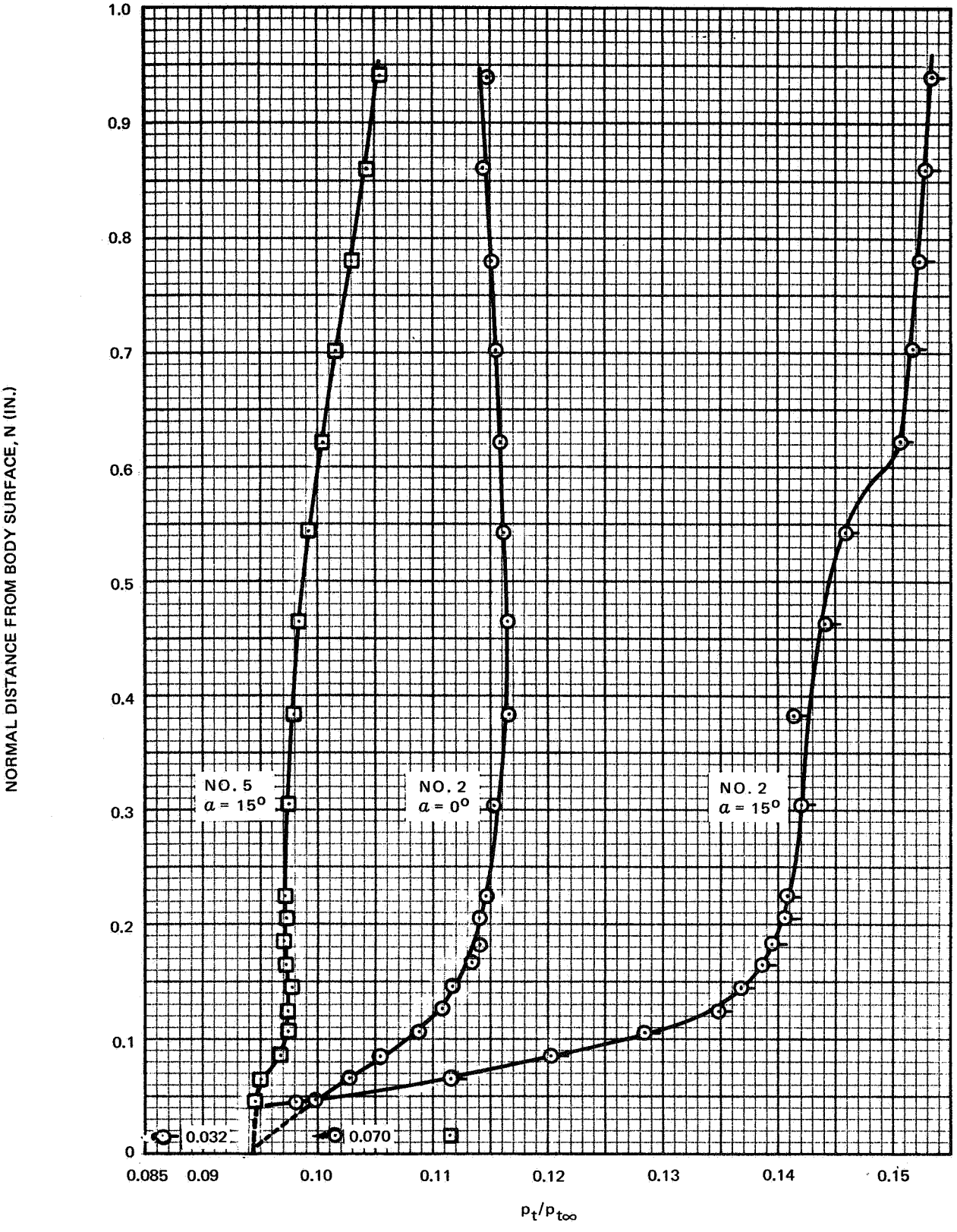

Figure 16. Shock Layer Total Pressure: Model A; Positions 2, 5; $\alpha = 0^0, 15^0$

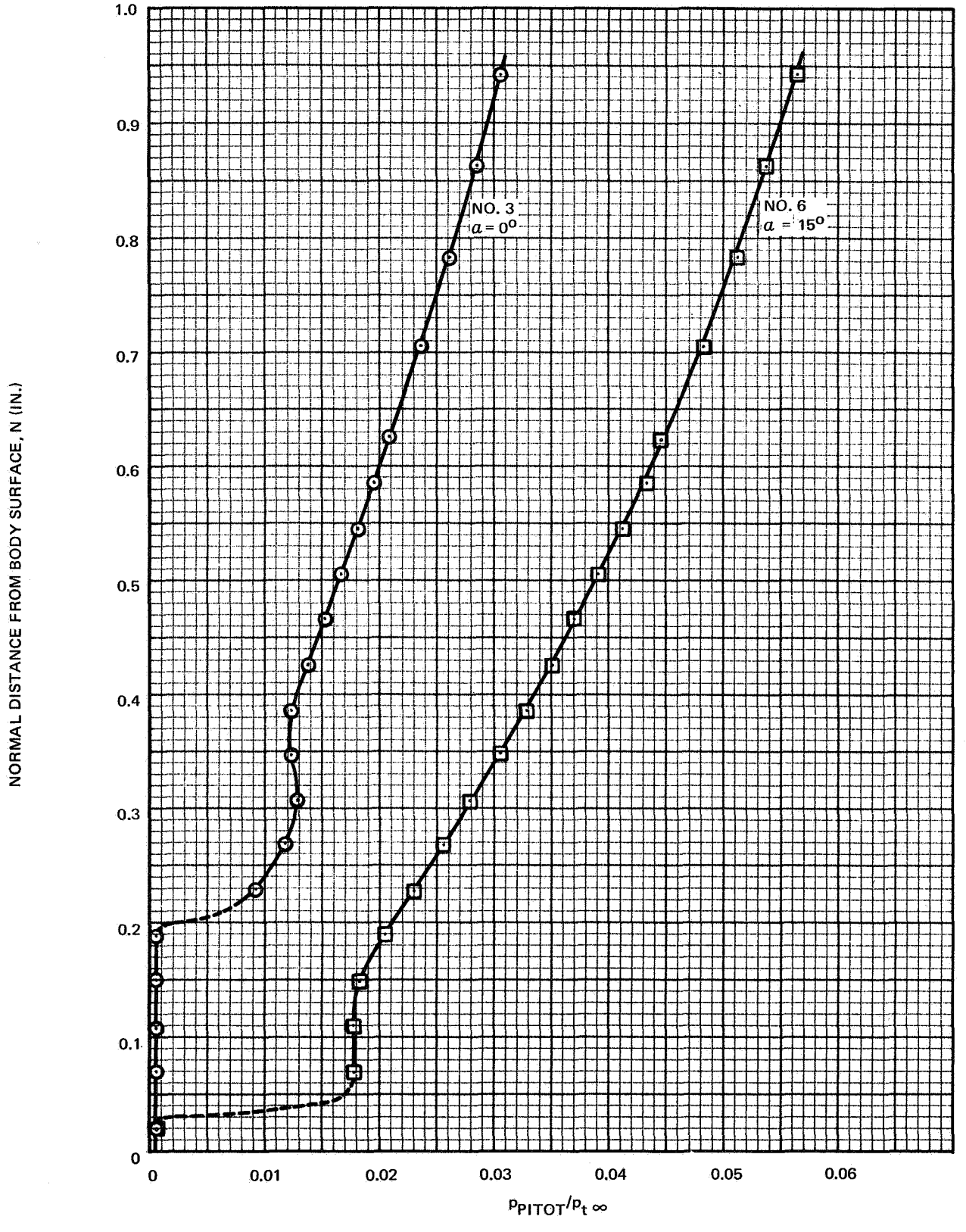

Figure 17. Shock Layer Pitot Pressure: Model A. Positions 3, 6; $\alpha = 0^o, 15^o$

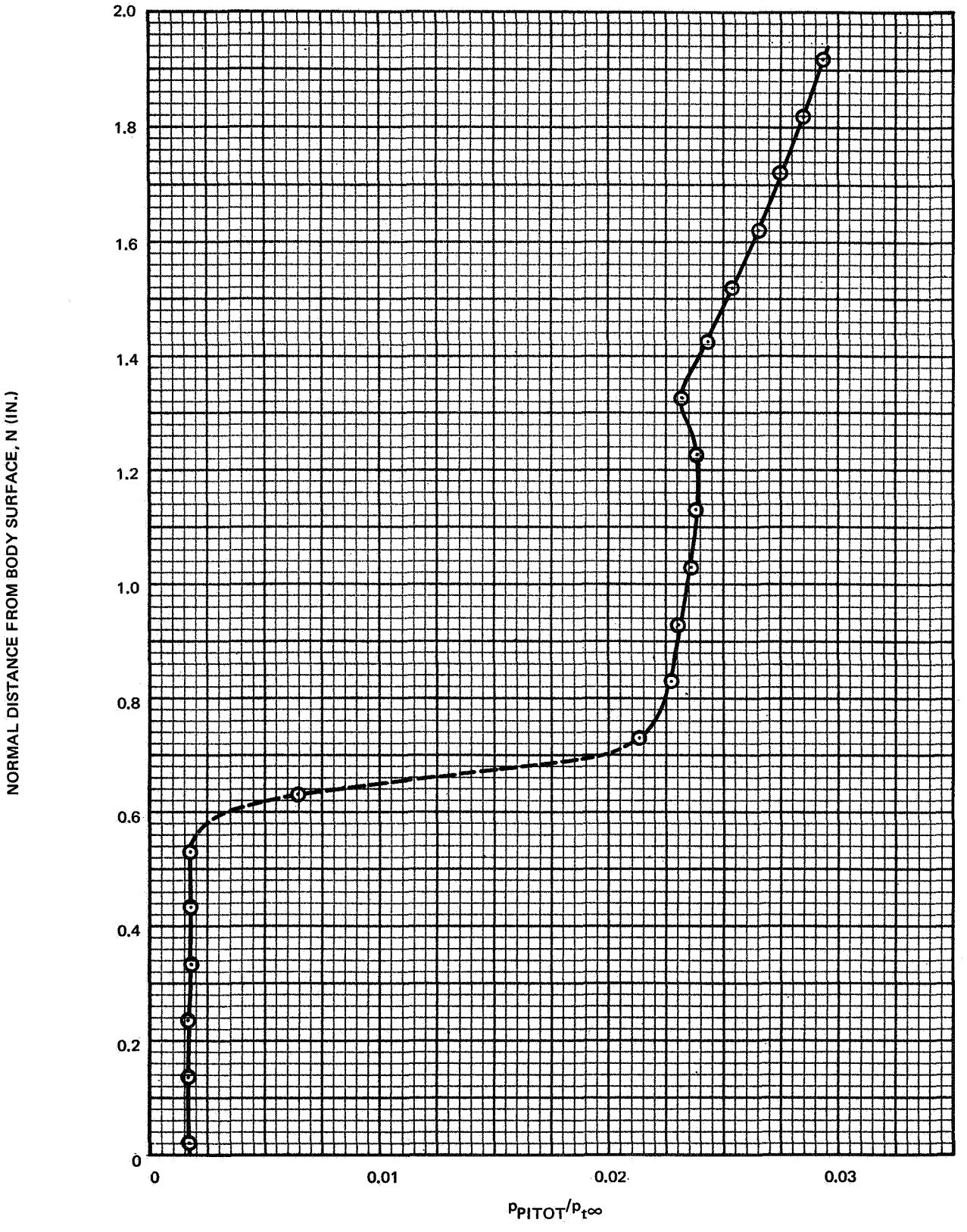

Figure 18. Shock Layer Pitot Pressure: Model A; Position 3; $\alpha = 15^0$

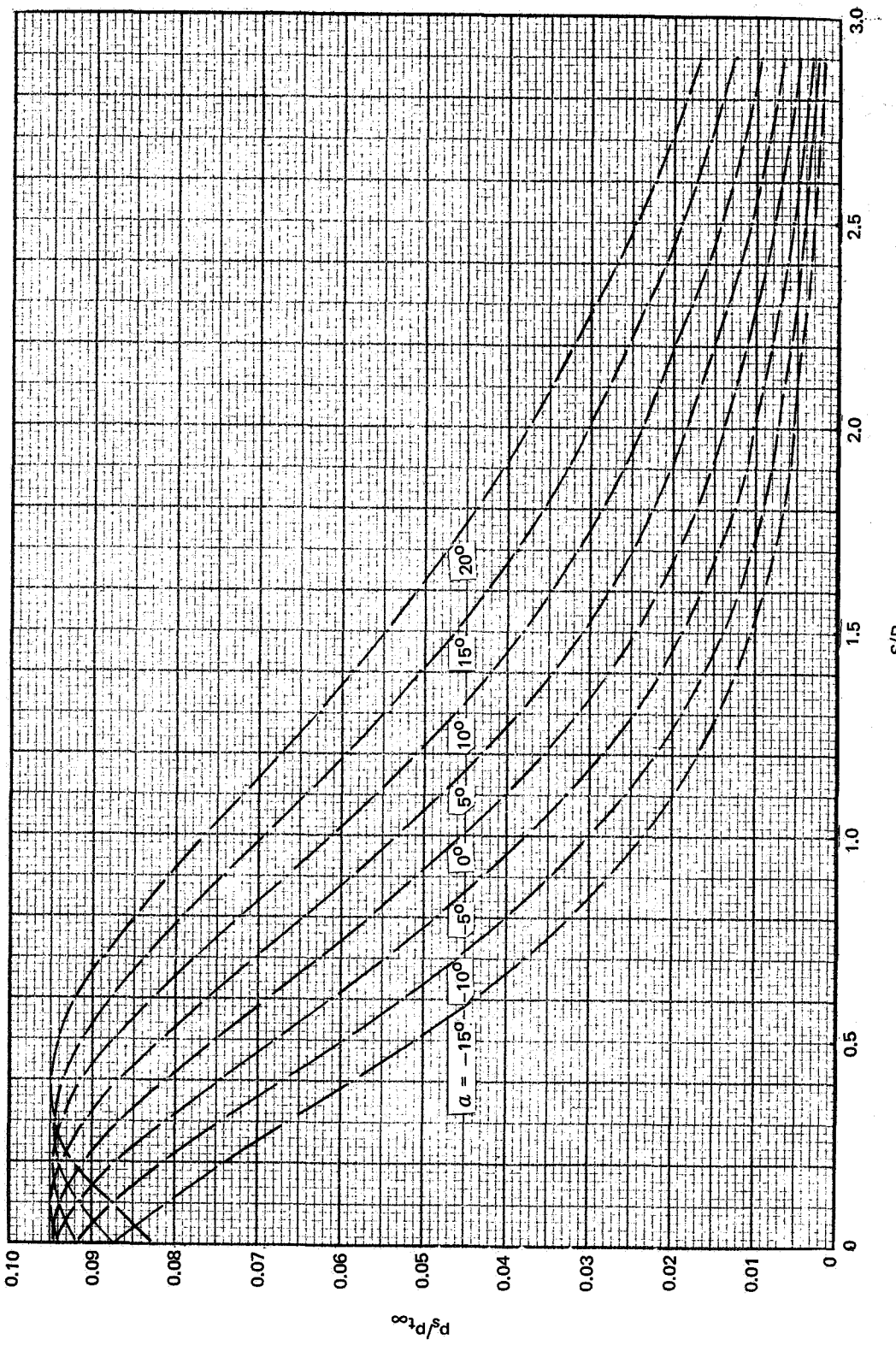

Figure 19. Surface Pressure Distributions: Model E; $\varphi = 0^\circ$ (Page 1 of 7)

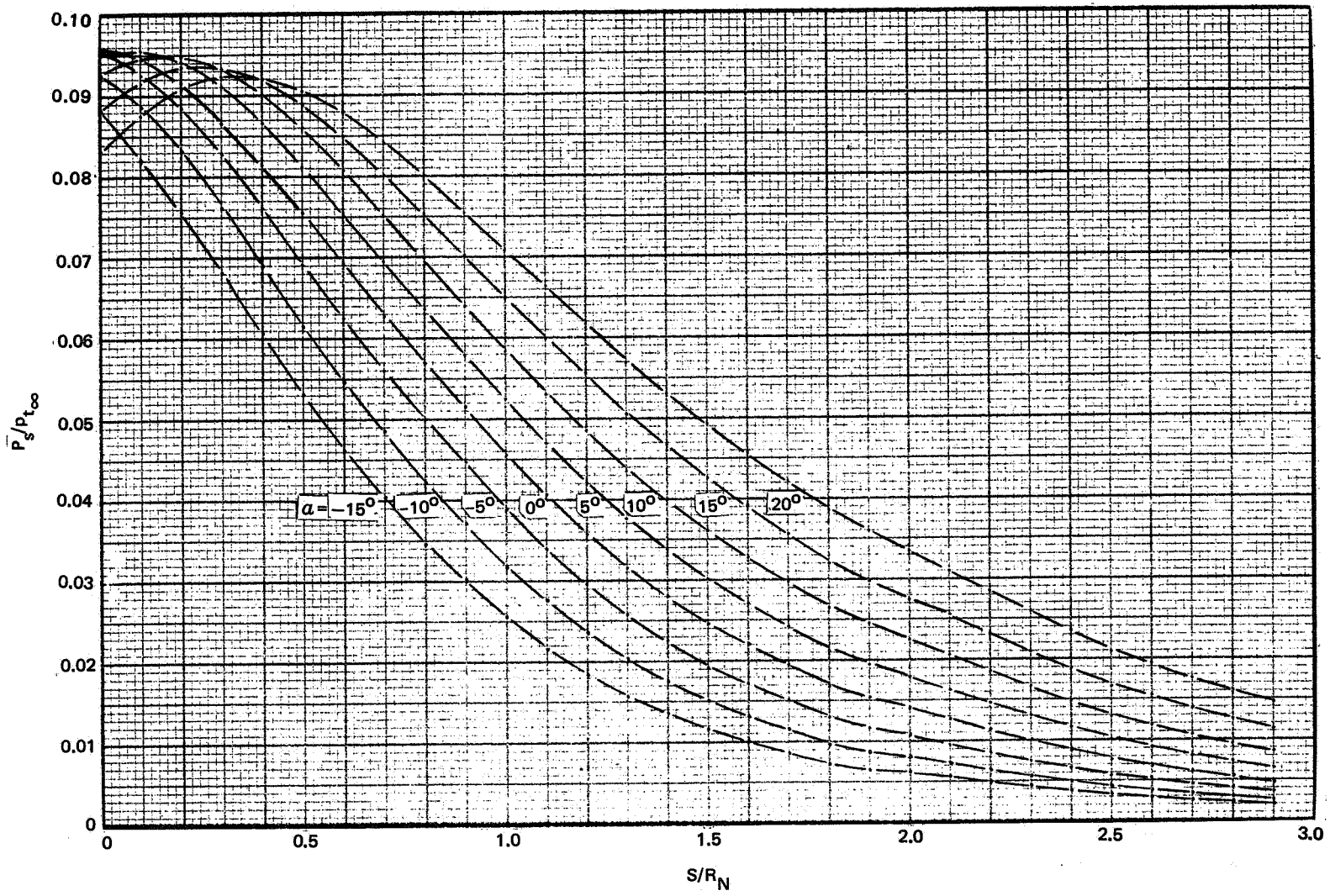

Figure 19. Surface Pressure Distributions: Model E; $\varphi = 30^0$ (Page 2 of 7)

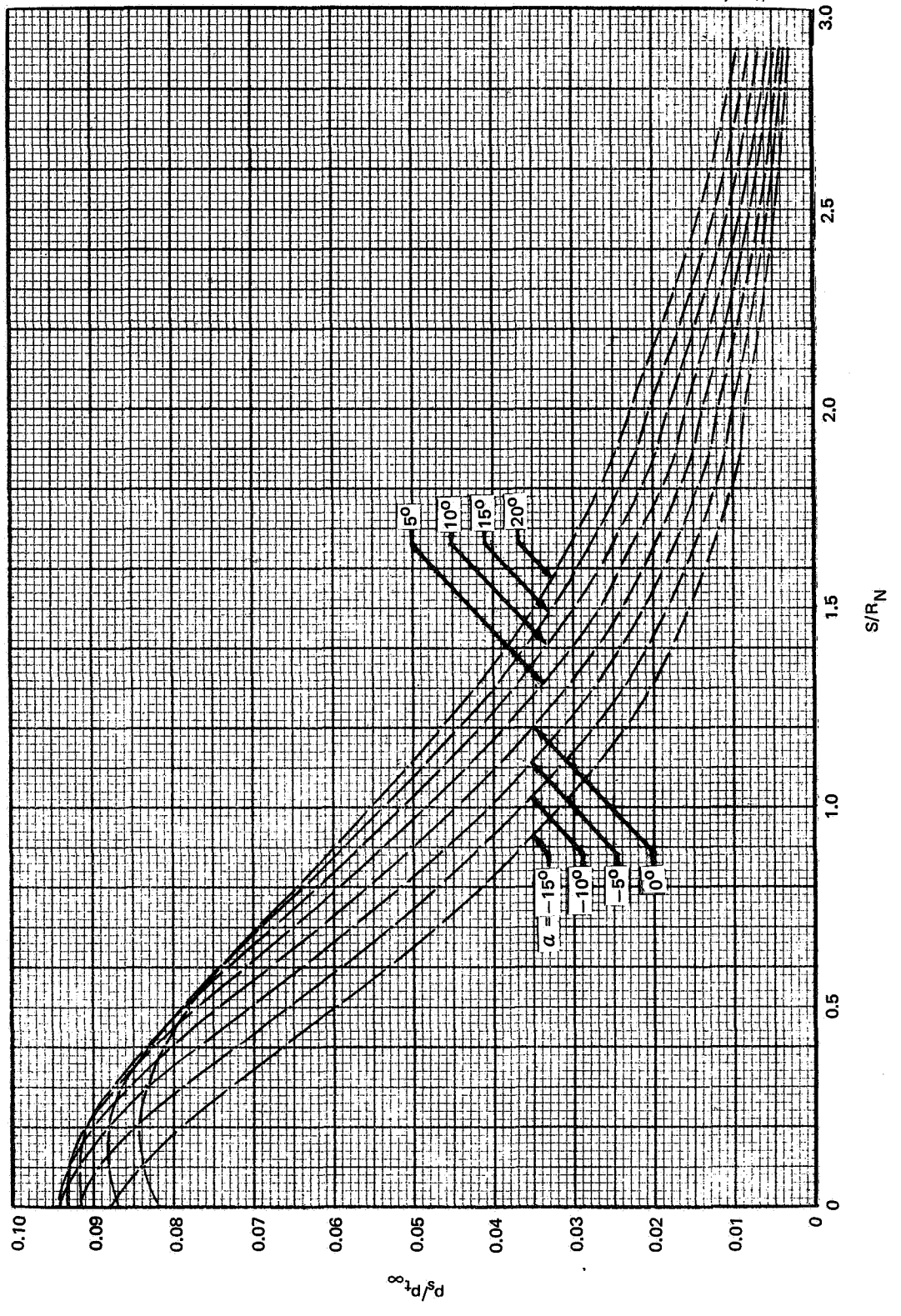

Figure 19. Surface Pressure Distributions: Model E; $\varphi = 60^o$ (Page 3 of 7)

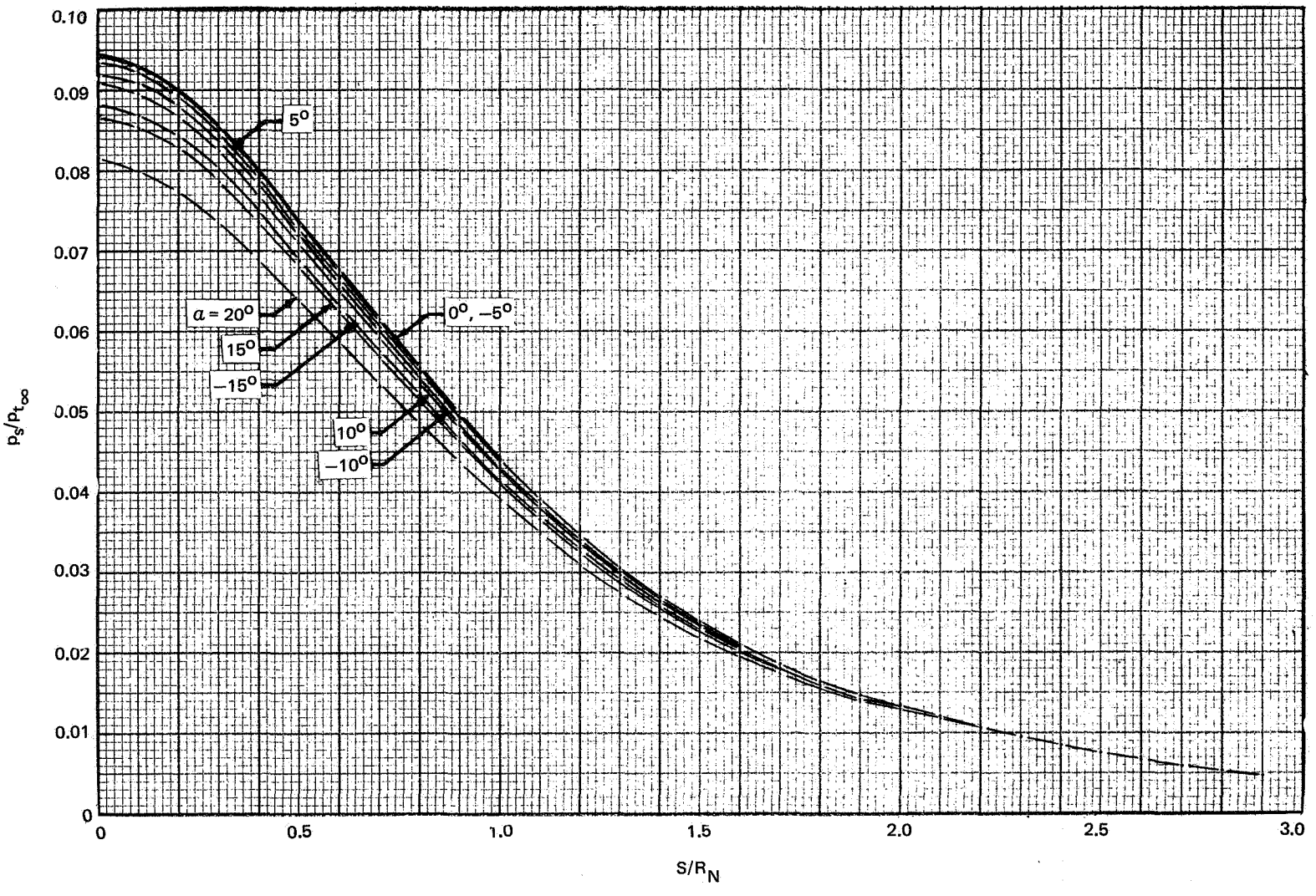

Figure 19. Surface Pressure Distributions: Model E; $\varphi = 90^0$ (Page 4 of 7)

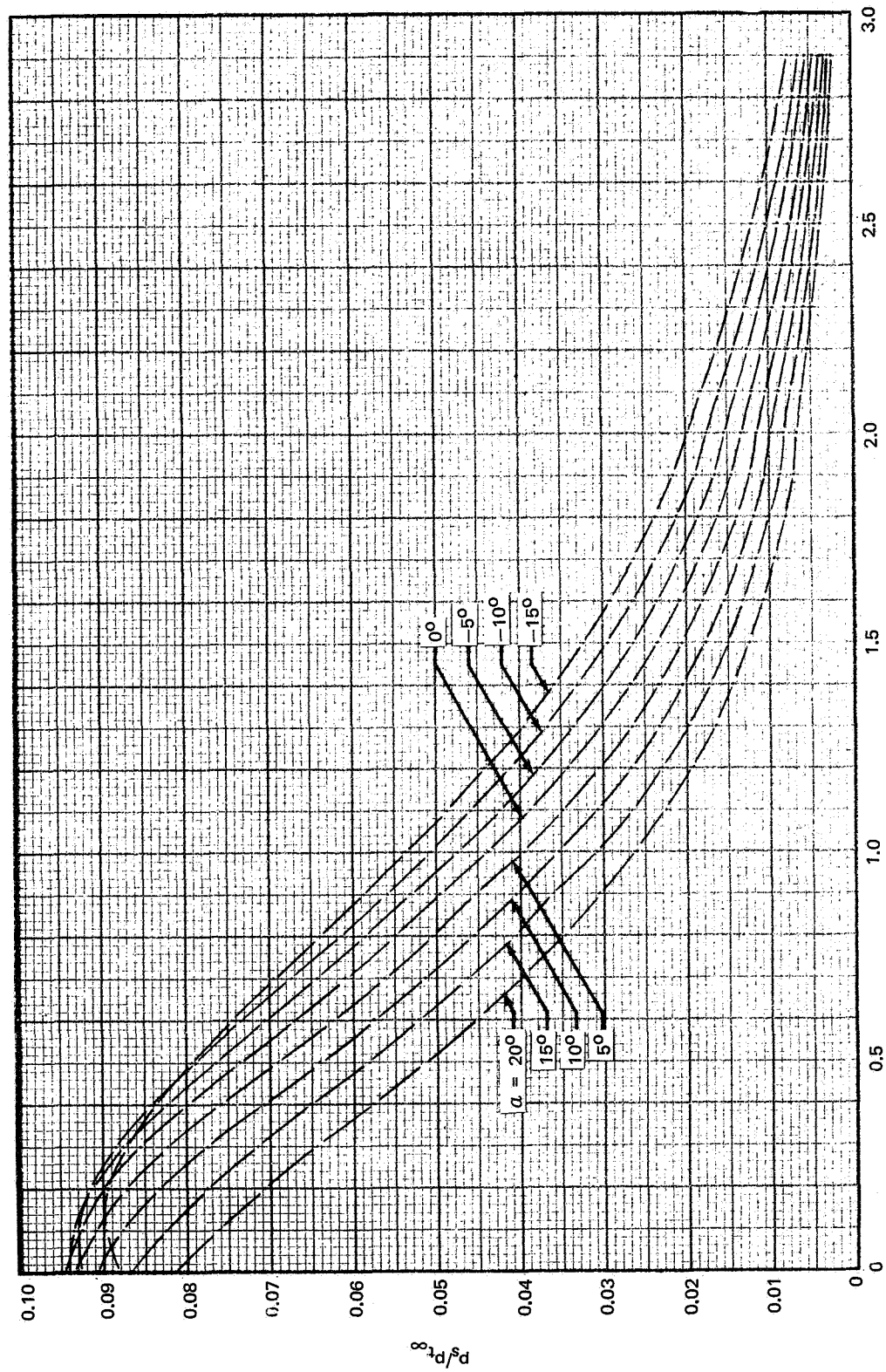

Figure 19. Surface Pressure Distributions: Model E; φ = 120° (Page 5 of 7)

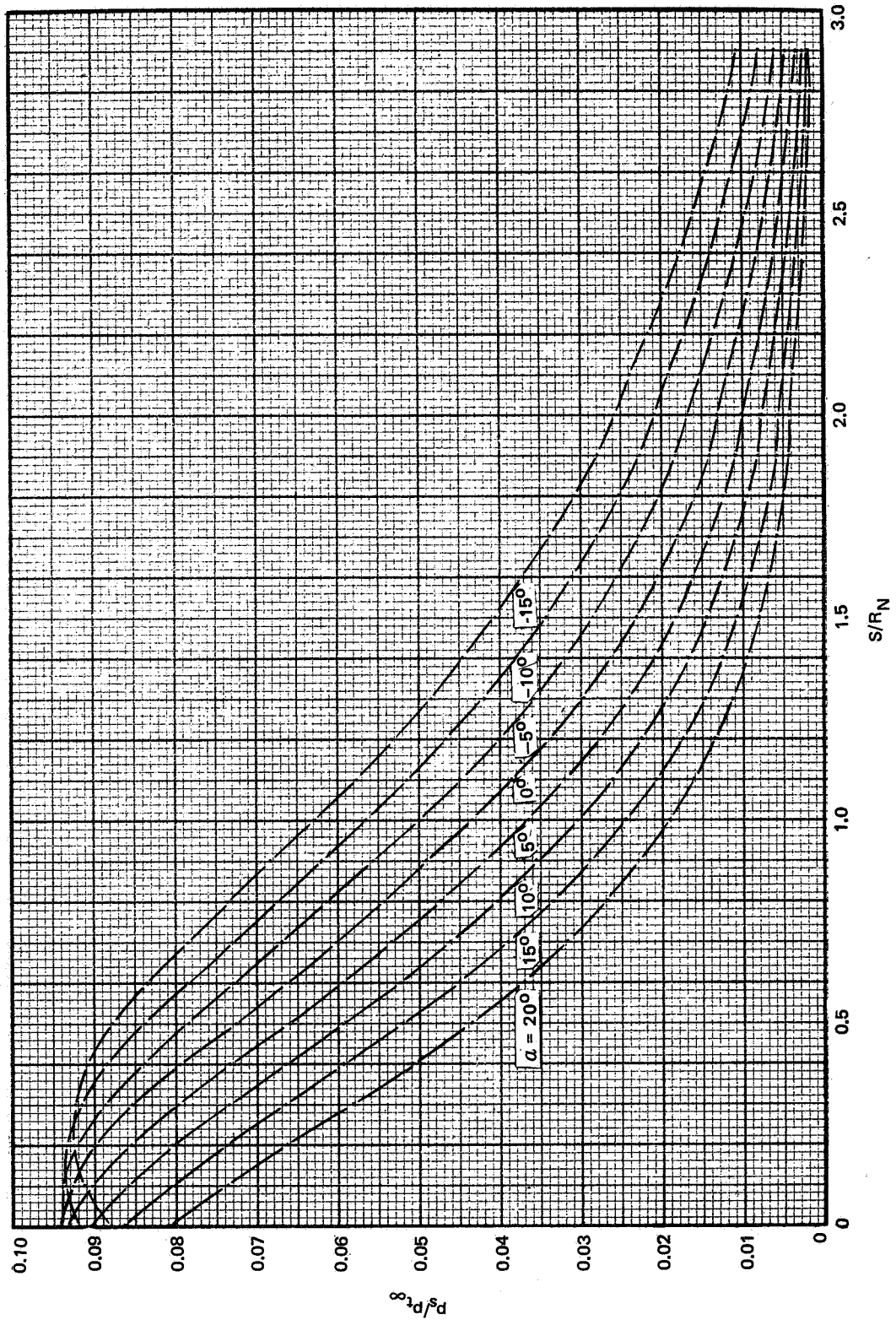

Figure 19. Surface Pressure Distributions: Model E; $\varphi = 150^0$ (Page 6 of 7)

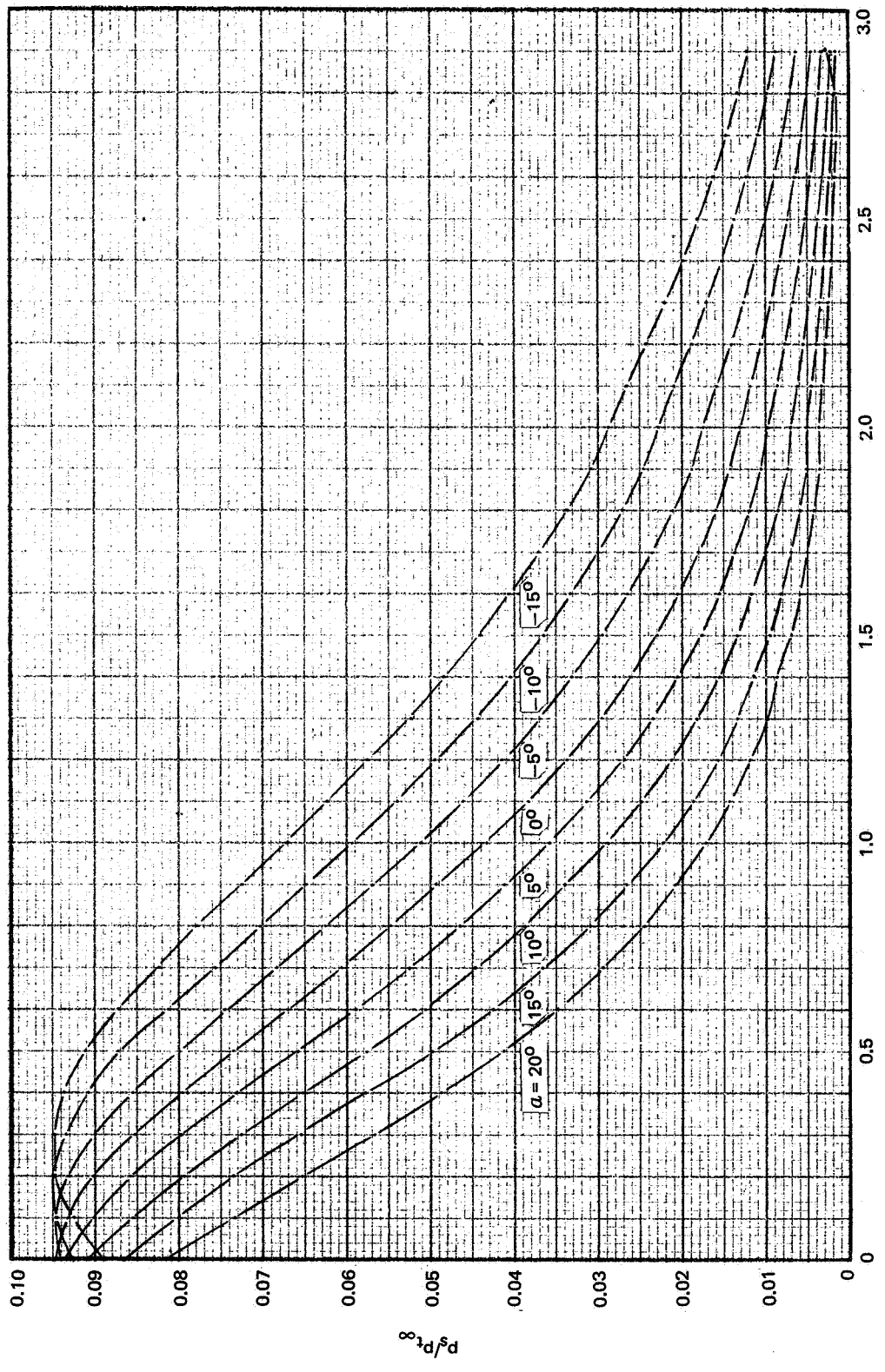

Figure 19. Surface Pressure Distributions: Model E; $\varphi = 180^0$ (Page 7 of 7)

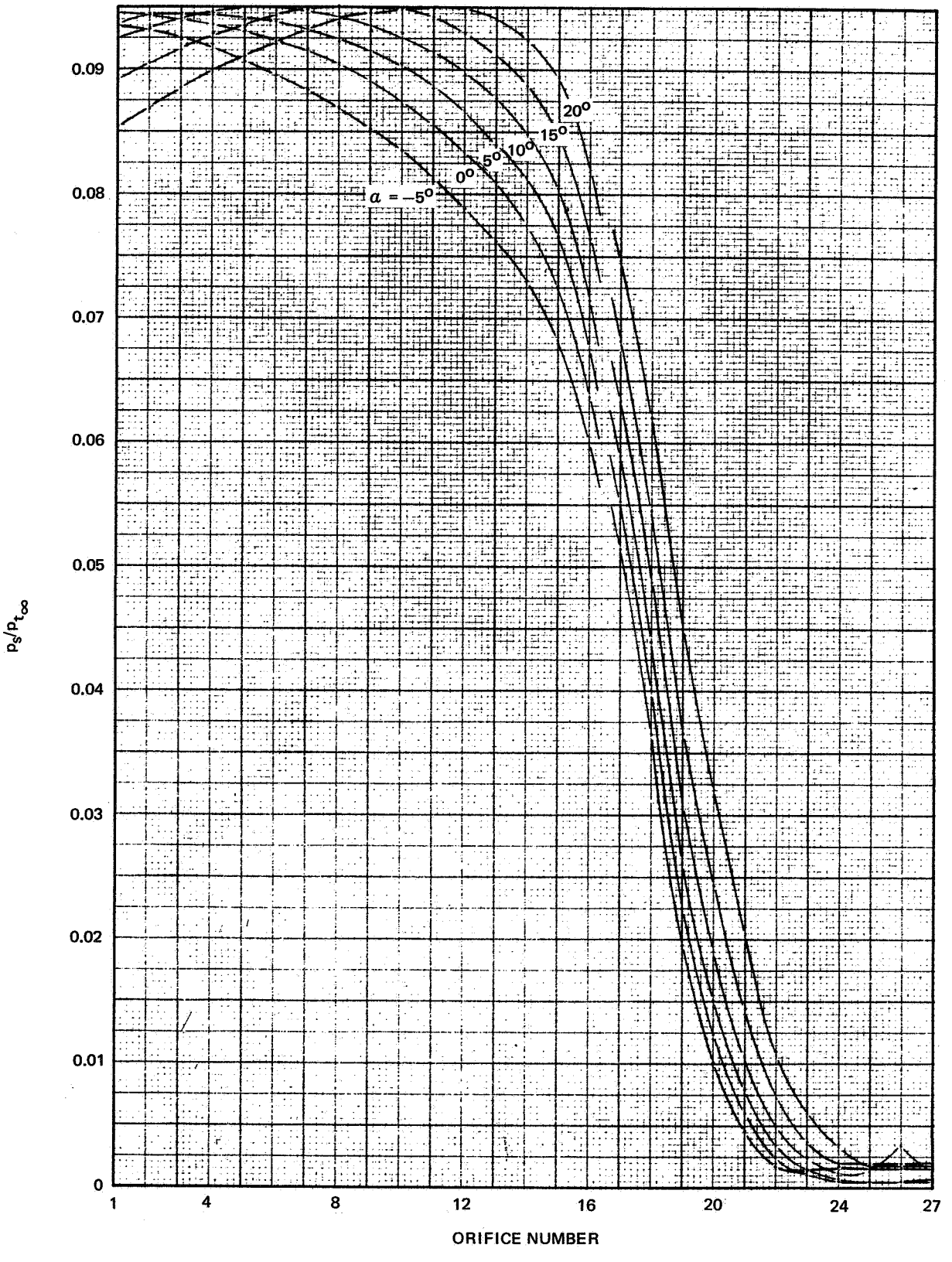

Figure 20. Surface Pressure Distributions: Model A; $\varphi = 0^0$ (Page 1 of 7)

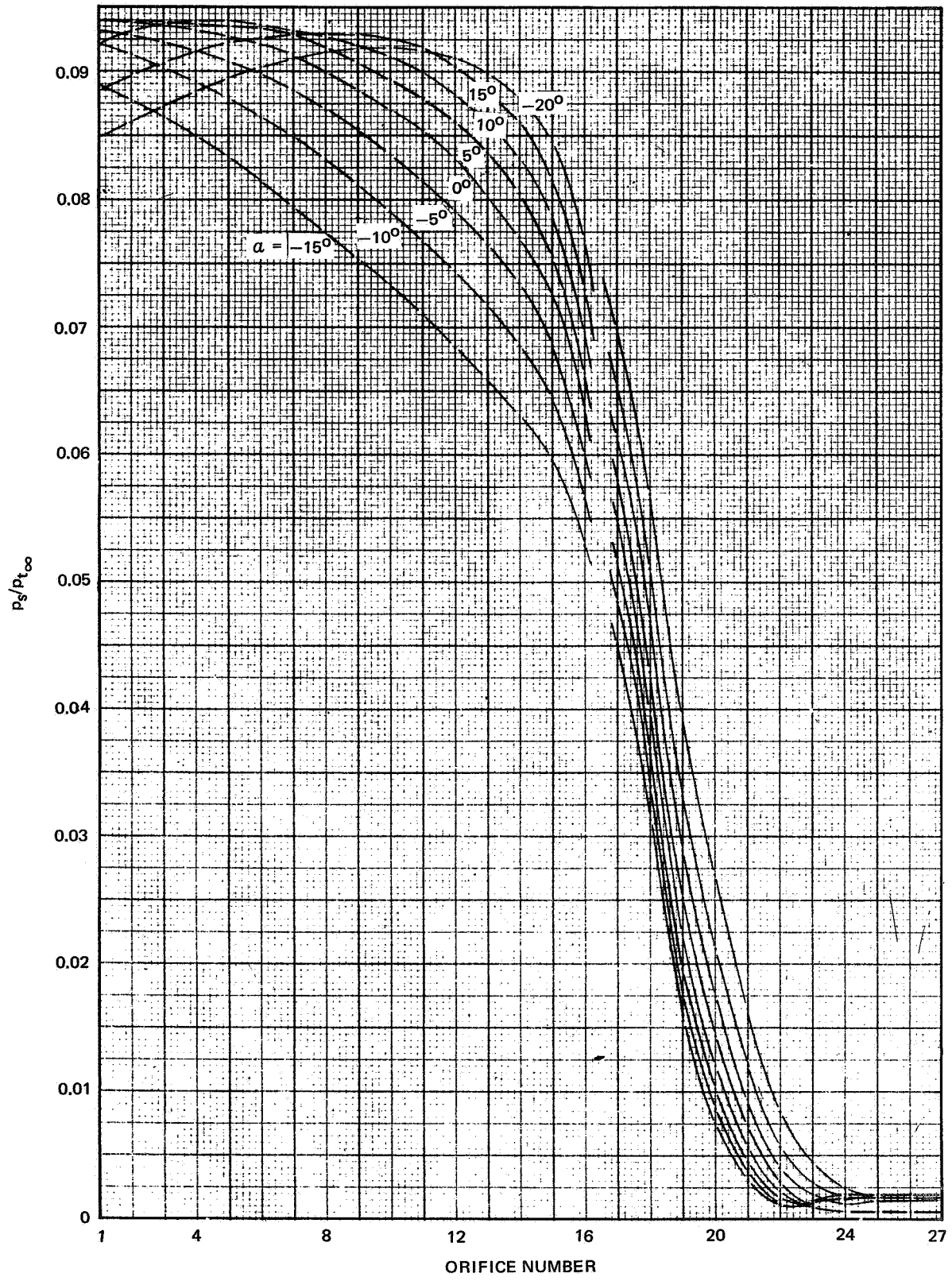

Figure 20. Surface Pressure Distributions: Model A; $\varphi = 30^0$ (Page 2 of 7)

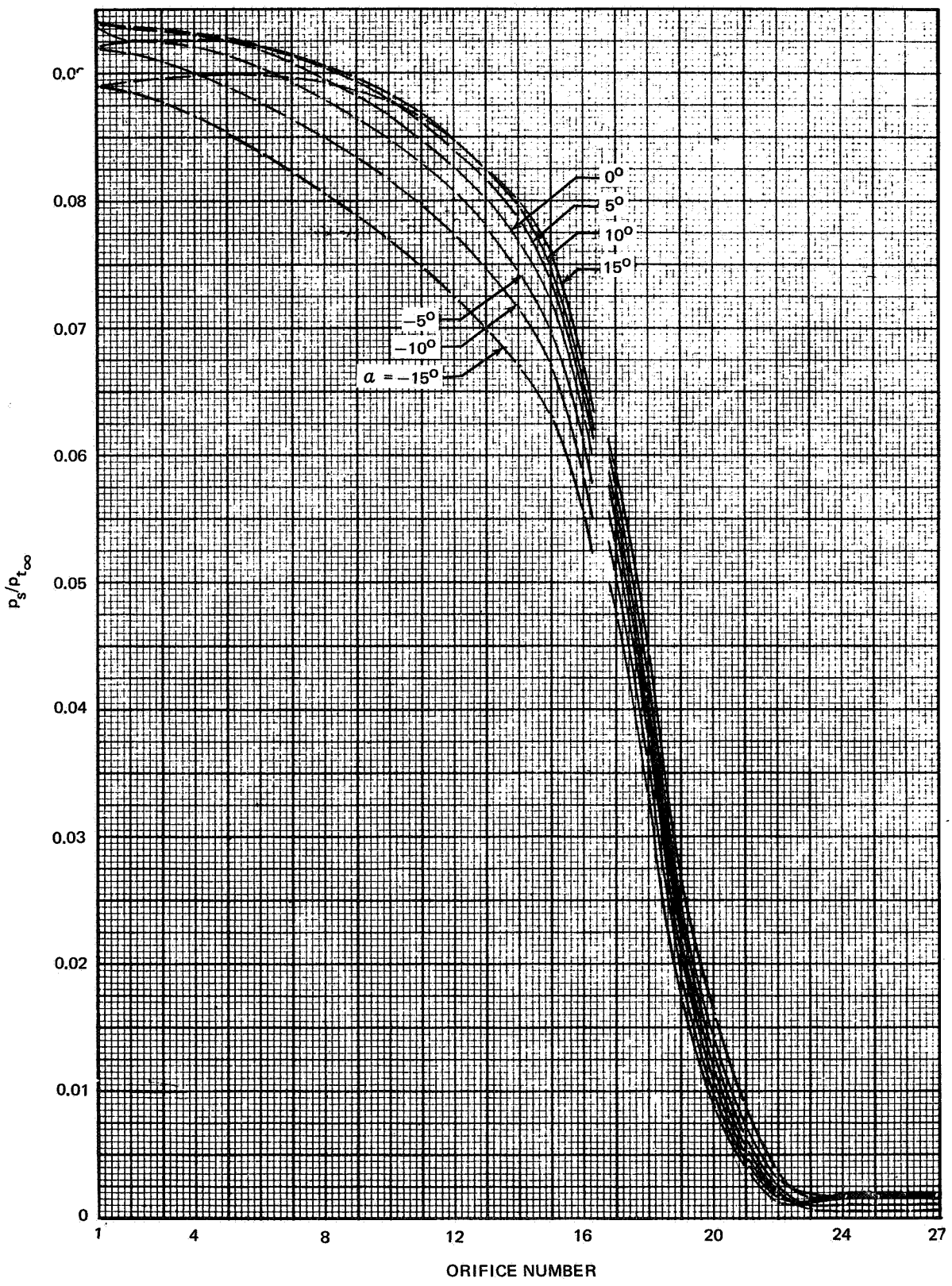

Figure 20. Surface Pressure Distribution: Model A; $\varphi = 60^0$ (Page 3 of 7)

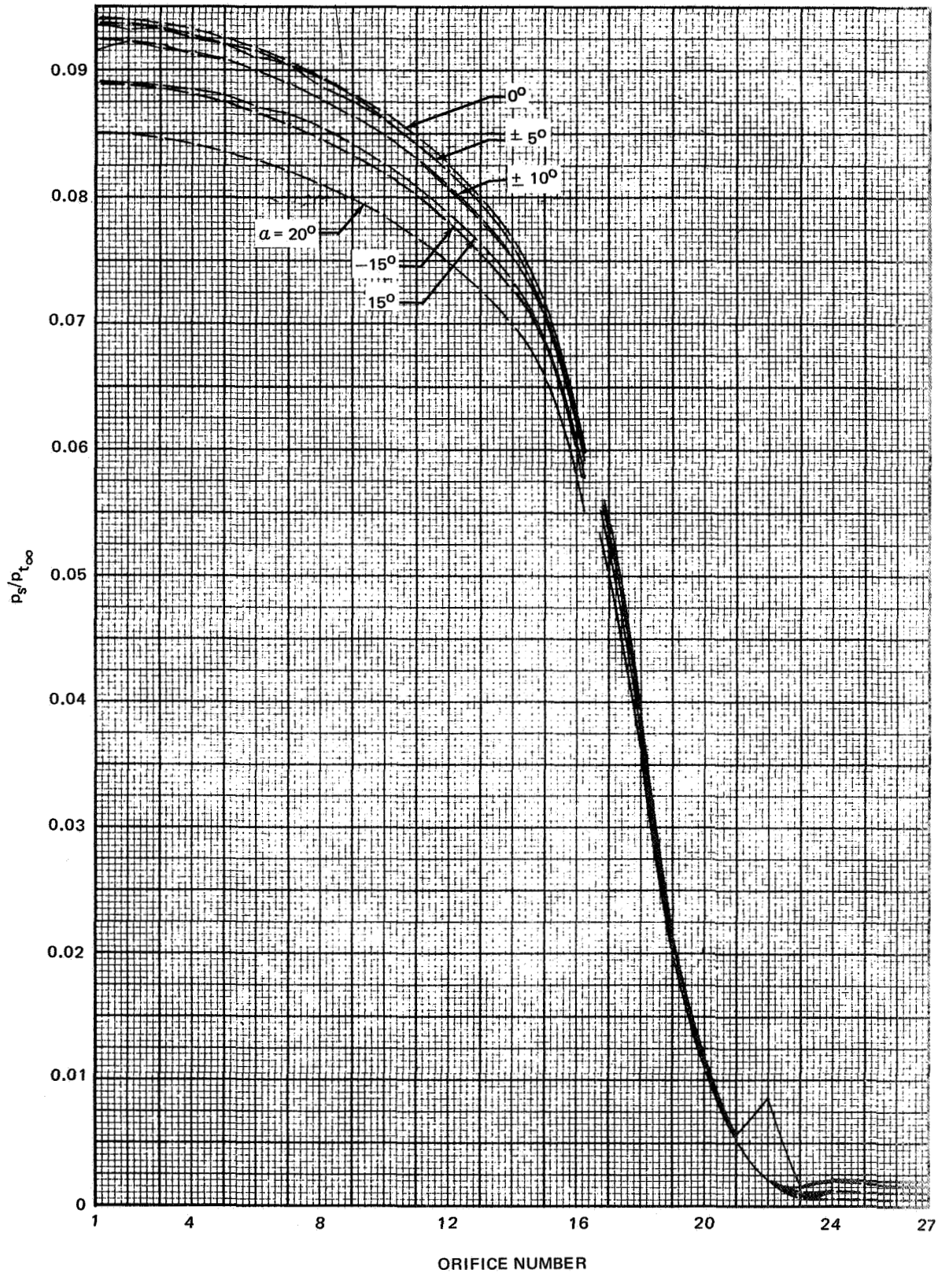

Figure 20. Surface Pressure Distributions: Model A; $\varphi = 90^0$ (Page 4 of 7)

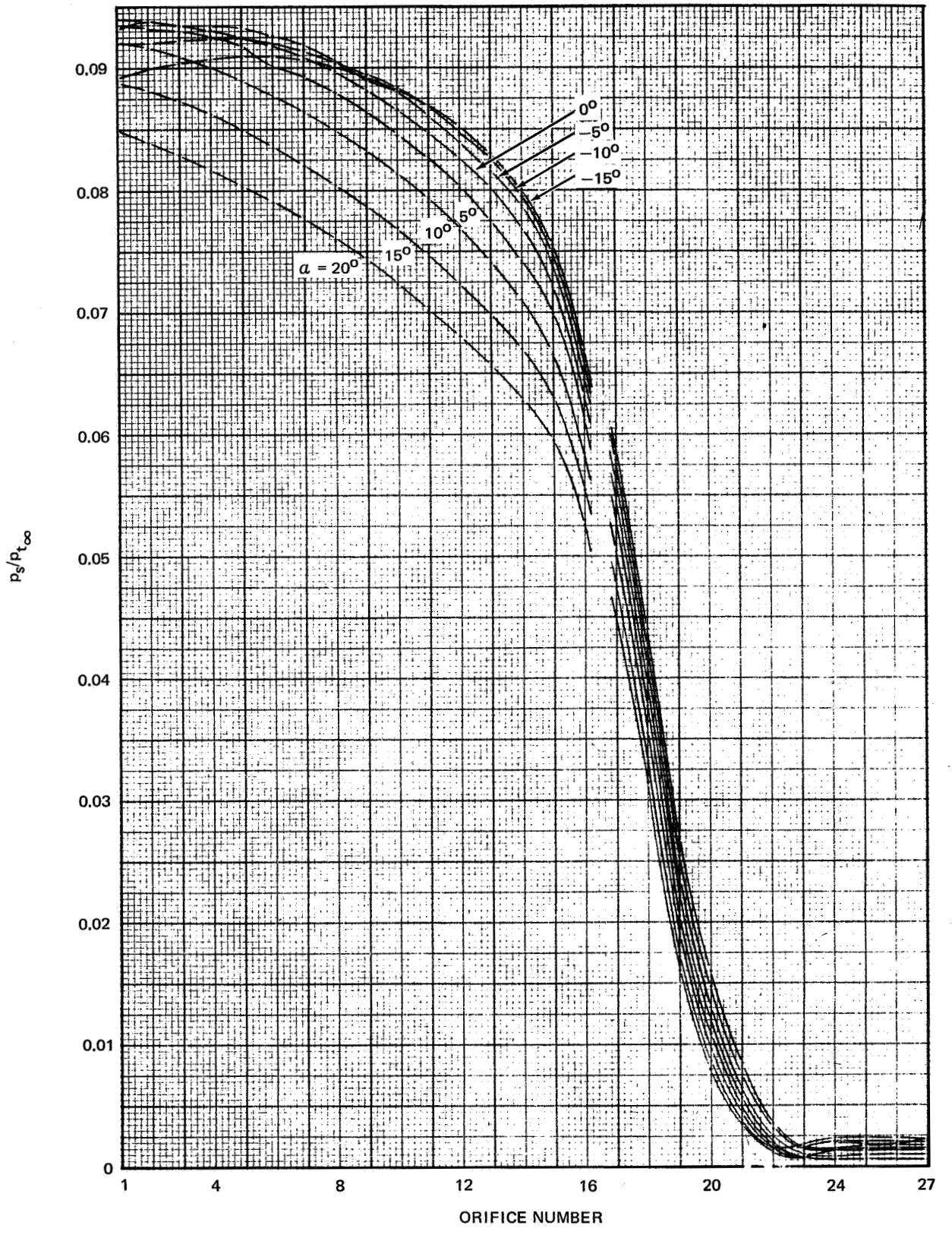

Figure 20. Surface Pressure Distributions: Model A; φ = 120° (Page 5 of 7)

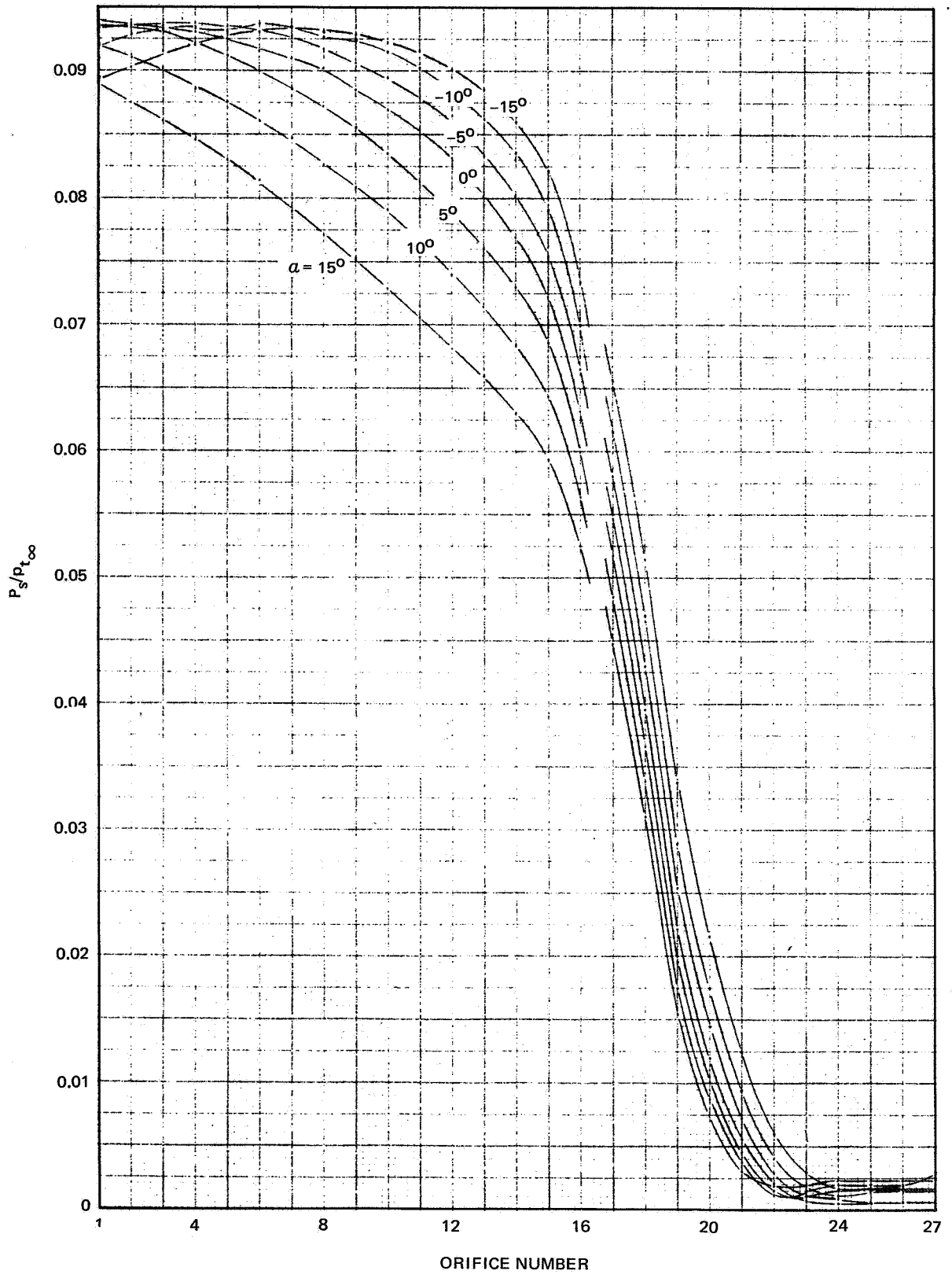

Figure 20. Surface Pressure Distributions: Model A; φ = 150° (Page 6 of 7)

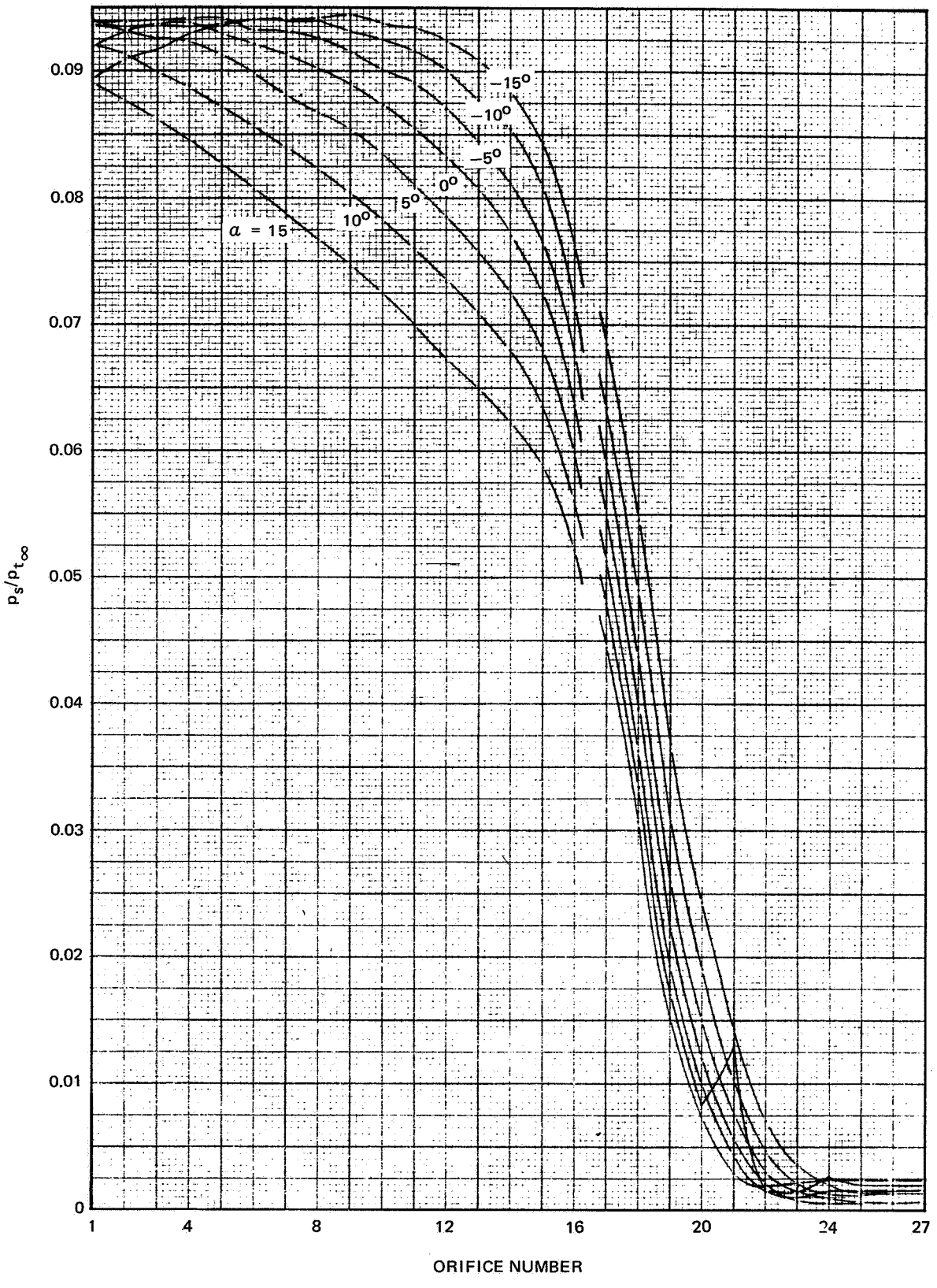

Figure 20. Surface Pressure Distributions: Model A; $\varphi = 180^0$ (Page 7 of 7)

support system was discovered during the runs which resulted in deviations from the nominal angles of attack noted on the figures. Table II presents corrected angles of attack for each tunnel run. Unfortunately, this small variation in α prevented overlapping of otherwise common data points obtained at positive and negative angles of attack. No correction was made for sting deflection due to model loads (deflection factor $\cong$ 0.00054°/lb normal load). In general the pressure data shows a reasonably smooth variation with both roll angle and angle of attack. Tabulated results are presented in appendix A for both models. All pressure readings for Model E stabilized within the allotted time increment while some fluctuations (denoted by a symbol, #, appearing next to the tabular value) were noted for Model A. The fluctuations at $\alpha = 20°$ are possibly due to a tunnel ceiling interference effect. As a result, the maximum angle of attack used during the Model A probe runs was limited to 15°.

The pressure distributions for Model A were plotted versus orifice number rather than normalized distance along the body surface in order to spread the family of curves in the rounded corner region. Consequently the curves are discontinuous between orifices 16 and 17. Referring back to fig. 6, orifices 1 through 16 are equally spaced in increments of 1.5° on a radius of 18 in. while orifices 17 through 24 are equally spaced in increments of 12.5° on a radius of 0.75 in. The occurrence of a weak shock just behind the leeward corner of Model A at $\alpha = -10°$ was noted visually (schlieren screen). This phenomena was extremely sensitive to angle of attack, since the shock wave appeared only intermittently during the $\alpha = -10°$ tunnel runs, and may account for the pressure peaks which appear in the data.

Referring to fig. 19, a persistent small rise in pressure appears just downstream of the point $S/R_N = 2.0$ on Model E indicating the possibility of a change in the viscous nature of the flow in this region.

A detailed examination of the surface pressure data in the stagnation region of Model E (orifices 1 through 7) leads to the observation that the maximum pressure occurring in the pitching plane of the model at angle of attack typically exceeds the symmetric flow stagnation value by approximately 1/2%. In spite of the close spacing of orifices, it was difficult to establish the exact magnitude and location of the maximum of the surface pressure curve. For Model A, this difficulty was increased owing to small fluctuations in pressure which occurred on the model face.

Sonic Line Determination

The approximate location of the sonic line was experimentally determined for Model A at $\alpha = 0°$ using the shock interaction technique described previously. The lower surface of the shock generator, which has a lateral span of 3 in., was set at 10° incidence to the free stream. The resulting shock interaction configuration was more complex than anticipated (fig. 21); however, the desired effect was obtained. A weak transmitted shock can be seen at the base of the "Mach stem" which grazes the sonic line in fig. 21(a), and intersects the sonic line in fig. 21(b). Using an optical comparator, a precise check of the influence of the interaction on the bow shock location indi-

Table II

NOMINAL VERSUS ACTUAL ANGLE OF ATTACK

MODEL E

NOMINAL ANGLE OF ATTACK	ROLL ANGLES AND RUN NUMBERS						
	0°	30°	60°	90°	120°	150°	180°
	3	4	5	6	7	8	9
-15	-15.07	-14.98	-14.78	-14.63	-14.37	-14.24	-14.18
-10	-10.10	-10.00	-9.81	-9.65	-9.41	-9.27	-9.22
-5	-5.09	-4.99	-4.81	-4.65	-4.41	-4.27	-4.21
0	-.02	+.05	+.26	+.42	+.66	+.79	+.84
5	4.98	5.05	5.26	5.43	5.67	5.79	5.83
10	9.98	10.04	10.24	10.42	10.66	10.79	10.83
15	15.00	15.04	15.24	15.42	15.66	15.80	15.84
20	19.99	20.03	20.24	20.41	20.64	20.79	20.83

MODEL A

NOMINAL ANGLE OF ATTACK	ROLL ANGLES AND RUN NUMBERS						
	0°	30°	60°	90°	120°	150°	180°
	14	17	18	19	20	21	22
-15	---	-15.06	-15.21	-15.24	-15.66	-15.24	-15.25
-10	---	-10.06	-10.20	-10.27	-10.64	-10.25	-10.27
-5	-4.99	-5.07	-5.21	-5.27	-5.65	-5.27	-5.26
0	.03	-.06	-.19	-.26	-.64	-.25	-.25
5	5.06	4.92	4.85	4.77	4.37	4.78	4.77
10	10.06	9.90	9.85	9.79	9.37	9.79	9.77
15	15.06	14.89	14.83	14.77	15.39	14.90	14.78
20	20.05	19.88	19.84	19.77	19.39	19.91	19.77

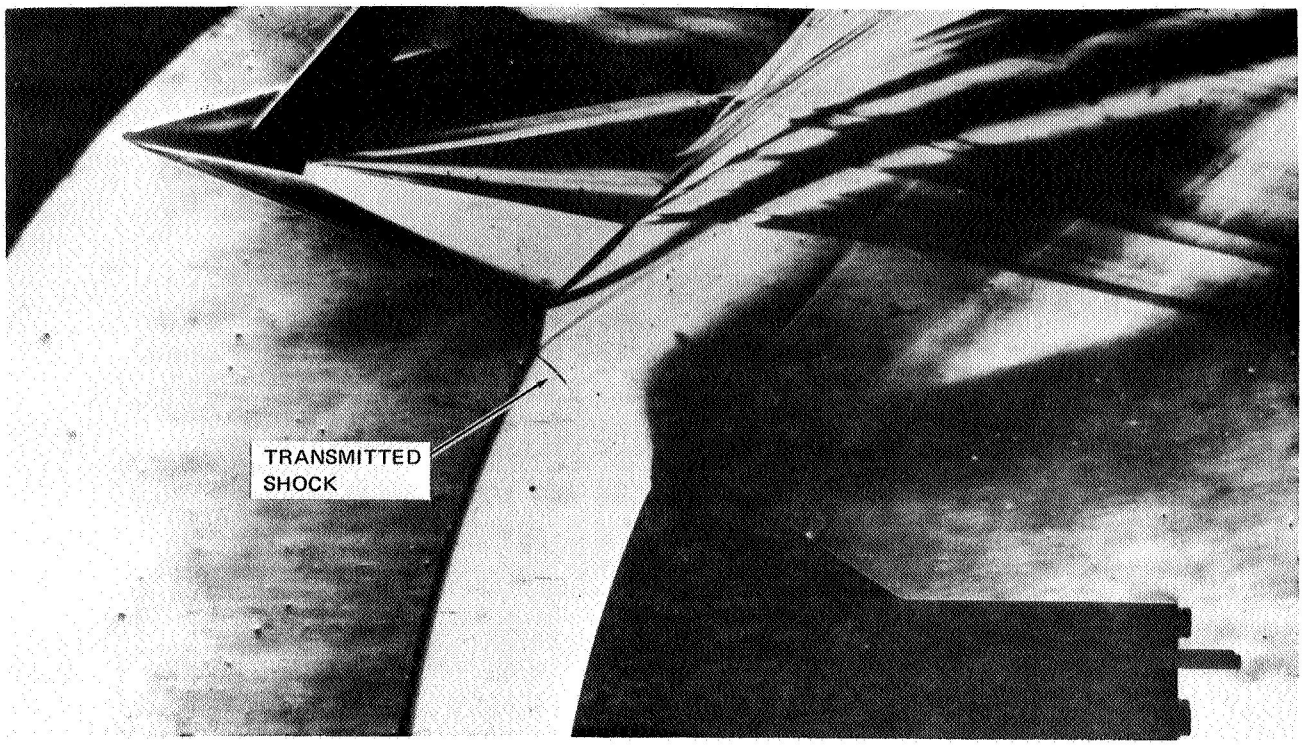

(a)

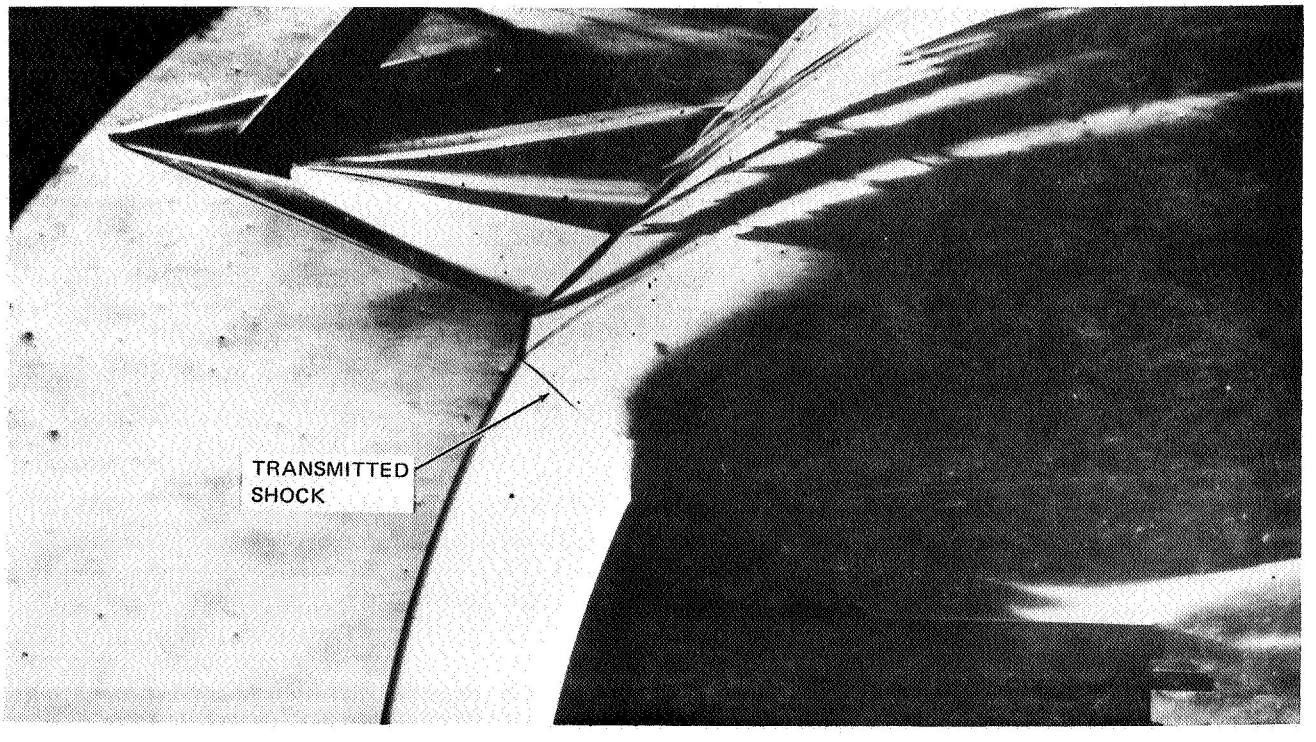

(b)

Figure 21. Sonic Line Location Technique

cated a negligible effect when the interaction takes place above the shock sonic point. Impinging the shock slightly below this point eliminated the triple-shock configuration and caused a small inflection in the bow shock in the immediate neighborhood of the interaction. For the sonic line geometry shown, it is probable that a zone of influence exists extending downstream to the limiting characteristic (for example, see ref. 7) within which a disturbance can still influence the subsonic region. No such effect was evident in the present case in spite of the strength of the impinging shock wave.

An obvious shortcoming in the interaction technique lies in the difficulty in establishing the location of the tip of the transmitted shock as it fades to zero strength at the sonic line. Also, if the interacting shock has significant lateral extent, one might anticipate a three dimensional effect which, when viewed on a schlieren photograph, would tend to record the portion of the transmitted shock out of the plane of symmetry as apparently lying below the true sonic line location.

The results of the schlieren measurements are shown in fig. 22. The data points correspond to the extreme discernible tip of the transmitted shocks. The range of data shown was obtained by manually translating the model in small vertical increments while viewing the schlieren screen. Photographs were continuously taken during the run at the rate of two per second. The shock sonic point was located on the basis of measured shock wave slope while the body sonic point was calculated from the surface pressure data ($p^*/p_{t_\infty} = 0.0497$ for $M_\infty = 4.468$).

The variation of sonic point location in the $\phi = 0$ or windward plane with angle of attack for both models is shown in figs. 23 and 24. At the negative angles of attack, the sonic line lies extremely close to the curvature discontinuity point on Model A.

Shock Wave Profiles

A sequence of shock wave profiles corresponding to the pitching plane of the model-sting configuration were determined through direct measurement of 70-mm schlieren negatives using a high resolution optical comparator. Results shown in figs. 25 and 26 have been normalized in terms of the maximum body radius, R_{MAX}. In addition, tabulated shock shape data are presented in Appendix B. The use of shock layer thickness as in ref. 21 (which investigates shock shapes for an Apollo-type configuration at large angles of attack) was considered but was not found convenient for displaying the shock profile beyond $r = R_{MAX}$. This parameter can be recovered, however, from the graphical or tabular data. A representative schlieren photograph (Model A with traversing probe in position 3) is shown in fig. 27. Shock wave measurements were made using a "clean" configuration with the forward probe ports sealed with flush mounted inserts.

Considering an orthogonal (x, y) coordinate system with origin at the stagnation point and y axis aligned with the free stream direction, denote the lateral location of the normal points on the shock and body by x_n and x_b, respectively. A relationship of the form $x_b = k\, x_n$ is equivalent to the statement that the lateral displacement between shock and body normal points is approximately

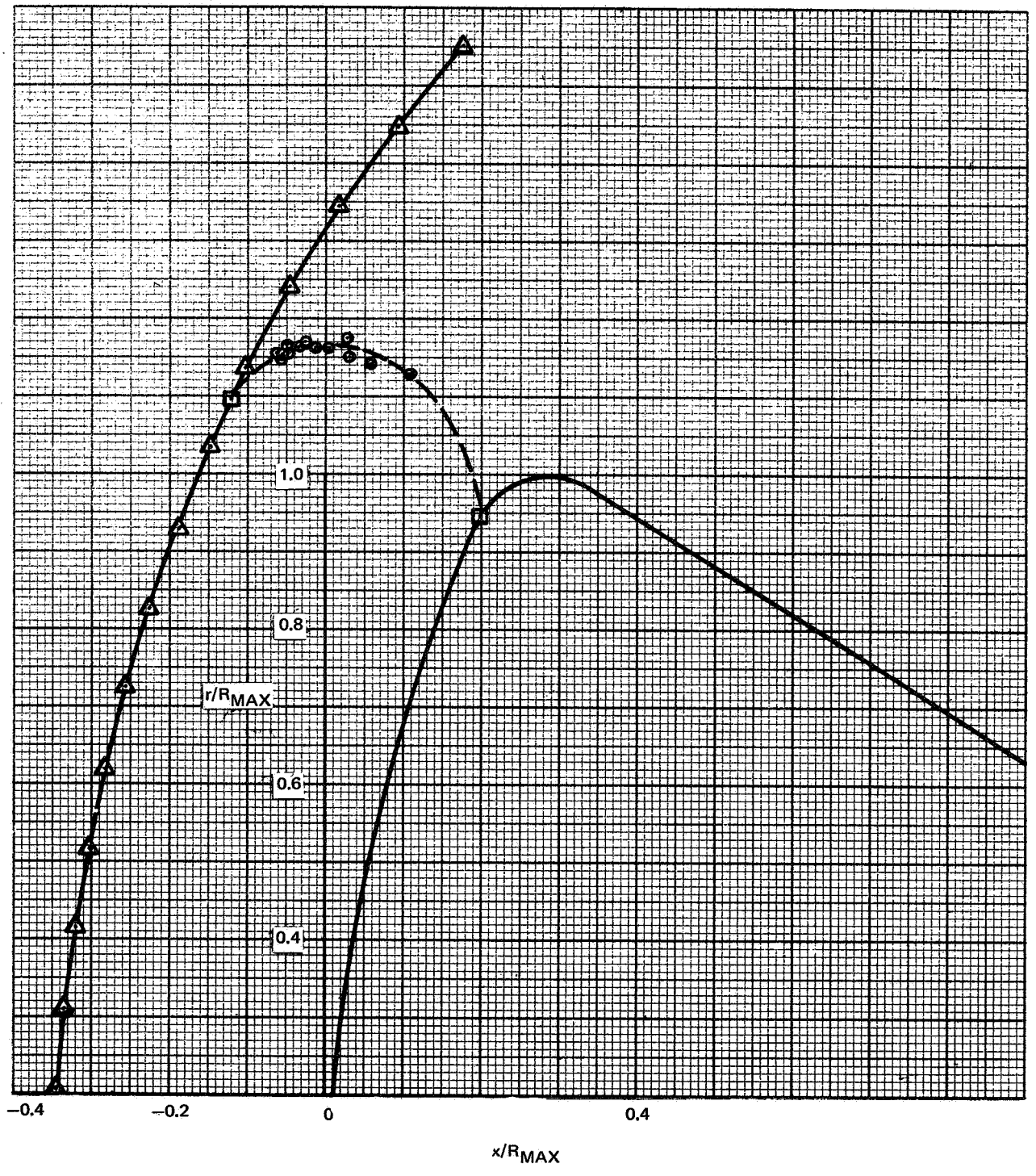

Figure 22. Sonic Line: Model A; $\alpha = 0^0$

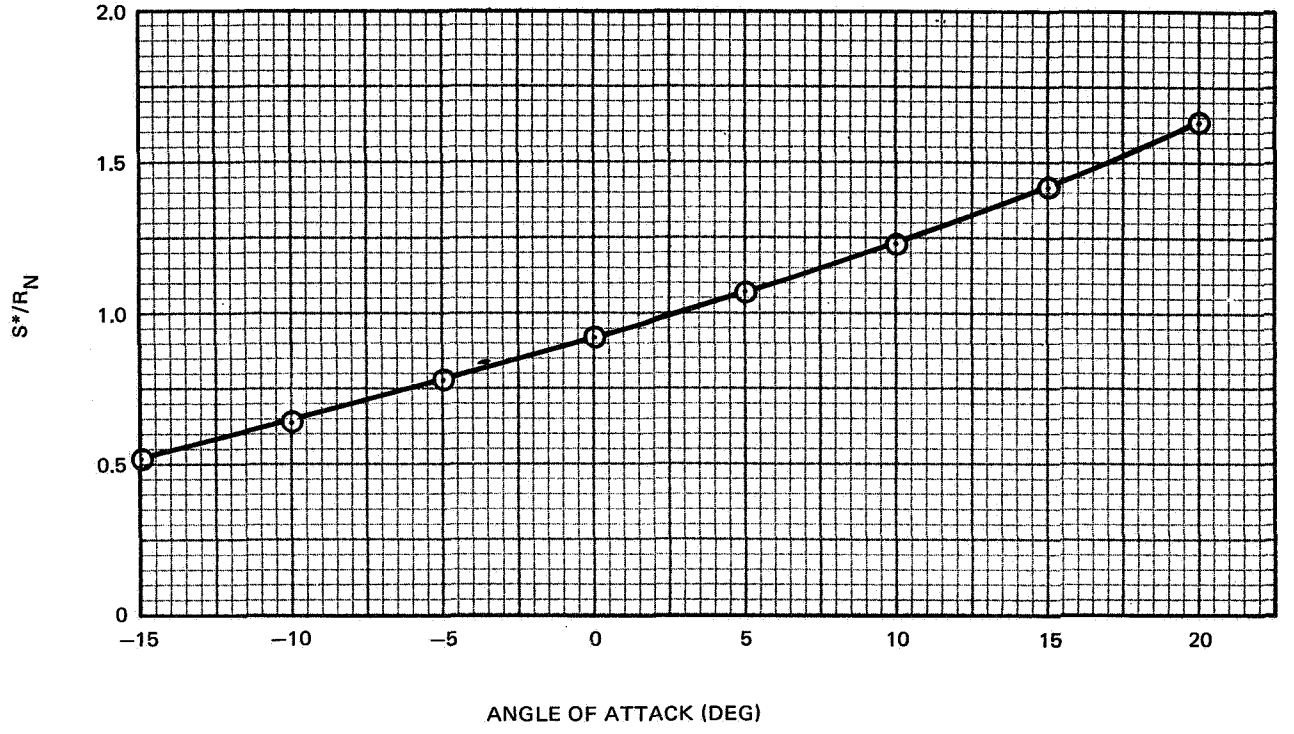

Figure 23. Sonic Point Location: Model E; $\varphi = 0^0$

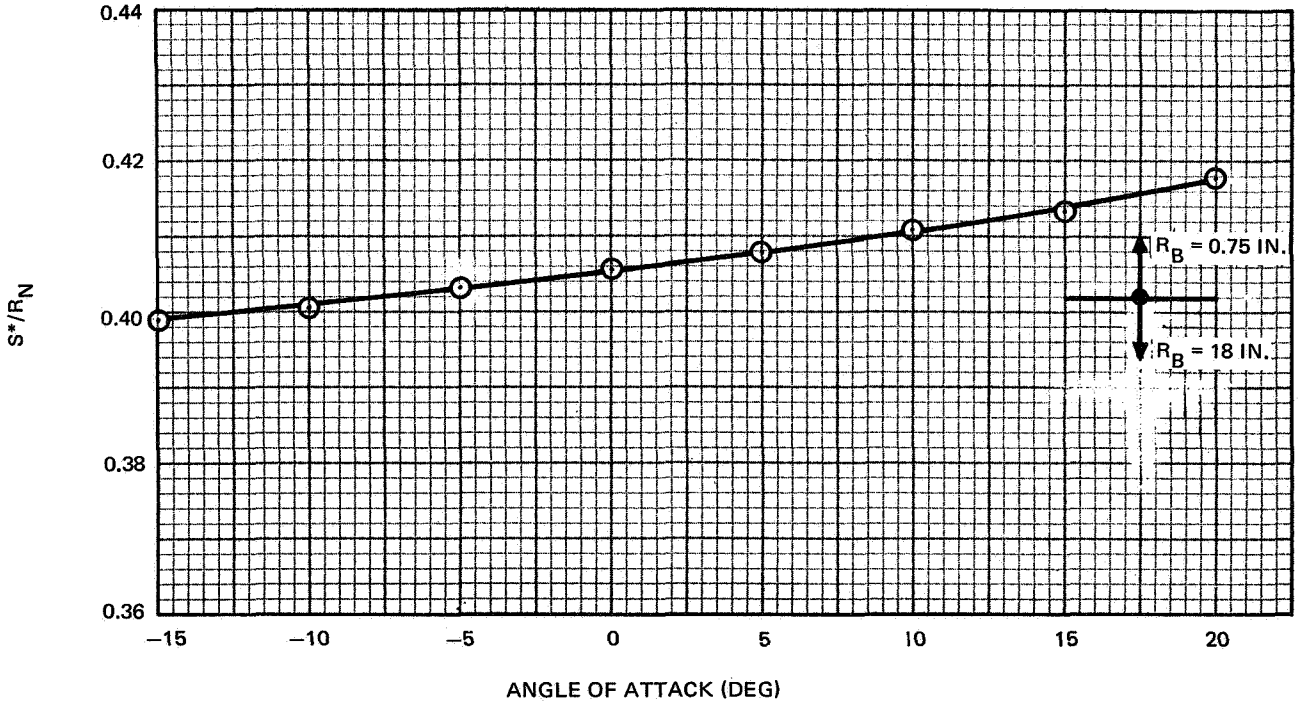

Figure 24. Sonic Point Location: Model A; $\varphi = 0^0$

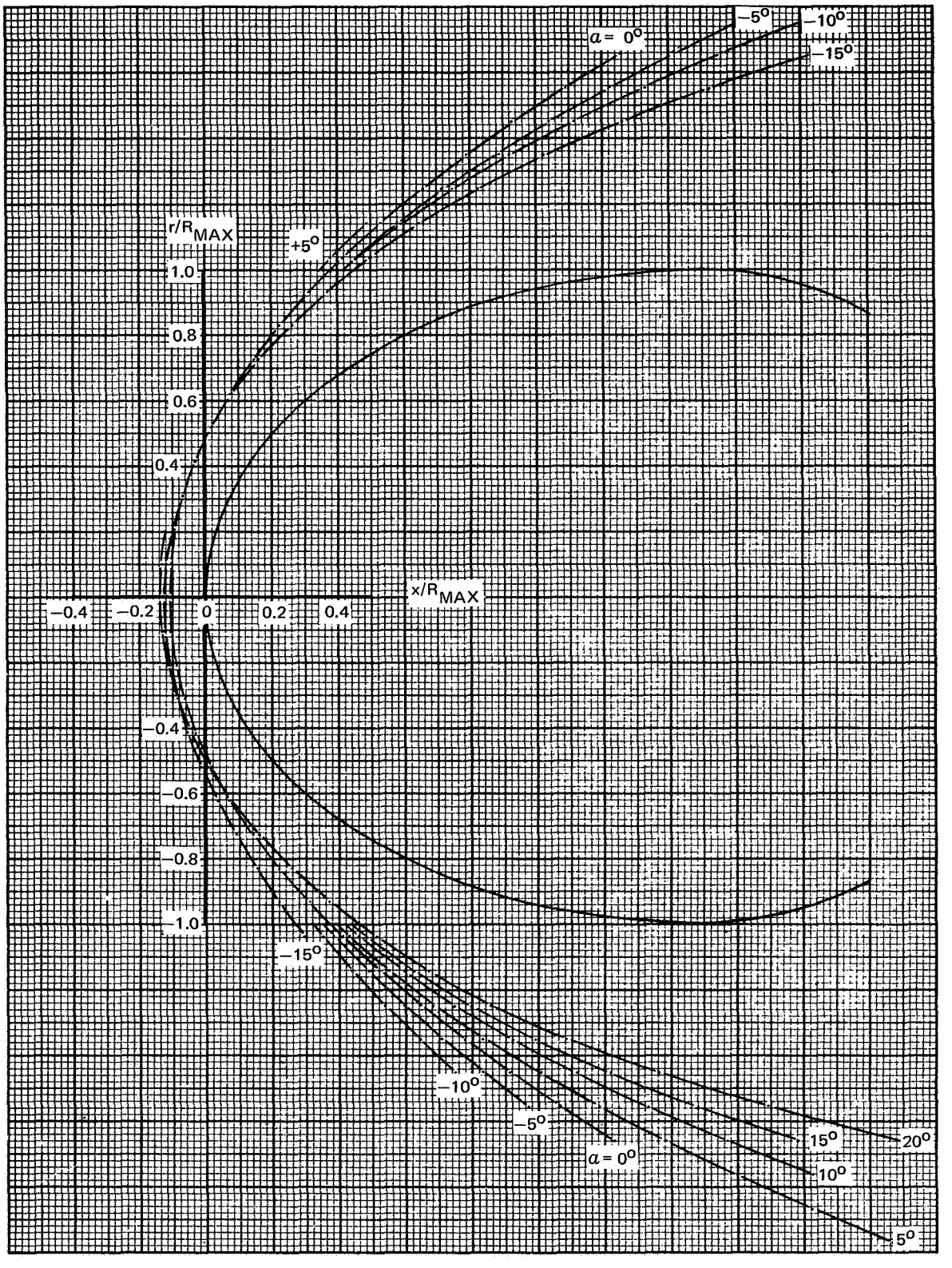

Figure 25. Shock Profiles: Model E

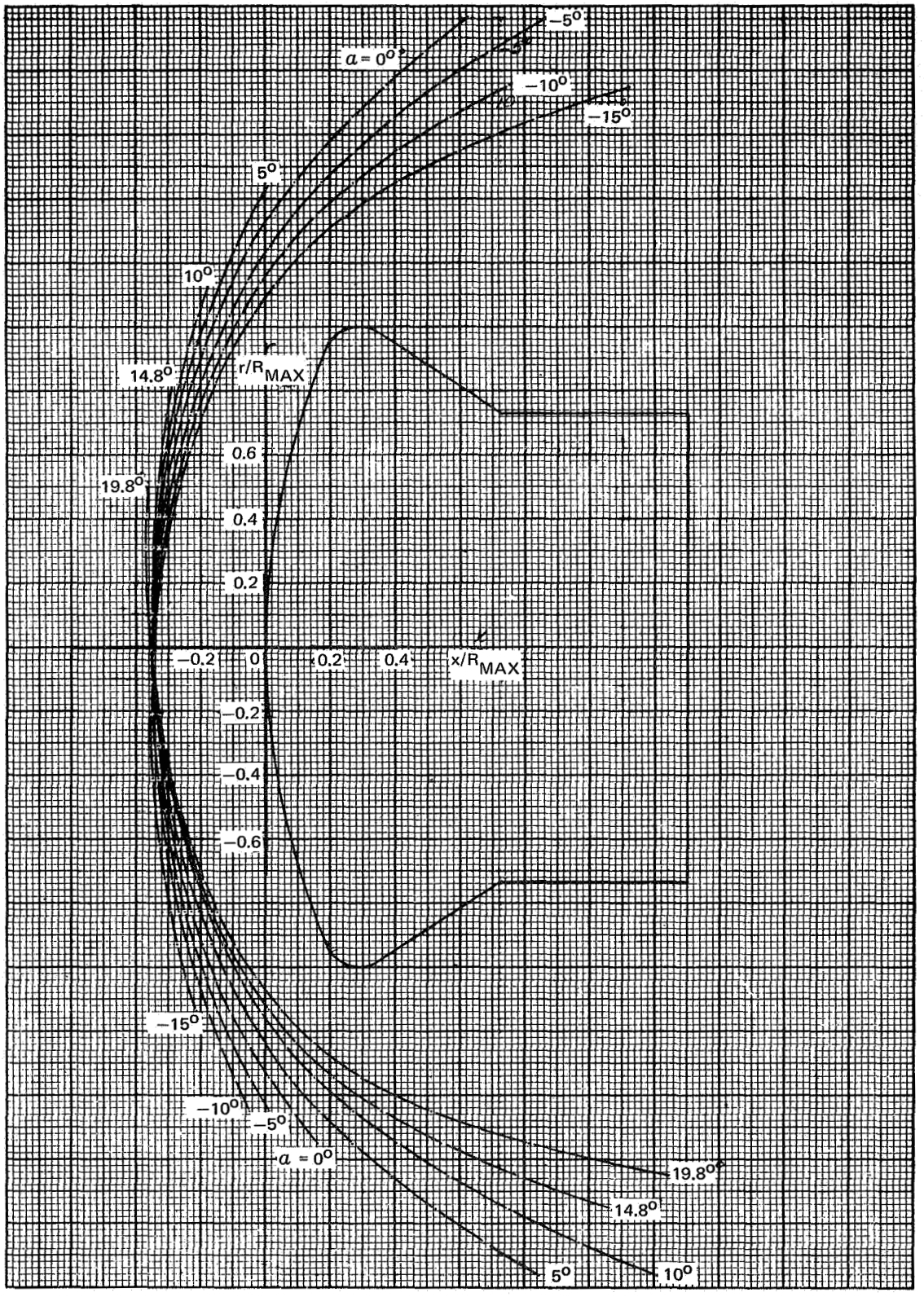

Figure 26. Shock Wave Profiles: Model A

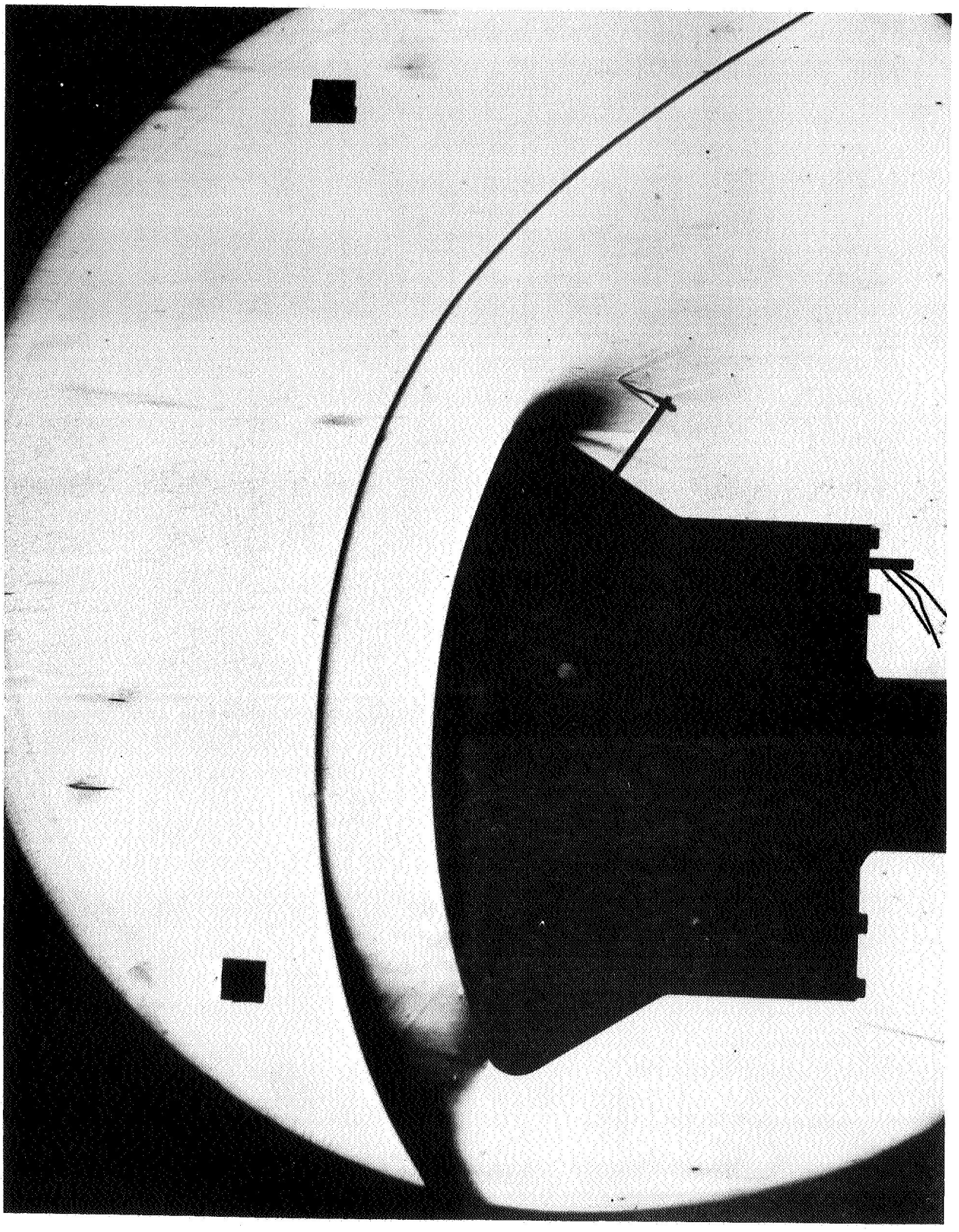

Figure 27. Representative Schlieren Photograph: Model A

k times the lateral shift in the stagnation streamline in the shock layer (see ref. 7). For example, the numerical results of ref. 3 give a value of $k \cong 6$. In the present study, a measurement of the quantity $\delta_{NP} = |x_b \pm x_n|$ was made using the shock profile schlierens (where the sign is determined by the relative position of the normal points and the stagnation point). The results, shown in figs. 28 and 29, are presented in this form owing to the lack of accurate data on stagnation point location. It is interesting to note that for increasing positive angle of attack, the slope of δ_{NP}/R_N (R_N = body radius of curvature at the axis of symmetry) decreases for Model E and increases for Model A.

CONCLUDING REMARKS

The shock layer pressure profile technique used in the present study for the determination of the "inviscid" value of body surface total pressure appears to yield valid results based on symmetric flow measurements. The effect of asymmetry on the measured value of $(p_t/p_{t_\infty})_{SURFACE}$ for the configurations and free stream conditions considered was found to be of the order of 0.5%. One may therefore conclude that the maximum entropy streamline does not, in general, coincide exactly with the stagnation streamline for three-dimensional flows. The impact of this behavior from a gross aerodynamic design standpoint is obviously small; however, consideration of this effect in the formulation of a three-dimensional analysis may be essential when precise, theoretically consistent solutions are being sought.

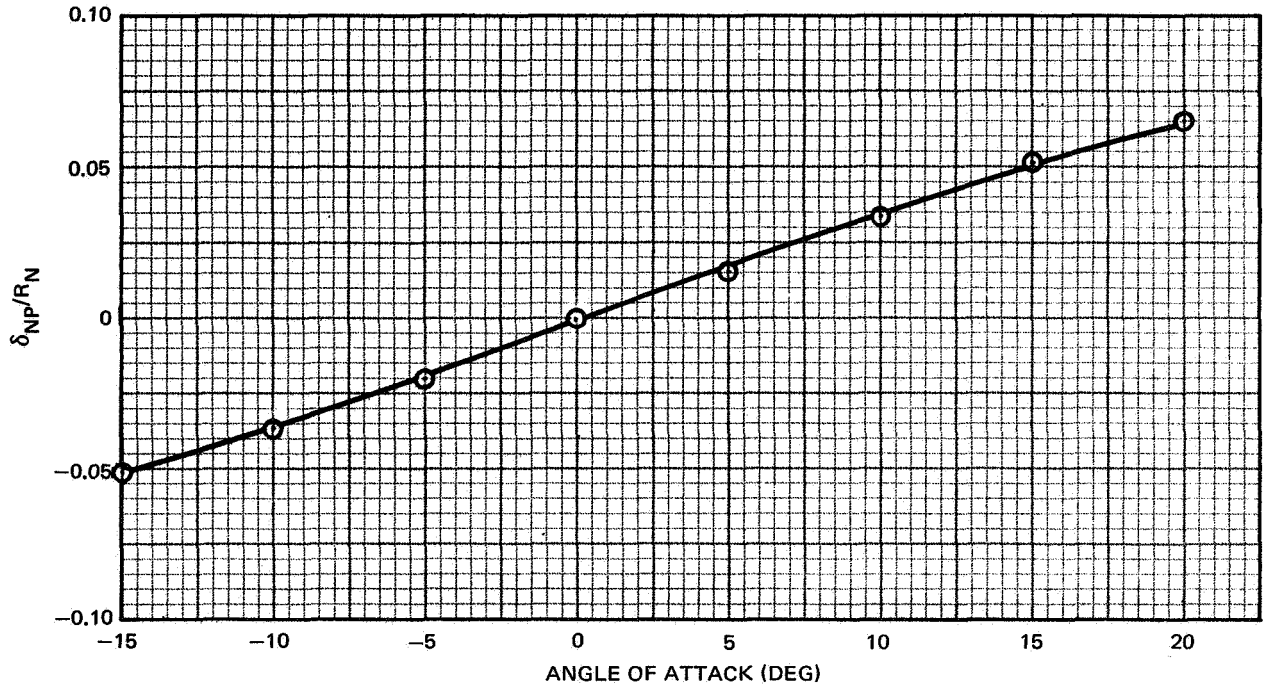

Figure 28. Lateral Displacement Between Shock and Body Normal Points: Model E

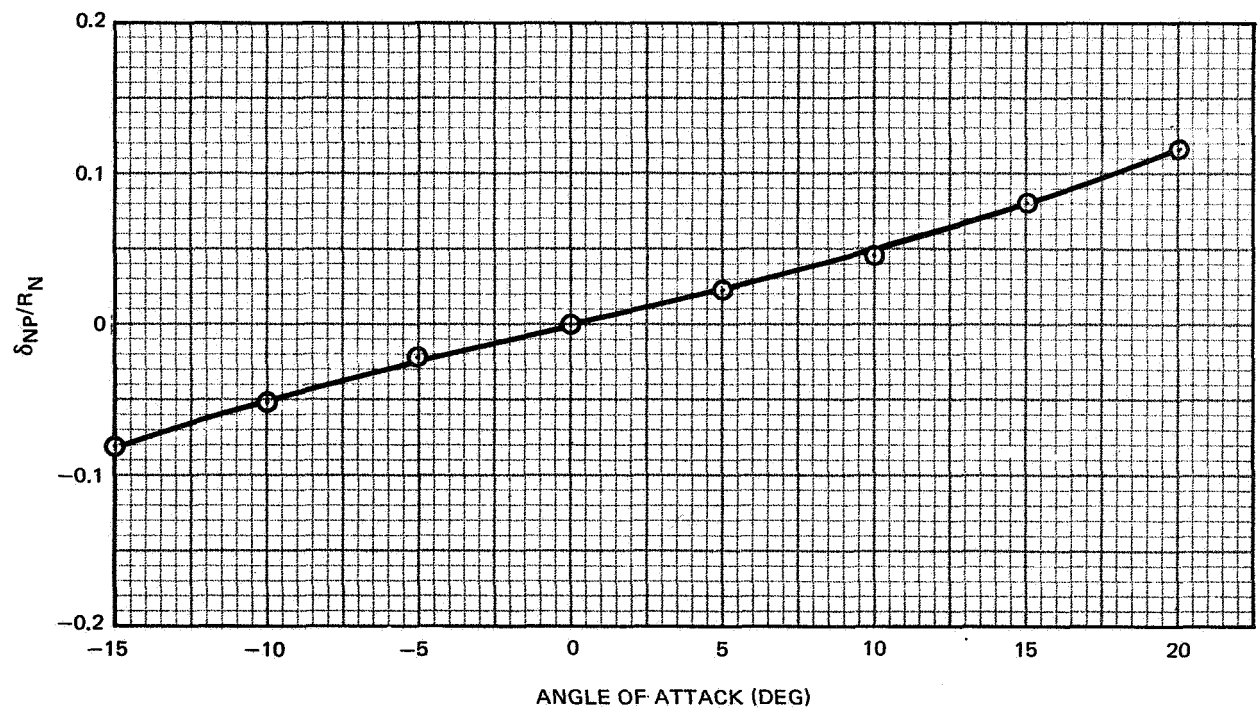

Figure 29. Lateral Displacement Between Shock and Body Normal Points: Model A

REFERENCES

1. K. W. Mangler, The Calculation of the Flow Field Between a Blunt Body and the Bow Wave. Hypersonic Flow. Butterworths Scientific Publications, London, 1960, Pages 219-238.

2. R. Vaglio-Laurin. On the PLK Method and the Supersonic Blunt-Body Problem, Journal of the Aerospace Sciences, Vol. 29, No. 2, February 1962, Pages 185-206 and 248.

3. R. J. Swigart. A Theory of Asymmetric Hypersonic Blunt-Body Flows. AIAA Journal, Vol. 1, No. 5, May 1963, Pages 1034-1042.

4. R. J. Swigart. The Direct Asymmetric Hypersonic Blunt-Body Problem. AIAA Paper No. 66-411, June 1966.

5. H. G. Webb, Jr., H. S. Dresser, B. K. Adler, and S. A. Waiter. Inverse Solution of Blunt-Body Flowfields at Large Angle of Attack. AIAA Journal, Vol. 5, No. 6, June 1967, Pages 1079-1085.

6. A. Muggia. Regione de Arresto per un Profilo a Bordo di Attaco Quasi-Circolare in Corrente Ipersonica non Simmetrica, (Stagnation Region of a Quasi-Circular Leading Edge Profile in Unsymmetric Hypersonic Flow), Atti Accad. Sci., Torino, Vol. 94, 1960, Pages 836-854.

7. W. D. Hayes and R. F. Probstein. Hypersonic Flow Theory: Volume 1. Inviscid Flows. Academic Press, New York, 1966, Chap. 4, 6.

8. W. J. Prosnak and E. Luczywek. The Direct Asymmetric Hypersonic Blunt-Body Problem. ICAS Paper No. 64-552, August 1964.

9. A. P. Bazhin. The Calculation of Supersonic Flow Past a Flat Plate With a Detached Shock Wave. Inzhenernyy Zhurnal (Moscow), Vol. 3, No. 2, 1963.

10. A Minailos. On the Calculation of Supersonic Flow Past Blunted Bodies of Revolution at Angles of Attack. U.S.S.R. Comput. Math. and Math. Phys., 1964, Pages 238-248.

11. G. D. Waldman. Integral Approach to the Yawed Blunt Body Problem. AIAA Paper No. 65-28. January 1965.

12. E. A. Brong and D. C. Leigh. Method of Belotserkovskii for Asymmetric Blunt-Body Flows. AIAA Journal, Vol. 2, No. 10, October 1964, Pages 1852-1853.

13. W. D. Hayes. Rotation Stagnation Point Flow. Journal of Fluid Mechanics, Vol. 19, 1964, Pages 366-374.

14. R. C. Boger and G. S. S. Ludford. Rotational Stagnation-Point Flow. Journal of Mathematics and Mechanics, Vol. 16, No. 12, 1967. Pages 1339-1359.

15. I. O. Bohachevsky and R. E. Mates. A Direct Method for Calculation of the Flow About an Axisymmetric Blunt Body at Angle of Attack. AIAA Journal. Vol. 4, No. 5, May 1966, Pages 776-782.

16. Moretti, G. and G. Bleich. Three Dimensional Flow Around Blunt Bodies. AIAA Journal, Vol. 5, No. 9, September 1967. Pages 1557-1 Pages 1557-1562.

17. J. Xerikos and W. A. Anderson. An Experimental Investigation of the Shock Layer Surrounding a Sphere in Supersonic Flow. AIAA Journal, Vol. 3, No. 3, March 1965.

18. I. M. Hall. The Displacement Effect of a Sphere in a Two-Dimensional Shear Flow. Journal of Fluid Mechanics, Vol. 1, 1956.

19. J. M. Kendall, Jr. Experiments on Supersonic-Blunt-Body Flows. Jet Propulsion Lab. Progress Report 20-372, 1959.

20. R. J. Polutchko. Hypersonic Flow Field About a Blunt Slab Wing at Angle of Attack: Phase I. ARL 64-213, Wright-Patterson AFB, December 1964.

21. R. J. Hakkinen. Supersonic Flow Near Two-Dimensional and Axially Symmetric Convex Corners and Curvature Discontinuities. Douglas Aircraft Company, Inc. Report No. SM-27747, July 1958.

22. G. E. Kaattari. Shock Envelopes of Blunt Bodies at Large Angles of Attack. NASA TN D-1980, December 1963.

APPENDIX A

SURFACE STATIC PRESSURE RATIO, $P_s/P_{t\infty}$

MODEL E

$\phi = 0^o$

RUN NUMBER 3

ORIFICE NUMBER	ANGLE OF ATTACK (NOMINAL)							
	-15^o	-10^o	-5^o	0^o	5^o	10^o	15^o	20^o
1	.0876	.0919	.0942	.0946	.0939	.0914	.0872	.0825
2	.0808	.0873	.0915	.0939	.0950	.0939	.0913	.0874
3	.0744	.0813	.0872	.0909	.0936	.0947	.0941	.0923
4	.0664	.0745	.0810	.0869	.0909	.0935	.0943	.0944
5	.0585	.0671	.0744	.0812	.0871	.0914	.0935	.0950
6	.0508	.0596	.0677	.0751	.0816	.0872	.0911	.0940
7	.0437	.0524	.0610	.0689	.0762	.0827	.0875	.0922
8	.0378	.0459	.0543	.0624	.0702	.0774	.0836	.0886
9	.0324	.0400	.0483	.0564	.0643	.0722	.0792	.0849
10	.0280	.0351	.0431	.0511	.0586	.0666	.0740	.0810
11	.0236	.0300	.0374	.0451	.0530	.0611	.0690	.0765
12	.0201	.0258	.0327	.0402	.0479	.0557	.0642	.0718
13	.0170	.0220	.0283	.0355	.0431	.0511	.0594	.0674
14	.0144	.0189	.0246	.0315	.0384	.0460	.0542	.0625
15	.0123	.0163	.0216	.0278	.0344	.0421	.0504	.0587
16	.0104	.0139	.0187	.0245	.0307	.0380	.0461	.0547
17	.0091	.0121	.0165	.0219	.0278	.0348	.0425	.0509
18	.0078	.0105	.0144	.0193	.0249	.0315	.0388	.0471
19	.0066	.0090	.0125	.0171	.0223	.0285	.0355	.0437
20	.0057	.0078	.0110	.0151	.0200	.0258	.0326	.0402
21	.0056	.0074	.0102	.0139	.0184	.0238	.0302	.0376
22	.0050	.0066	.0091	.0125	.0168	.0218	.0279	.0349
23	.0044	.0058	.0080	.0111	.0150	.0197	.0255	.0322
24	.0038	.0051	.0071	.0099	.0135	.0178	.0233	.0297
25	.0034	.0045	.0062	.0087	.0119	.0158	.0209	.0268
26	.0030	.0040	.0055	.0078	.0107	.0144	.0191	.0247
27	.0026	.0035	.0048	.0069	.0095	.0129	.0172	.0225
28	.0023	.0031	.0042	.0060	.0084	.0115	.0155	.0203
29	.0020	.0027	.0037	.0054	.0075	.0104	.0140	.0186
30	.0018	.0024	.0033	.0048	.0067	.0094	.0126	.0170
31	.0780	.0705	.0626	.0547	.0463	.0387	.0315	.0246

MODEL E

$\phi = 30^{\circ}$

RUN NUMBER 4

ORIFICE NUMBER	ANGLE OF ATTACK (NOMINAL)							
	-15°	-10°	-5°	0°	5°	10°	15°	20°
1	.0881	.0925	.0953	.0957	.0949	.0922	.0881	.0832
2	.0820	.0886	.0925	.0944	.0955	.0947	.0914	.0875
3	.0757	.0832	.0884	.0916	.0941	.0948	.0935	.0908
4	.0681	.0761	.0827	.0866	.0910	.0932	.0931	.0923
5	.0607	.0690	.0761	.0815	.0866	.0900	.0920	.0921
6	.0531	.0615	.0691	.0754	.0812	.0860	.0888	.0904
7	.0461	.0546	.0626	.0692	.0752	.0808	.0849	.0880
8	.0403	.0484	.0560	.0628	.0694	.0752	.0801	.0841
9	.0345	.0422	.0499	.0569	.0636	.0699	.0753	.0800
10	.0302	.0371	.0447	.0514	.0579	.0639	.0702	.0754
11	.0254	.0317	.0388	.0454	.0525	.0583	.0650	.0708
12	.0218	.0276	.0339	.0406	.0470	.0530	.0599	.0663
13	.0183	.0235	.0295	.0357	.0422	.0485	.0557	.0617
14	.0157	.0203	.0257	.0315	.0376	.0434	.0506	.0569
15	.0135	.0175	.0225	.0280	.0338	.0399	.0468	.0531
16	.0115	.0150	.0196	.0245	.0301	.0361	.0426	.0493
17	.0100	.0131	.0172	.0220	.0271	.0328	.0392	.0457
18	.0086	.0114	.0151	.0195	.0242	.0297	.0357	.0422
19	.0072	.0096	.0129	.0168	.0212	.0264	.0320	.0385
20	.0065	.0086	.0117	.0153	.0194	.0244	.0298	.0360
21	.0063	.0081	.0108	.0141	.0179	.0224	.0275	.0334
22	.0056	.0072	.0096	.0127	.0163	.0205	.0254	.0310
23	.0049	.0063	.0085	.0113	.0146	.0185	.0232	.0285
24	.0043	.0056	.0075	.0100	.0131	.0167	.0210	.0260
25	.0038	.0049	.0066	.0088	.0116	.0147	.0188	.0234
26	.0033	.0042	.0057	.0076	.0101	.0129	.0166	.0209
27	.0029	.0038	.0052	.0069	.0092	.0119	.0154	.0195
28	.0026	.0033	.0045	.0061	.0081	.0106	.0138	.0176
29	.0023	.0029	.0041	.0054	.0073	.0095	.0125	.0161
30	.0020	.0026	.0036	.0048	.0065	.0086	.0113	.0146
31	.0737	.0683	.0624	.0554	.0480	.0410	.0342	.0274

MODEL E

$\phi = 60^{\circ}$

RUN NUMBER 5

ORIFICE NUMBER	ANGLE OF ATTACK (NOMINAL)							
	-15°	-10°	-5°	0°	5°	10°	15°	20°
1	.0878	.0918	.0944	.0942	.0932	.0914	.0869	.0819
2	.0841	.0893	.0917	.0930	.0929	.0917	.0881	.0837
3	.0790	.0848	.0881	.0900	.0909	.0908	.0881	.0843
4	.0731	.0788	.0834	.0855	.0870	.0875	.0864	.0832
5	.0663	.0722	.0769	.0802	.0826	.0835	.0831	.0812
6	.0595	.0653	.0701	.0744	.0770	.0787	.0788	.0781
7	.0531	.0591	.0637	.0678	.0709	.0732	.0740	.0740
8	.0470	.0528	.0575	.0616	.0649	.0675	.0690	.0692
9	.0412	.0469	.0515	.0557	.0594	.0621	.0636	.0644
10	.0366	.0417	.0464	.0503	.0539	.0566	.0586	.0599
11	.0313	.0361	.0404	.0446	.0483	.0507	.0537	.0554
12	.0273	.0317	.0357	.0397	.0431	.0462	.0488	.0506
13	.0236	.0275	.0314	.0349	.0385	.0417	.0444	.0465
14	.0204	.0239	.0275	.0308	.0340	.0372	.0398	.0420
15	.0178	.0210	.0242	.0272	.0304	.0335	.0361	.0385
16	.0154	.0183	.0212	.0239	.0268	.0298	.0326	.0348
17	.0135	.0161	.0187	.0214	.0242	.0269	.0297	.0319
18	.0118	.0140	.0164	.0190	.0216	.0242	.0269	.0294
19	.0102	.0122	.0143	.0166	.0190	.0216	.0242	.0266
20	.0089	.0107	.0127	.0149	.0171	.0194	.0219	.0242
21	.0086	.0101	.0119	.0138	.0159	.0181	.0204	.0227
22	.0077	.0090	.0107	.0124	.0143	.0164	.0186	.0210
23	.0067	.0080	.0094	.0110	.0128	.0147	.0167	.0190
24	.0060	.0071	.0084	.0098	.0114	.0132	.0151	.0172
25	.0053	.0063	.0073	.0087	.0100	.0116	.0134	.0154
26	.0047	.0055	.0066	.0078	.0090	.0105	.0122	.0141
27	.0042	.0049	.0058	.0069	.0080	.0093	.0109	.0126
28	.0036	.0043	.0051	.0061	.0070	.0083	.0097	.0112
29	.0032	.0038	.0045	.0054	.0063	.0074	.0088	.0103
30	.0029	.0034	.0040	.0048	.0056	.0067	.0079	.0093
31	.0636	.0615	.0587	.0551	.0506	.0457	.0409	.0351

MODEL E

$\phi = 90^{\circ}$

RUN NUMBER 6

ORIFICE NUMBER	ANGLE OF ATTACK (NOMINAL)							
	-15°	-10°	-5°	0°	5°	10°	15°	20°
1	.0882	.0919	.0941	.0945	.0933	.0909	.0867	.0816
2	.0869	.0909	.0928	.0928	.0921	.0895	.0852	.0799
3	.0842	.0879	.0899	.0900	.0892	.0867	.0829	.0774
4	.0801	.0835	.0852	.0853	.0846	.0824	.0786	.0734
5	.0750	.0782	.0799	.0801	.0791	.0768	.0734	.0690
6	.0687	.0719	.0735	.0738	.0727	.0710	.0680	.0639
7	.0631	.0660	.0675	.0677	.0667	.0649	.0624	.0587
8	.0574	.0601	.0611	.0615	.0603	.0592	.0567	.0530
9	.0521	.0542	.0553	.0553	.0548	.0535	.0514	.0485
10	.0468	.0488	.0498	.0502	.0497	.0484	.0463	.0437
11	.0413	.0430	.0438	.0441	.0438	.0428	.0411	.0390
12	.0370	.0384	.0390	.0392	.0390	.0379	.0366	.0347
13	.0328	.0339	.0345	.0345	.0342	.0335	.0324	.0308
14	.0290	.0300	.0304	.0303	.0301	.0296	.0285	.0273
15	.0258	.0265	.0270	.0268	.0268	.0262	.0255	.0245
16	.0228	.0234	.0238	.0236	.0236	.0231	.0225	.0217
17	.0204	.0209	.0211	.0210	.0211	.0206	.0201	.0194
18	.0180	.0185	.0186	.0186	.0187	.0184	.0179	.0174
19	.0159	.0163	.0165	.0164	.0164	.0162	.0159	.0154
20	.0142	.0145	.0147	.0146	.0145	.0144	.0142	.0138
21	.0133	.0134	.0135	.0135	.0135	.0133	.0133	.0129
22	.0120	.0121	.0121	.0121	.0121	.0121	.0119	.0117
23	.0106	.0107	.0108	.0107	.0108	.0107	.0107	.0105
24	.0095	.0096	.0097	.0095	.0096	.0095	.0095	.0094
25	.0085	.0085	.0085	.0084	.0085	.0084	.0084	.0083
26	.0076	.0076	.0076	.0075	.0076	.0075	.0076	.0075
27	.0067	.0067	.0067	.0067	.0066	.0066	.0067	.0066
28	.0059	.0059	.0059	.0059	.0058	.0058	.0059	.0059
29	.0052	.0053	.0053	.0052	.0052	.0052	.0053	.0053
30	.0047	.0047	.0047	.0046	.0047	.0047	.0047	.0047
31	.0522	.0541	.0552	.0557	.0554	.0541	.0519	.0490

MODEL E

$\phi = 120^{\circ}$

RUN NUMBER 7

ORIFICE NUMBER	ANGLE OF ATTACK (NOMINAL)							
	-15°	-10°	-5°	0°	5°	10°	15°	20°
1	.0881	.0924	.0940	.0947	.0935	.0907	.0867	.0814
2	.0897	.0929	.0935	.0924	.0908	.0877	.0825	.0762
3	.0894	.0914	.0912	.0899	.0872	.0832	.0776	.0707
4	.0871	.0885	.0875	.0854	.0822	.0774	.0714	.0644
5	.0838	.0842	.0823	.0799	.0759	.0707	.0652	.0577
6	.0793	.0789	.0765	.0736	.0691	.0641	.0581	.0520
7	.0745	.0735	.0706	.0672	.0624	.0576	.0522	.0448
8	.0694	.0673	.0643	.0610	.0562	.0513	.0462	.0399
9	.0641	.0614	.0586	.0549	.0504	.0454	.0404	.0346
10	.0587	.0559	.0532	.0497	.0453	.0405	.0360	.0306
11	.0536	.0506	.0474	.0438	.0395	.0352	.0308	.0261
12	.0487	.0458	.0424	.0388	.0349	.0307	.0267	.0225
13	.0442	.0412	.0376	.0342	.0305	.0267	.0230	.0193
14	.0395	.0367	.0334	.0301	.0266	.0233	.0199	.0166
15	.0358	.0330	.0298	.0267	.0233	.0204	.0173	.0144
16	.0322	.0293	.0263	.0234	.0204	.0177	.0150	.0124
17	.0291	.0265	.0236	.0208	.0181	.0155	.0132	.0108
18	.0262	.0237	.0210	.0184	.0159	.0136	.0115	.0094
19	.0236	.0210	.0185	.0162	.0139	.0119	.0100	.0081
20	.0214	.0188	.0165	.0144	.0123	.0104	.0087	.0071
21	.0198	.0175	.0153	.0133	.0115	.0099	.0083	.0069
22	.0181	.0159	.0139	.0120	.0103	.0088	.0074	.0062
23	.0163	.0142	.0124	.0106	.0091	.0078	.0065	.0054
24	.0147	.0128	.0111	.0095	.0081	.0069	.0058	.0048
25	.0130	.0113	.0098	.0083	.0071	.0060	.0051	.0042
26	.0118	.0102	.0088	.0075	.0063	.0054	.0045	.0037
27	.0106	.0090	.0077	.0065	.0056	.0047	.0039	.0033
28	.0094	.0079	.0068	.0057	.0049	.0041	.0034	.0028
29	.0084	.0070	.0061	.0051	.0043	.0037	.0030	.0025
30	.0076	.0063	.0054	.0046	.0038	.0033	.0027	.0022
31	.0415	.0467	.0516	.0559	.0597	.0629	.0644	.0650

MODEL E

$\phi = 150^{o}$

RUN NUMBER 8

ORIFICE NUMBER	ANGLE OF ATTACK (NOMINAL)							
	-15^{o}	-10^{o}	-5^{o}	0^{o}	5^{o}	10^{o}	15^{o}	20^{o}
1	.0879	.0919	.0939	.0942	.0932	.0904	.0863	.0808
2	.0911	.0936	.0940	.0926	.0903	.0858	.0801	.0736
3	.0925	.0934	.0920	.0899	.0855	.0804	.0739	.0663
4	.0922	.0916	.0887	.0852	.0798	.0735	.0665	.0582
5	.0909	.0885	.0839	.0795	.0734	.0665	.0593	.0508
6	.0878	.0837	.0784	.0727	.0661	.0594	.0521	.0436
7	.0835	.0786	.0729	.0666	.0594	.0523	.0450	.0370
8	.0785	.0730	.0670	.0602	.0534	.0462	.0390	.0318
9	.0735	.0674	.0614	.0542	.0473	.0403	.0334	.0268
10	.0682	.0620	.0557	.0491	.0420	.0355	.0290	.0230
11	.0628	.0566	.0500	.0434	.0365	.0305	.0244	.0192
12	.0576	.0516	.0449	.0384	.0321	.0262	.0208	.0162
13	.0533	.0468	.0402	.0337	.0277	.0226	.0175	.0135
14	.0484	.0419	.0358	.0297	.0241	.0194	.0148	.0113
15	.0445	.0381	.0321	.0263	.0210	.0168	.0126	.0096
16	.0404	.0342	.0285	.0231	.0183	.0144	.0107	.0081
17	.0372	.0312	.0256	.0205	.0162	.0126	.0093	.0069
18	.0338	.0281	.0229	.0181	.0142	.0109	.0079	.0059
19	.0307	.0252	.0203	.0159	.0124	.0094	.0068	.0050
20	.0279	.0228	.0183	.0141	.0109	.0082	.0058	.0043
21	.0258	.0209	.0168	.0131	.0101	.0077	.0057	.0043
22	.0239	.0192	.0152	.0118	.0090	.0068	.0050	.0038
23	.0216	.0173	.0136	.0105	.0079	.0060	.0044	.0033
24	.0197	.0156	.0121	.0093	.0071	.0053	.0039	.0029
25	.0176	.0139	.0107	.0082	.0062	.0046	.0034	.0025
26	.0160	.0126	.0096	.0073	.0055	.0041	.0030	.0022
27	.0144	.0112	.0085	.0064	.0049	.0036	.0026	.0020
28	.0129	.0100	.0075	.0056	.0043	.0031	.0023	.0017
29	.0116	.0089	.0067	.0050	.0038	.0027	.0020	.0015
30	.0105	.0080	.0060	.0045	.0033	.0024	.0018	.0018
31	.0346	.0417	.0489	.0560	.0626	.0689	.0747	.0788

MODEL E

$\phi = 179.8^{o}$

RUN NUMBER 9

ORIFICE NUMBER	ANGLE OF ATTACK (NOMINAL)							
	-15^{o}	-10^{o}	-5^{o}	0^{o}	5^{o}	10^{o}	15^{o}	20^{o}
1	.0888	.0926	.0941	.0945	.0936	.0908	.0867	.0816
2	.0924	.0945	.0947	.0932	.0901	.0855	.0800	.0732
3	.0947	.0949	.0931	.0901	.0859	.0793	.0735	.0653
4	.0947	.0933	.0898	.0852	.0798	.0726	.0654	.0567
5	.0937	.0907	.0854	.0796	.0731	.0652	.0578	.0488
6	.0911	.0863	.0799	.0734	.0658	.0576	.0498	.0413
7	.0871	.0812	.0745	.0670	.0589	.0505	.0426	.0347
8	.0823	.0756	.0683	.0606	.0525	.0447	.0366	.0294
9	.0779	.0702	.0626	.0547	.0464	.0388	.0310	.0245
10	.0723	.0648	.0569	.0493	.0412	.0340	.0267	.0209
11	.0670	.0593	.0511	.0433	.0358	.0289	.0223	.0172
12	.0622	.0539	.0461	.0383	.0313	.0249	.0187	.0143
13	.0574	.0494	.0414	.0337	.0269	.0213	.0158	.0119
14	.0522	.0443	.0369	.0296	.0234	.0182	.0133	.0099
15	.0483	.0404	.0331	.0262	.0205	.0156	.0113	.0083
16	.0440	.0364	.0294	.0229	.0177	.0133	.0095	.0069
17	.0406	.0332	.0265	.0204	.0156	.0117	.0082	.0059
18	.0371	.0300	.0236	.0180	.0137	.0100	.0070	.0050
19	.0337	.0271	.0211	.0159	.0119	.0085	.0059	.0042
20	.0308	.0244	.0188	.0141	.0104	.0073	.0051	.0035
21	.0287	.0228	.0174	.0131	.0098	.0071	.0051	.0037
22	.0265	.0209	.0158	.0118	.0087	.0062	.0045	.0033
23	.0242	.0188	.0141	.0104	.0077	.0055	.0039	.0028
24	.0220	.0170	.0126	.0093	.0068	.0048	.0034	.0025
25	.0197	.0151	.0111	.0082	.0060	.0042	.0030	.0022
26	.0181	.0137	.0100	.0073	.0053	.0038	.0027	.0020
27	.0162	.0122	.0089	.0064	.0047	.0032	.0023	.0017
28	.0146	.0108	.0079	.0057	.0041	.0028	.0020	.0015
29	.0133	.0097	.0070	.0050	.0036	.0025	.0018	.0016
30	.0121	.0088	.0063	.0045	.0032	.0022	.0016	.0028
31	.0324	.0400	.0482	.0565	.0642	.0720	.0787	.0852

MODEL A

$\phi = 0^{o}$

RUN NUMBER 14

ORIFICE NUMBER	ANGLE OF ATTACK (NOMINAL)							
	-15^{o}	-10^{o}	-5^{o}	0^{o}	5^{o}	10^{o}	15^{o}	20^{o}
1	xxxxx	xxxxx	.0935	.0945	.0935	.0925	.0892	.0854
2	xxxxx	xxxxx	.0932	.0943	.0943	.0933	.0905	.0868
3	xxxxx	xxxxx	.0923	.0938	.0943	.0940	.0915	.0885
4	xxxxx	xxxxx	.0920	.0936	.0943	.0946	.0929	.0899
5	xxxxx	xxxxx	.0907	.0931	.0939	.0949	.0934	.0910
6	xxxxx	xxxxx	.0895	.0920	.0938	.0947	.0943	.0922
7	xxxxx	xxxxx	.0883	.0916	.0934	.0948	.0948	.0932
8	xxxxx	xxxxx	.0868	.0903	.0922	.0937	.0951	.0942
9	xxxxx	xxxxx	.0852	.0893	.0910	.0932	.0948	.0945
10	xxxxx	xxxxx	.0835	.0872	.0904	.0929	.0949	.0949
11	xxxxx	xxxxx	.0812	.0857	.0885	.0914	.0942	.0949
12	xxxxx	xxxxx	.0788	.0833	.0867	.0896	.0929	.0949
13	xxxxx	xxxxx	.0762	.0810	.0839	.0877	.0911	.0939
14	xxxxx	xxxxx	.0731	.0775	.0814	.0848	.0887	.0923
15	xxxxx	xxxxx	.0682	.0726	.0766	.0805#	.0847	.0893
16	xxxxx	xxxxx	.0600	.0637	.0675	.0714	.0763	.0818
17	xxxxx	xxxxx	.0514	.0552	.0589	.0633	.0682	.0747
18	xxxxx	xxxxx	.0365	.0400	.0439	.0487	.0545	.0620
19	xxxxx	xxxxx	.0195	.0225	.0262	.0307	.0366	.0449
20	xxxxx	xxxxx	.0101	.0123	.0151	.0190	.0243	.0320
21	xxxxx	xxxxx	.0046	.0060	.0079	.0106	.0144	.0203
22	xxxxx	xxxxx	.0017	.0024	.0034	.0049	.0072	.0107
23	xxxxx	xxxxx	.0014	.0010	.0015	.0024	.0037	.0060
24	xxxxx	xxxxx	.0017	.0005	.0007	.0012	.0019	.0033
25	xxxxx	xxxxx	.0016	.0005	.0005	.0013	.0018	.0017
26	xxxxx	xxxxx	.0016	.0005	.0005	.0034	.0019	.0018
27	xxxxx	xxxxx	.0016	.0005	.0006	.0014	.0019	.0018
28	xxxxx	xxxxx	.0260	.0222	.0193	.0172	.0154	.0183

MODEL A

$\phi = 30^{o}$

RUN NUMBER 17

ORIFICE NUMBER	ANGLE OF ATTACK (NOMINAL)							
	-15^{o}	-10^{o}	-5^{o}	0^{o}	5^{o}	10^{o}	15^{o}	20^{o}
1	.0889	.0922	.0932	.0936	.0940	.0921	.0885	.0848
2	.0877	.0913	.0932	.0938	.0940	.0931	.0898	.0860
3	.0865	.0902	.0922	.0936	.0937	.0936	.0906	.0872
4	.0849	.0892	.0916	.0932	.0936	.0938	.0915	.0882
5	.0834	.0878	.0907	.0925	.0936	.0939	.0923	.0896
6	.0814	.0864	.0899	.0921	.0934	.0936	.0926	.0903
7	.0793	.0850	.0885	.0914	.0929	.0932	.0930	.0909
8	.0774	.0831	.0870	.0898	.0915	.0928	.0930	.0915
9	.0753	.0811	.0856	.0884	.0907	.0919	.0929	.0917
10	.0734	.0791	.0835	.0869	.0894	.0911	.0925	.0918
11	.0710	.0767	.0817	.0854	.0878	.0901	.0919	.0916
12	.0683	.0744	.0792	.0831	.0861	.0882	.0903	.0911
13	.0659	.0718	.0764	.0801	.0837	.0860	.0883	.0898
14	.0632	.0686	.0735	.0771	.0805	.0832	.0861	.0879
15	.0596	.0643	.0686	.0725	.0756	.0788	.0816	.0847
16	.0529	.0566	.0601	.0635	.0664	.0697	.0730	.0768
17	.0452	.0484	.0517	.0548	.0580	.0614	.0653	.0698
18	.0313	.0338	.0368	.0398	.0429	.0469	.0511	.0569
19	.0156	.0175	.0197	.0223	.0252	.0288	.0332	.0393
20	.0076	.0087	.0102	.0120	.0143	.0175	.0212	.0270
21	.0032	.0038	.0046	.0057	.0073	.0094	.0121	.0165
22	.0011	.0012	.0016	.0022	.0030	.0041	.0057	.0084
23	.0015	.0014	.0013	.0008	.0012	.0019	.0028	.0045
24	.0019	.0018	.0017	.0006	.0007	.0012	.0016	.0025
25	.0019	.0018	.0017	.0006	.0006	.0015	.0020	.0020
26	.0019	.0018	.0017	.0006	.0006	.0015	.0020	.0021
27	.0019	.0018	.0017	.0006	.0006	.0015	.0019	.0021
28	.0340	.0291	.0254	.0222	.0196	.0174	.0157	.0169

MODEL A

$\phi = 60^{\circ}$

RUN NUMBER 18

ORIFICE NUMBER	ANGLE OF ATTACK (NOMINAL)							
	-15°	-10°	-5°	0°	5°	10°	15°	20°
1	.0890	.0919	.0936	.0941	.0938	.0921	.0890	.0853#
2	.0885	.0916	.0924	.0934	.0937	.0925	.0894	.0856#
3	.0877	.0909	.0923	.0933	.0935	.0926#	.0897	.0860
4	.0866	.0898	.0921	.0929	.0931	.0926	.0899	.0866
5	.0855	.0890	.0914	.0928	.0928	.0926	.0899	.0866
6	.0836	.0877	.0904	.0918	.0921	.0922	.0898	.0869
7	.0820	.0864	.0892	.0909	.0914	.0913	.0896	.0868
8	.0805	.0851	.0880	.0894	.0904	.0906	.0893	.0868
9	.0788	.0836	.0863	.0883	.0894	.0897	.0886	.0862
10	.0771	.0817	.0846	.0868	.0878	.0883	.0878	.0853
11	.0748	.0798	.0832	.0847	.0864	.0870	.0865	.0844
12	.0724	.0770	.0801	.0825	.0840	.0847	.0847	.0834
13	.0697	.0746	.0780	.0802	.0817	.0824	.0829	.0815#
14	.0670	.0716	.0741	.0767	.0785	.0795	.0800	.0790#
15	.0630	.0671	.0697	.0720	.0738	.0746#	.0758	.0748#
16	.0554	.0586	.0612	.0631	.0648	.0657	.0672	.0668#
17	.0474	.0504	.0528	.0547	.0562	.0574	.0589	.0592
18	.0332	.0358	.0378	.0394	.0411	.0426	.0447	.0456
19	.0172	.0190	.0206	.0220	.0235	.0249	.0269	.0284
20	.0087	.0098	.0109	.0118	.0131	.0143	.0161	.0177
21	.0039	.0044	.0050	.0056	.0064	.0073	.0085	.0101
22	.0012	.0015	.0018	.0021	.0025	.0030	.0037	.0142
23	.0013	.0012	.0011	.0007	.0009	.0019	.0016	.0130
24	.0017	.0017	.0016	.0006	.0010	.0017	.0020	.0151
25	.0018	.0017	.0016	.0006	.0011	.0018	.0020	.0107
26	.0018	.0017	.0016	.0006	.0010	.0019	.0020	.0120
27	.0017	.0017	.0015	.0007	.0010	.0017	.0019	.0136
28	.0275	.0258	.0239	.0225	.0208	.0190	.0174	.0162

MODEL A

$\phi = 90^{o}$

RUN NUMBER 19

ORIFICE NUMBER	ANGLE OF ATTACK (NOMINAL)							
	-15^{o}	-10^{o}	-5^{o}	0^{o}	5^{o}	10^{o}	15^{o}	20^{o}
1	.0891	.0915	.0936	.0942	.0938	.0924#	.0888	.0851
2	.0892	.0922	.0932	.0939	.0937	.0923	.0890	.0850
3	.0887	.0917	.0932	.0933	.0929	.0920	.0884	.0846
4	.0885	.0915	.0927	.0933	.0925	.0912	.0880	.0842
5	.0881	.0907	.0919	.0923	.0921	.0908	.0876	.0836
6	.0871	.0898	.0910	.0918	.0916	.0900	.0868	.0829
7	.0866	.0889	.0904	.0907	.0904	.0890	.0857	.0821
8	.0854	.0878	.0894	.0895	.0887	.0878	.0846	.0809
9	.0841	.0864	.0880	.0882	.0876	.0863	.0834	.0799
10	.0826	.0850	.0862	.0867	.0861	.0850	.0819	.0786
11	.0810	.0832	.0842	.0848	.0842	.0831	.0803	.0769
12	.0787	.0806	.0822	.0826	.0820	.0808	.0781	.0749
13	.0763	.0780	.0795	.0799	.0795	.0784#	.0756	.0726
14	.0734	.0753	.0761	.0767	.0761	.0753	.0727	.0699
15	.0687	.0705	.0716	.0717	.0712	.0707	.0683	.0657
16	.0605	.0619	.0626	.0629	.0625	.0619	.0600	.0578
17	.0524	.0534	.0541	.0543	.0541	.0537	.0520	.0500
18	.0378	.0385	.0390	.0393	.0391	.0388	.0374	.0360
19	.0210	.0214	.0217	.0219	.0217	.0215	.0207	.0200
20	.0115	.0117	.0118	.0118	.0117	.0117	.0113	.0110
21	.0055	.0055	.0056	.0056	.0056	.0056	.0054	.0053
22	.0021	.0021	.0021	.0021	.0021	.0085	.0021	.0020
23	.0012	.0009	.0007	.0007	.0007	.0014	.0016	.0014
24	.0017	.0016	.0012	.0006	.0012	.0022	.0021	.0019
25	.0018	.0016	.0012	.0006	.0011	.0017	.0021	.0019
26	.0018	.0016	.0012	.0006	.0011	.0016	.0021	.0019
27	.0017	.0015	.0012	.0006	.0011	.0016	.0021	.0018
28	.0214	.0218	.0222	.0223	.0222	.0222	.0213	.0207

MODEL A

$\phi = 120^{o}$

RUN NUMBER 20

ORIFICE NUMBER	ANGLE OF ATTACK (NOMINAL)							
	-15^{o}	-10^{o}	-5^{o}	0^{o}	5^{o}	10^{o}	15^{o}	20^{o}
1	.0892	.0920	.0931	.0940	.0935	.0921	.0888	.0850
2	.0899	.0920	.0938	.0937	.0932	.0917	.0880	.0839
3	.0903	.0923	.0934	.0935	.0930	.0908	.0873	.0829
4	.0907	.0923	.0934	.0931	.0925	.0900	.0862	.0817
5	.0908	.0925	.0934	.0923	.0918	.0889	.0849	.0803
6	.0909	.0917	.0926	.0918	.0901	.0876	.0835	.0791
7	.0906	.0914	.0919	.0908	.0893	.0864	.0821	.0778
8	.0900	.0903	.0906	.0897	.0879	.0849	.0804	.0758
9	.0890	.0894	.0893	.0881	.0863	.0830	.0786	.0746
10	.0881	.0884	.0883	.0866	.0844	.0813	.0769	.0723
11	.0869	.0868	.0861	.0847	.0828	.0793	.0748	.0702
12	.0851	.0847	.0839	.0826	.0802	.0767	.0723	.0681
13	.0830	.0826	.0815	.0801	.0775	.0740	.0699	.0659
14	.0801	.0795	.0787	.0768	.0742	.0710	.0670	.0627
15	.0756	.0749	.0736	.0722	.0699	.0666	.0630	.0595
16	.0668	.0660	.0647	.0631	.0612	.0584	.0554	.0526
17	.0587	.0578	.0563	.0546	.0528	.0503	.0475	.0447
18	.0441	.0428	.0412	.0396	.0377	.0355	.0332	.0314
19	.0268	.0253	.0235	.0222	.0205	.0188	.0172	.0161
20	.0160	.0146	.0131	.0120	.0108	.0097	.0087	.0080
21	.0085	.0075	.0064	.0057	.0050	.0043	.0038	.0035
22	.0036	.0031	.0025	.0021	.0018	.0015	.0014	.0012
23	.0016	.0013	.0010	.0008	.0007	.0013	.0018	.0016
24	.0015	.0014	.0008	.0006	.0014	.0019	.0023	.0021
25	.0017	.0015	.0009	.0006	.0013	.0018	.0023	.0021
26	.0017	.0015	.0009	.0006	.0013	.0018	.0023	.0020
27	.0017	.0014	.0009	.0006	.0013	.0024	.0022	.0020
28	.0173	.0189	.0205	.0220	.0238	.0254	.0278	.0297

MODEL A

$\phi = 150^{o}$

RUN NUMBER 21

ORIFICE NUMBER	ANGLE OF ATTACK (NOMINAL)							
	-15^{o}	-10^{o}	-5^{o}	0^{o}	5^{o}	10^{o}	15^{o}	20^{o}
1	.0894#	.0919#	.0933	.0939	.0935	.0921	.0889	.0850#
2	.0902	.0928	.0936	.0937	.0933	.0910	.0875	.0835#
3	.0915	.0932	.0937	.0935	.0931	.0902	.0861	.0817#
4	.0921	.0933	.0937	.0931	.0919	.0886	.0846	.0801#
5	.0928	.0931	.0934	.0925	.0912	.0876	.0830	.0783
6	.0930	.0937	.0930	.0916	.0899	.0861	.0814	.0767
7	.0933	.0934	.0927	.0910	.0886	.0847	.0790	.0752
8	.0930	.0926	.0917	.0902	.0872	.0826	.0771	.0737
9	.0928	.0924	.0906	.0885	.0855	.0808	.0752	.0724
10	.0922	.0915	.0894	.0869	.0835	.0791	.0729	.0692
11	.0916	.0902	.0878	.0853	.0813	.0767	.0706	.0689
12	.0901	.0886	.0859	.0832	.0788	.0739	.0681	.0677
13	.0885	.0862	.0833	.0802	.0761	.0714	.0659	.0660#
14	.0859	.0836	.0802	.0769	.0729	.0683	.0630	.0646#
15	.0821	.0791	.0755	.0722	.0686	.0643	.0593	.0620#
16	.0733	.0699	.0665	.0632	.0599	.0563#	.0525	.0555#
17	.0656	.0615	.0580	.0547	.0517	.0484	.0447	.0475
18	.0514	.0469	.0429	.0395	.0366	.0338	.0310	.0334
19	.0337	.0288	.0253	.0221	.0195	.0174	.0154	.0175
20	.0216	.0174	.0144	.0119	.0101	.0087	.0075	.0090
21	.0124	.0093	.0072	.0056	.0045	.0037	.0030	.0134
22	.0059	.0041	.0029	.0021	.0015	.0012	.0018	.0109
23	.0029	.0018	.0011	.0007	.0010	.0014	.0018	.0136
24	.0016	.0011	.0008	.0005	.0015	.0019	.0023	.0110
25	.0017	.0014	.0006	.0005	.0016	.0019	.0023	.0150
26	.0017	.0014	.0006	.0006	.0015	.0018	.0023	.0143
27	.0017	.0014	.0006	.0006	.0015	.0028	.0023	.0152
28	.0156	.0174	.0194	.0218	.0249	.0289	.0336	.0407

MODEL A

$\phi = 180^{o}$

RUN NUMBER 22

ORIFICE NUMBER	ANGLE OF ATTACK (NOMINAL)							
	-15^{o}	-10^{o}	-5^{o}	0^{o}	5^{o}	10^{o}	15^{o}	20^{o}
1	.0893	.0919	.0938	.0940	.0937	.0924	.0890	.0853#
2	.0908	.0931	.0938	.0935	.0933	.0913	.0877	.0836
3	.0916	.0936	.0940	.0937	.0925	.0898	.0862	.0819
4	.0930	.0934	.0941	.0938	.0923	.0888	.0846	.0801
5	.0935	.0937	.0942	.0928	.0912	.0872	.0826	.0783
6	.0941	.0941	.0932	.0921	.0898	.0858	.0807	.0760
7	.0941	.0939	.0932	.0914	.0881	.0838	.0789	.0741
8	.0942	.0939	.0926	.0901	.0867	.0822	.0767	.0717
9	.0944	.0932	.0915	.0892	.0853	.0804	.0747	.0701
10	.0937	.0925	.0901	.0873	.0835	.0784	.0725	.0701
11	.0933	.0916	.0891	.0855	.0809	.0760	.0699	.0693
12	.0923	.0901	.0870	.0832	.0786	.0733	.0672	.0690
13	.0907	.0877	.0845	.0805	.0757	.0709#	.0648	.0668
14	.0885	.0854	.0812	.0770	.0726	.0679	.0622	.0658
15	.0843	.0808	.0766	.0725	.0679	.0636	.0587	.0645
16	.0762	.0714	.0675	.0637	.0598	.0561	.0522	.0576
17	.0684	.0633	.0590	.0549	.0513	.0479	.0444	.0497
18	.0546	.0490	.0437	.0397	.0363	.0334	.0307	.0349
19	.0368	.0307	.0259	.0222	.0193	.0171	.0152	.0183
20	.0243	.0190	.0150	.0120	.0099	.0084	.0074	.0092
21	.0143	.0104	.0076	.0057	.0044	.0131	.0029	.0040
22	.0071	.0047	.0031	.0021	.0015	.0017	.0019	.0014
23	.0036	.0022	.0013	.0007	.0011	.0015	.0019	.0018
24	.0020	.0013	.0008	.0006	.0016	.0026	.0024	.0023
25	.0013	.0012	.0005	.0006	.0016	.0020	.0024	.0023
26	.0016	.0013	.0006	.0006	.0016	.0019	.0024	.0023
27	.0016	.0013	.0006	.0006	.0015	.0019	.0024	.0023
28	.0152	.0169	.0191	.0220	.0256	.0303	.0364	.0449

APPENDIX B

SHOCK WAVE COORDINATES
X/R_{max} Versus r/R_{max}

MODEL E

r/R_{max}	ANGLE OF ATTACK							
	-15°	-10°	-5°	0°	5°	10°	15°	20°
-1.9703					2.0655			
-1.8666					1.8214			
-1.7629					1.5978	1.8260		
-1.6592				1.2320	1.3831	1.5660	1.7817	2.0922
-1.5555			.9717	1.0658	1.1806	1.3275	1.4795	1.6875
-1.4518		.7514	.8326	.9127	1.0072	1.1160	1.2155	1.3610
-1.3481		.6416	.7082	.7769	.8320	.9209	.9884	1.0822
-1.2444		.5379	.5935	.6454	.6841	.7459	.7945	.8555
-1.1407		.4393	.4869	.5206	.5466	.5949	.6252	.6681
-1.0370	.2941	.3466	.3815	.4073	.4291	.4568	.4779	.5089
-.9333	.2204	.2653	.2857	.3101	.3175	.3430	.3520	.3713
-.8296	.1538	.1819	.2080	.2170	.2197	.2393	.2386	.2575
-.7259	.0913	.1158	.1327	.1417	.1408	.1491	.1497	.1569
-.6222	.0335	.0571	.0710	.0734	.0668	.0740	.0730	.0763
-.5185	-.0158	.0023	.0131	.0154	.0173	.0164	.0133	.0052
-.4148	-.0567	-.0406	-.0300	-.0293	-.0338	-.0317	-.0367	-.0420
-.3111	-.0863	-.0755	-.0650	-.0626	-.0699	-.0726	-.0786	-.0843
-.2074	-.1095	-.0907	-.0908	-.0894	-.0974	-.0985	-.1038	-.1171
-.1037	-.1211	-.1091	-.1045	-.1038	-.1089	-.1074	-.1212	-.1341
0	-.1352	-.1121	-.1116	-.1091	-.1117	-.1200	-.1301	-.1399
.1037	-.1221	-.1081	-.1052	-.1032	-.1068	-.1140	-.1266	-.1330
.2074	-.0989	-.0970	-.0864	-.0940	-.0939	-.0979	-.1132	-.1247
.3111	-.0743	-.0732	-.0608	-.0684	-.0643	-.0736	-.0884	
.4148	-.0363	-.0337	-.0185	-.0320	-.0259	-.0373	-.0557	
.5185	.0192	.0096	.0273	.0168	.0184	.0021	-.0175	
.6222	.0751	.0723	.0935	.0759	.0709	.0541		
.7259	.1622	.1457	.1614	.1458	.1417	.1151		
.8296	.2633	.2346	.2430	.2232	.2059	.1850		
.9333	.3675	.3354	.3419	.3164	.2891	.2561		
1.0370	.4955	.4556	.4559	.4152	.3824	.3421		
1.1407	.6449	.5898	.5777	.5321	.4863			
1.2444	.8223	.7489	.7149	.6577				
1.3481	1.0225	.9180	.8740	.7896				
1.4518	1.2589	1.1150	1.0414	.9271				
1.5555	1.5260	1.3295	1.2247	1.0887				
1.6592	1.8384	1.5639	1.4169	1.2547				
1.7629		1.8334	1.6349					

MODEL A

r/R_{max}	ANGLE OF ATTACK							
	-15°	-10°	-5°	0°	5°	10°	14.8°	19.8°
-2.1714					1.2284			
-2.0680					1.0261			
-1.9646					.8418	1.2075		
-1.8612					.6754	.9660		
-1.7578					.5237	.7535	1.0728	
-1.6544					.3887	.5643	.7795	1.2563
-1.5510				.1640	.2691	.4039	.5452	.8125
-1.4476		-.0491	.0079	.0801	.1657	.2685	.3553	.5099
-1.3442		-.0981	-.0507	.0100	.0745	.1525	.2117	.2980
-1.2408		-.1424	-.1019	-.0550	.0002	.0581	.0970	.1497
-1.1374	-.2157	-.1801	-.1478	-.1082	-.0650	-.0180	.0120	.0491
-1.0340	-.2467	-.2132	-.1875	-.1552	-.1198	-.0815	-.0593	-.0308
-.9306	-.2729	-.2424	-.2208	-.1959	-.1659	-.1344	-.1177	-.0959
-.8272	-.2926	-.2676	-.2499	-.2293	-.2054	-.1795	-.1667	-.1487
-.7238	-.3126	-.2898	-.2761	-.2596	-.2396	-.2170	-.2075	-.1942
-.6204	-.3266	-.3071	-.2971	-.2847	-.2676	-.2500	-.2442	-.2327
-.5170	-.3386	-.3218	-.3170	-.3051	-.2928	-.2768	-.2736	-.2668
-.4136	-.3484	-.3332	-.3301	-.3223	-.3131	-.2985	-.2989	-.2926
-.3102	-.3537	-.3407	-.3416	-.3356	-.3281	-.3162	-.3184	-.3144
-.2068	-.3581	-.3452	-.3486	-.3447	-.3399	-.3290	-.3346	-.3338
-.1034	-.3520	-.3477	-.3524	-.3507	-.3465	-.3402	-.3456	-.3488
0	-.3478	-.3454	-.3499	-.3530	-.3503	-.3461	-.3485	-.3586
.1034	-.3373	-.3392	-.3457	-.3499	-.3509	-.3485	-.3526	-.3652
.2068	-.3243	-.3283	-.3378	-.3441	-.3470	-.3479	-.3499	-.3696
.3102	-.3082	-.3150	-.3252	-.3345	-.3409	-.3429	-.3491	-.3693
.4136	-.2868	-.2968	-.3094	-.3200	-.3279	-.3334	-.3423	-.3677
.5170	-.2618	-.2734	-.2886	-.3032	-.3142	-.3220	-.3315	-.3664
.6204	-.2333	-.2467	-.2651	-.2820	-.2965	-.3068	-.3203	
.7238	-.1955	-.2146	-.2358	-.2567	-.2739	-.2871	-.3058	
.8272	-.1536	-.1755	-.1998	-.2256	-.2463	-.2643	-.2846	
.9306	-.1007	-.1320	-.1601	-.1893	-.2155	-.2382		
1.0340	-.0394	-.0789	-.1131	-.1469	-.1802	-.2075		
1.1374	.0346	-.0141	-.0580	-.1019	-.1381	-.1745		
1.2408	.1271	.0635	.0067	-.0484	-.0943			
1.3442	.2501	.1577	.0825	.0164	-.0426			
1.4476	.4034	.2687	.1740	.0911	.0172			
1.5510	.6021	.4055	.2807	.1747				
1.6544	.8391	.5679	.4004	.2694				
1.7578		.7538	.5397	.3771				
1.8612			.6950	.4941				
1.9646			.8630	.6224				
2.0680				.7548				